Chronic Impact of Nanoparticles on *Caenorhabditis elegans*: Neurodegeneration, Behavioral Impairments, and Molecular Mechanisms

Inaugural dissertation

for the attainment of the title of doctor
in the Faculty of Mathematics and Natural Sciences

at the Heinrich Heine University Düsseldorf

presented by

DANG TRI LE

from Can Tho

Duesseldorf, …../2024

from the IUF - Leibniz Research Institute for Environmental Medicine GmbH
at the Heinrich Heine University Düsseldorf

Published by permission of the
Faculty of Mathematics and Natural Sciences at
Heinrich Heine Universität Düsseldorf

Supervisor: Prof. Dr. rer. nat. Anna von Mikecz
Co-supervisor: Prof. Dr. rer. nat. Dieter Willbold

Date of the oral examination: …../…../2024

TABLE OF CONTENTS

SUMMARY

The use of nanoparticles (NPs) in industry and consumer products has been steadily increasing, leading to their accumulation in environmental sinks like soil and sediments as they are released through usage and disposal. While much of nanotoxicology research has largely focused on the immediate effects and uptake pathways of nanoparticles, the long-term consequences, especially those that emerge with age, are still not well understood. In this context, investigating chronic NP-bio-interactions is essential for a deeper understanding of their potential impacts. To explore age-dependent NP bio-interactions, *Caenorhabditis elegans* serves as a key target organism for NP research and functions as an animal model for neurotoxicology, lifespan studies, and the analysis of molecular pathways involved in neurodegeneration.

This doctoral thesis investigates into the long-term effects of silica NPs on *Caenorhabditis elegans*, with a particular emphasis on neurodegeneration and resulting behavioral defects. GABAergic neurons undergo neuronal loss when treated with silica NPs. This neuronal loss is correlated with a reduction in locomotion, as GABAergic motor neurons are responsible for controlling movement. Besides, the exposure to silica NPs accelerated protein aggregation in serotonergic and dopaminergic neurons, which is associated with an increase in behavioral defects.

Proteomic data analysis shows a reduction in prominent gene ontology group of glutamate metabolic process. Since glutamate is a compulsory component for GABA synthesis, the significant downregulation of *gdh-1* (Glutamate dehydrogenase) and *got-1.2* (Glutamate oxaloacetate transaminase) is particularly important in understanding the loss of GABAergic neurons following silica NPs exposure.

In addition to these biochemical and cellular findings, a single-worm tracking platform (SWT) was developed to automate the quantification of thrashing rates and swimming tracks. This platform proved to be robust and effective under various experimental conditions, including different types of particles and concentrations. This capability provides a scalable and efficient alternative for large-scale studies. The successful implementation of this platform represents a significant advancement, as it lays the groundwork for future high-throughput screening of a wide range of pollutants, intervention therapeutics, aging processes as well as various mutants and disease models of *C. elegans*.

ZUSAMMENFASSUNG

Der Einsatz von Nanopartikeln (NPs) in Industrie und Konsumgütern hat kontinuierlich zugenommen, was zu ihrer Anreicherung in Umwelt-Senken wie Boden und Sedimenten führt, wenn sie durch Nutzung und Entsorgung freigesetzt werden. Während sich die Nanotoxikologie überwiegend auf die akuten Effekte und Aufnahmewege von Nanopartikeln konzentriert hat, sind die langfristigen Konsequenzen, insbesondere solche, die mit dem Alter auftreten, noch nicht gut verstanden. In diesem Kontext ist die Untersuchung chronischer NP-Bio-Interaktionen entscheidend, um ein tieferes Verständnis ihrer potenziellen Auswirkungen zu erlangen. Zur Erforschung altersabhängiger NP-Bio-Interaktionen dient *Caenorhabditis elegans* als wichtiger Zielorganismus für die NP-Forschung und fungiert als Tiermodell für die Neurotoxikologie, für Studien zur Lebensspanne und die Analyse molekularer Wege, die an der Neurodegeneration beteiligt sind.

Diese Dissertation untersucht die langfristigen Effekte von Silica-Nanopartikeln auf *Caenorhabditis elegans*, mit besonderem Schwerpunkt auf Neurodegeneration und den daraus resultierenden Verhaltensdefekten. Bei der Behandlung mit Silica-NPs kommt es zu einem Verlust von GABAergen Motorneuronen, der mit einer Reduktion der Bewegung korreliert ist, da diese für die Bewegungssteuerung verantwortlich sind. Darüber hinaus induziert die Exposition gegenüber Silica-NPs eine Proteinaggregation in serotonergen und dopaminergen Neuronen, was mit einer Zunahme von Verhaltensdefekten assoziiert ist.

Proteomische Daten zeigen eine Verringerung in der prominenten Gen Ontologie-Gruppe des Glutamat-Stoffwechselprozesses. Da Glutamat ein wesentlicher Bestandteil der GABA-Synthese ist, ist die signifikante Herunterregulierung von *gdh-1* (Glutamatdehydrogenase) und *got-1.2* (Glutamat-Oxalacetat-Transaminase) besonders wichtig für das Verständnis des Verlusts von GABAergen Neuronen nach der Exposition gegenüber Silica-NPs.

Zur Bestätigung der Ergebnisse wurde eine Einzelwurm-Tracking-Plattform (SWT) etabliert, um die Quantifizierung von Schwimmbewegungen zu automatisieren. Diese Plattform bildet die Grundlage für zukünftige Screenings von Schadstoffen, Therapeutika, Alterungsprozessen sowie *C. elegans* Mutanten- und Krankheitsmodellen.

1. INTRODUCTION

1.1 Engineered nanoparticles

1.1.1 Application and distribution in the environment

The advancement of nanotechnology has led to a substantial increase in the production of engineered nanomaterials over recent decades, with these materials finding applications in nearly every aspect of our daily lives (Bayda et al., 2019). Silica NPs possess a nano-scale size and distinct physicochemical properties, including higher surface reactivity and an increased surface-to-volume ratio (Napierska et al., 2010). Silica NPs are extensively utilized in various fields, including biomedical applications, cosmetics, food products, car tires, and paints (Mebert et al., 2017) . According to the 2017 World Health Organization (WHO) guidelines, the annual production volume of silica NPs was 1.5 million tons.

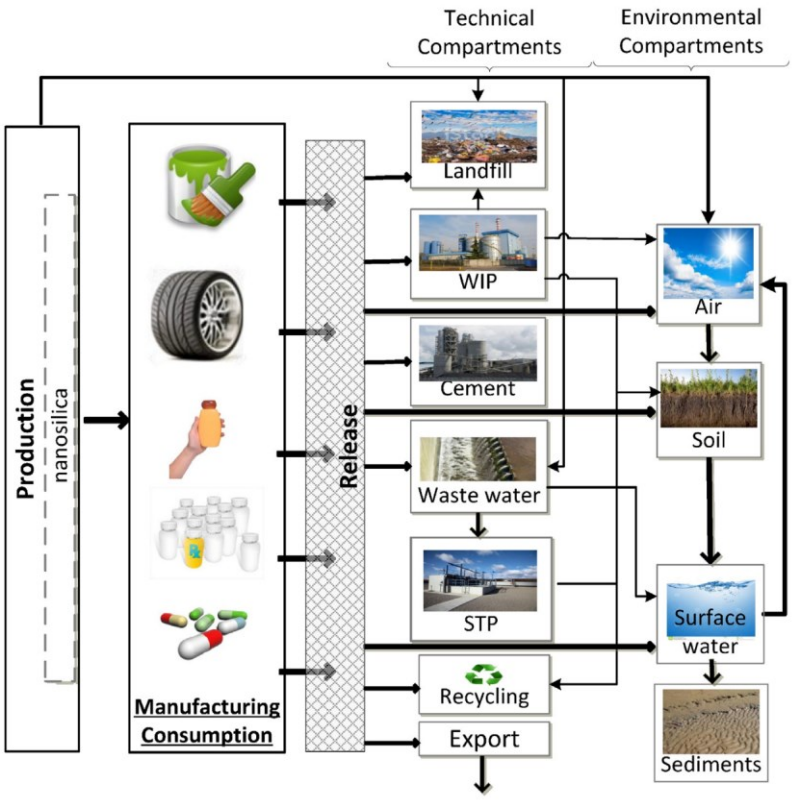

Figure 1. Lifecycle and distribution of nanoparticles in the environment. (Wang et al., 2016)

Silica NPs are produced and incorporated into various products, such as paint, tires, food

containers, and pharmaceuticals (Figure 1). During consumption, they can be released into the environment through landfills, waste incineration plants, cement production, wastewater streams, sewage treatment plants, recycling, and export channels. In landfills, they accumulate as waste; in incineration plants, they may be released into the air; and in cement production, silica NPs integrate into construction materials. Treated wastewater containing silica NPs is released back into the environment. From these technical compartments, silica nanoparticles can transition into the air, soil, or surface water, where they may settle into sediments. Recycling and export processes further distribute these particles in environmental sinks air, soil, surface waters and sediments (Figure 1).

The estimated median concentration of silica nanoparticles (NPs) in central European surface waters is 3.5 µg/L. In comparison, the median concentrations of silica NPs are 160 µg/kg in natural or urban soils, 390 µg/kg in soil treated with sewage sludge, and 490 µg/kg in landfill waste (Y. Wang et al., 2016).

1.1.2 Environmental effects of nanoparticles

Nanoparticles pose significant risks to the environment due to their potential toxicity and widespread applications across various industries. Industries such as ceramic manufacturing are particularly at risk of airborne particle formation and emission, exposing workers to potential health hazards associated with nanoparticles (Bessa et al., 2020). One significant concern is the potential risks associated with nanoparticles in aquatic environments. A study has demonstrated that nanoparticles like colloidal silver NPs can accumulate in rainbow trout fish (*Oncorhynchus mykiss*), reducing the hatching rates and sperm motility at 0.1 mg/L (Johari, 2014). The toxicity of various types of cadmium sulfide (CdS) nanoparticles has been demonstrated in a range of aquatic organisms, including the bacterium *Vibrio fischeri*, the microalgae *Raphidocelis subcapitata* and *Chlorella vulgaris*, and the crustacean *Daphnia magna* (Silva et al., 2016). Notably, the adverse effects of these nanoparticles extend beyond plankton, bacteria, and microalgae, impacting aquatic plants such as *Spirodela polyrrhiza* (Khataee et al., 2014). Additionally, the toxicity of zinc sulfide (ZnS) nanoparticles has been evaluated using the clam *Ruditapes decussatus* (Labiadh et al., 2017). Although extensive research has been conducted to assess the toxicological impacts of various nanoparticles on diverse life forms, the precise mechanisms underlying the toxic actions of metal sulfide nanoparticles remain inadequately understood.

Nanoparticles present risks to human health due to their unique physicochemical properties, which can lead to adverse effects on various biological systems. Silica nanoparticles have been shown to trigger the production of reactive oxygen species (ROS) and induce autophagy in human hepatocytes (Yu et al., 2014), cause spermatogenesis damage (Xu et al., 2014), and disrupt vascular homeostasis (Nemmar et al., 2014) The toxic effects of intraperitoneally administered 50 nm silica NPs (0.25 mg/kg) on systemic circulation, oxidative stress, inflammation, and DNA damage have been observed in the lungs, heart, liver, kidneys, and brain of mice (Nemmar et al., 2016) The generation of ROS induced by nanoparticles is partly due to mitochondrial dysfunction and the activation of stress-related cell signaling pathways. This process also leads to DNA damage, resulting in cell cycle arrest and apoptosis (Khanna et al., 2015; Teodoro et al., 2016). Furthermore, titanium dioxide nanoparticles have been shown to induce the release of nitric acid and glutamic acid in the brains of mice (J. Wang et al., 2008; Ze et al., 2013). These nanoparticles are also believed to activate inflammatory signaling pathways, specifically p38 MAP kinase, NF-Kb, and c-Src pathways, leading to an increased release of inflammatory cytokines from macrophages, particularly after accumulating in macrophage-rich organs such as the liver and spleen (Moon et al., 2010). Hemmerich and von Mikecz showed that nano polystyrene and nano silica were taken up by human epithelial cells (HEp-2 cells) within seconds via a dynamin dependent transport. NPs distribute in living cells in the cytoplasm or translocate via diffusion or active transport into the cell nucleus (Hemmerich & von Mikecz, 2013).In the nucleus, silica nanoparticles induced an abnormal redistribution of transcription and splicing factors, as well as components from protein homeostasis or proteostasis, such as 20S proteasomes in nuclear inclusions. These inclusions resemble the inclusions in neurodegenerative diseases (Chen and von Mikecz, 2005).

1.2 *Caenorhabditis elegans*

Caenorhabditis elegans (*C. elegans*) is a 1 mm long transparent nematode that ubiquitously inhabits the soil's solid-liquid interface, where it subsists on bacteria found on decomposing plant material. Within this microbe-rich habitat, *C. elegans* is part of a complex web of interactions involving various microbes and soil invertebrates. These organisms may serve as food, vectors, or competitors. Additionally, nematodes face threats from predators, pathogens, and parasites (Schulenburg & Félix, 2017). Through its interactions with other terrestrial organisms and its role in the food chain, *C. elegans* contributes to the ecological balance of nutrient cycling and

decomposition processes. This makes it a valuable bioindicator for detecting soil contamination and ecological imbalances (Neher, 2001; Schulenburg & Félix, 2017).

1.2.1 The model organism *C. elegans*

50 years ago, *C. elegans*, a 1 mm long nematode, was isolated by Sydney Brenner, who subsequently introduced it into the laboratory and established it as a model organism for scientific research (Brenner 1974; Corsi et al, 2015). Since then, *C. elegans* has become a cornerstone of laboratory research due to its simplicity and the wealth of genetic tools available for its study. In laboratory settings, the worm is typically cultured on agar plates or in liquid medium, where it is fed Escherichia coli (*E. Coli*) as a primary food source (Michaelson, 2000). The reproductive potential (300–350 offspring per worm) and short boom-bust life cycle of adult hermaphrodite *C. elegans* (2–3 weeks) facilitates the maintenance and study of large populations.

C. elegans exists in two sexes: hermaphrodites (XX) and males (XO). However, males are quite rare in laboratory cultures, making up only 0.1-0.2% of the population. This rarity is due to the fact that males arise from the mis-segregation of homologous chromosomes during cell division. Hermaphrodites possess both oocytes and sperm, allowing them to reproduce either through self-fertilization or by mating with males, which can introduce genetic diversity. The generation time for *C. elegans* is influenced by environmental factors such as temperature and food availability. Under optimal conditions (approximately 20°C), the generation time is about three days post-fertilization. During this period, the worm undergoes embryogenesis followed by four successive larval stages (L1-L4), before maturing into an adult (Figure 2).

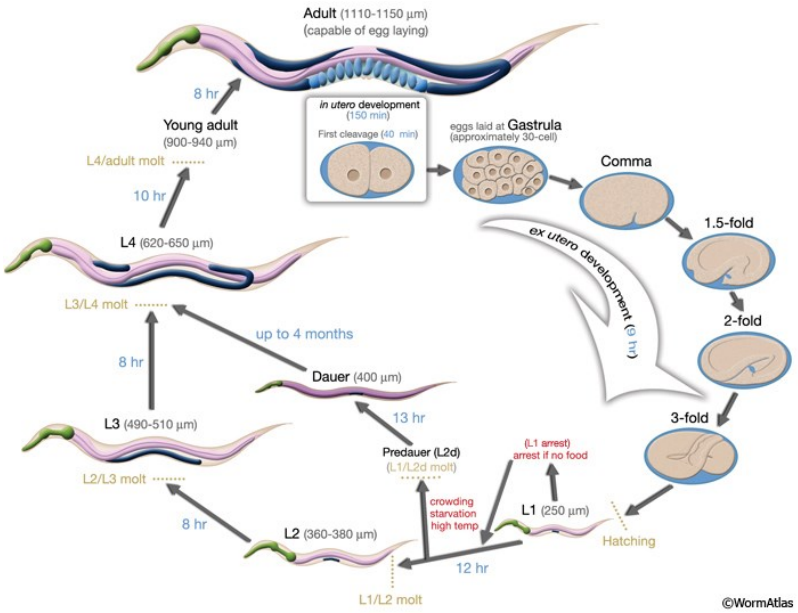

Figure 2. Life cycle of *C. elegans* at 22°C (Altun & Hall, 2009)

Adult *C. elegans* have a relatively short lifespan of 2-3 weeks, during which they can produce around 300 offspring. This rapid lifecycle and high reproductive rate make *C. elegans* an ideal organism for genetic and developmental studies, as it allows researchers to quickly observe the effects of genetic manipulations over multiple generations (Brenner, 1974; Corsi et al., 2015). The transparency of the worm's cuticle is another advantageous trait, as it permits the direct observation of internal organs, including the pharynx, intestine, reproductive system, and gonads, under a microscope. Fluorescent proteins, which are stably integrated into the genome, enable researchers to visualize specific tissues and cellular processes in living worms

The genome of *C. elegans* has been fully sequenced, revealing that 60-80% of its genes are homologous to those in the human genome (The *C. elegans* Sequencing Consortium, 1998). This high degree of genetic similarity makes *C. elegans* a powerful model for studying human biology and disease. Many of the molecular signaling pathways, including those involved in stress responses, are conserved between *C. elegans* and humans, allowing insights gained from studies in worms to be applicable to human health and disease. Consequently, *C. elegans* is widely used in various research fields such as developmental biology, cell biology, molecular biology, neurobiology, genetics, aging research, and toxicology (Corsi et al., 2015).

C. elegans' role in scientific research continues to expand as new techniques and technologies are developed, further consolidating its status as a model organism that provides invaluable insights into fundamental biological processes.

In its terrestrial ecosystem, *C. elegans* encounters nanoparticles that enter the soil, for instance, through the application of sewage sludge from wastewater treatment plants onto agricultural fields (Y. Wang et al., 2016). *C. elegans* assimilates NPs primarily through two pathways: ingestion via the mouth and subsequent pharynx, leading to the intestinal tract, and absorption through the vulva, affecting the reproductive system The translocation of nano-silica into specific vulval cells or pharyngeal tissues is associated with functional impairments of these organs (Pluskota et al., 2009; Scharf et al, 2013).

1.2.2 The nervous system of *C. elegans*

The nervous system of *C. elegans* is a highly organized and intricate network that provides a comprehensive model for studying neural function and development. It comprises several key components, including the nerve ring, which encircles the pharynx, the ventral nerve cord, the dorsal nerve cord, and the neuropil located in the tail region (Corsi et al., 2015). The nerve ring acts as a central hub, coordinating sensory and motor signals throughout the worm's body. The invariant structure and stereotypical positioning of neurons in the adult worm facilitate the precise identification and detailed mapping of each of the 302 individual neurons present in its nervous system (Apfeld & Kenyon, 1999; White et al., 1986). This anatomical consistency is a significant advantage for neurobiological research, allowing scientists to study neural circuits and their functions with remarkable accuracy.

The neural cell bodies in *C. elegans* are predominantly organized into ganglia, primarily located in the head, along the ventral nerve cord, and in the tail (Figure 3). This arrangement supports efficient signal transmission and integration within the nervous system (Corsi et al., 2015). In addition to neurons, *C. elegans* has 56 glia-like cells that play crucial roles in supporting and modulating neural activity. These glia-like cells are particularly important for surrounding and protecting sensory neurons, contributing to the overall functionality and resilience of the nervous system (Oikonomou & Shaham, 2011).

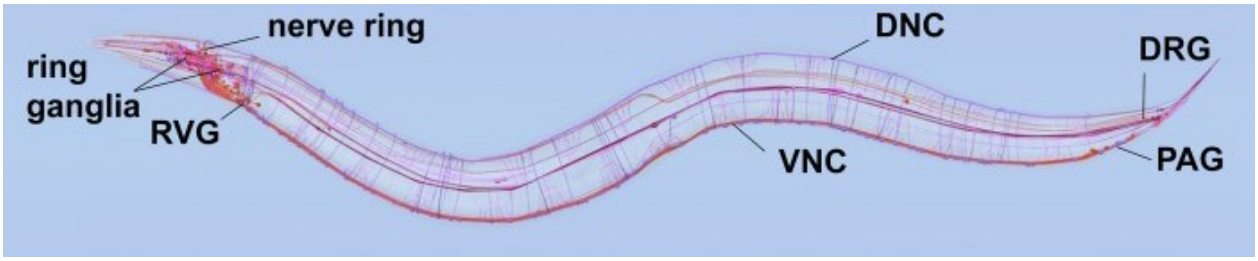

Figure 3. Diagram of the *C. elegans* nervous system identifying some major nerve bundles and ganglia. Major nerve tracts include the ventral nerve cord (VNC), dorsal nerve cord (DNC), and nerve ring. Major ganglia include the ring ganglia, retro vesicular ganglion (RVG), pre-anal ganglion (PAG), and dorsal-root ganglion (DRG). Adapted from Corsi et al., 2015.

The *C. elegans* nervous system features an extensive network of connections, comprising 6393 chemical synapses, 890 cell contacts (gap junctions), and 1410 neuromuscular junctions (tight junctions) (Brenner et al., 1986; Varshney et al., 2011). These connections enable neurons to communicate through neurotransmitters and neuropeptides, facilitating complex behaviors and physiological responses. Key neurotransmitters, such as acetylcholine (ACh), serotonin, dopamine, and γ-aminobutyric acid (GABA), are released from synaptic vesicles and play important roles in signal transmission (Bargmann, 1998) . This diverse array of neurotransmitters allows for a wide range of neural functions, from simple motor control sophisticated sensory processing.

C. elegans is also equipped with a highly sensitive sensory system capable of detecting environmental toxins and pathogens through its 60 sensory neurons. These neurons are specialized to perceive various stimuli, including chemosensory, olfactory, gustatory, mechanosensory, and thermosensory inputs. Upon detecting these stimuli, the sensory neurons relay signals either through interneurons or directly to motor neurons, initiating appropriate behavioral responses (Melo & Ruvkun, 2012; Zhang et al., 2005). Among these sensory neurons, 12 pairs of amphid neurons (ADF, ADL, AFD, ASE, ASG, ASH, ASI, ASJ, ASK, AWA, AWB, AWC) are located in the pharynx and have direct or indirect contact with the external environment. These amphid neurons extend from the oral cavity along the pharynx to the nerve ring, making them the largest chemosensory organs in nematodes (Altun & Hall, 2009)

Motor neurons in *C. elegans* play a critical role in coordinating movement and other physiological processes. They stimulate body wall muscle cells using acetylcholine (ACh) and inhibit them using γ-aminobutyric acid (GABA). Similarly, the pharyngeal muscles are excited by ACh but inhibited

by glutamate, ensuring precise control over muscle contractions and feeding behaviors (Bargmann, 1998). The ability of the *C. elegans* nervous system to integrate sensory inputs and generate appropriate motor outputs allows the worm to navigate its environment effectively, avoiding toxins and pathogens through coordinated behavioral responses (Melo & Ruvkun, 2012; Zhang et al., 2005).

GABAergic nervous system

The neurotransmitter γ-aminobutyric acid (GABA) plays a crucial role in the central nervous systems of vertebrates, primarily functioning at inhibitory synapses. In *Caenorhabditis elegans*, GABA operates mainly at neuromuscular synapses, being essential for muscle relaxation during locomotion and contraction during defecation (Jorgensen, 2005). This distinct role in basic motor functions has facilitated genetic analyses, identifying various proteins necessary for GABA function, including biosynthetic enzymes, transporters, receptors, and transcription factors.

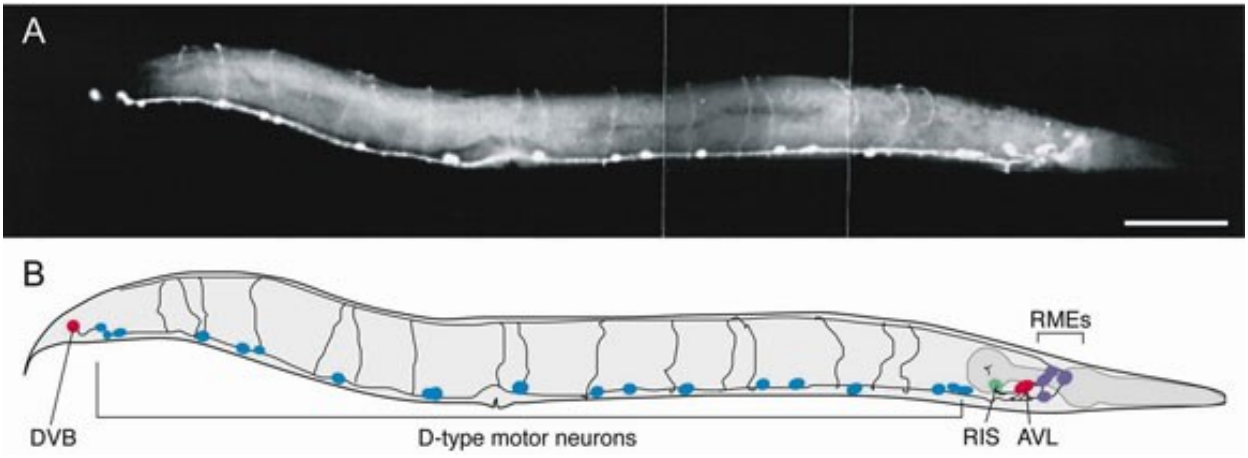

Figure 4. The GABA nervous system in *C. elegans*.
(A) Fluorescent micrograph of an adult *C. elegans* hermaphrodite stained with an antiGABA antiserum. (B) Schematic drawing of the positions of the 26 GABA-containing neurons (Schuske et al., 2004).

In *C. elegans*, GABA acts through two main receptor types: $GABA_A$ receptors, which are GABA-gated chloride channels that inhibit cells by hyperpolarization or creating a current shunt (Schofield et al., 1987), and $GABA_B$ receptors, which inhibit excitability by opening potassium channels and inhibiting calcium channels through G-protein-coupled mechanisms (Kaupmann et al., 1997). These receptors help regulate various physiological processes, including muscle relaxation and contraction.

The GABAergic system in *C. elegans* includes 26 neurons, consisting of motor neurons (DD, VD, RME, AVL, DVB) and the interneuron RIS (Figure 4). These neurons have specific roles: the D-type neurons inhibit body muscles during locomotion, creating the worm's sinusoidal movement (McIntire et al., 1993). The RME neurons regulate head foraging movements, preventing exaggerated flexures; and the AVL and DVB neurons stimulate enteric muscles during defecation, essential for expelling intestinal contents.

Genetic screens have identified several critical genes for GABA function in *C. elegans*. The gene unc-25 encodes glutamic acid decarboxylase (GAD), the enzyme required for GABA synthesis (Jin et al., 1999). The gene *unc-47* encodes the vesicular GABA transporter (VGAT), which packages GABA into synaptic vesicles (McIntire et al., 1997). The gene *unc-46* likely acts as an accessory protein for VGAT, regulating its activity or localization (McIntire et al., 1993). The gene *unc-30* is a transcription factor that regulates the expression of GAD and VGAT in D-type neurons (Jin et al., 1994). The gene *unc-49* encodes a $GABA_A$ receptor subunit essential for muscle inhibition (Bamber et al., 1999), while *exp-1* encodes a novel GABA-gated cation channel involved in excitatory functions during defecation (Beg & Jorgensen, 2003).

Despite the evolutionary divergence between nematodes and vertebrates, many aspects of the GABAergic systems are conserved. Both possess $GABA_A$ and $GABA_B$ receptors and share mechanisms for GABA synthesis and transport. However, nematodes also have a unique GABA-gated cation channel (EXP-1) not found in vertebrates (Jorgensen, 2005).

The study of GABA in *C. elegans* has provided significant insights into the roles of GABA in motor function and the genetic regulation of GABAergic neurons. These findings have broader implications for understanding similar mechanisms in vertebrates and underscore the evolutionary conservation of neurotransmitter systems.

1.2.3 Behavior phenotypes

The relatively simple nervous system of the nematode *C. elegans* compared to vertebrates provides an excellent model for the analysis of various behavioral phenotypes, such as locomotion, egg-laying, pumping frequency, defecation, and chemo sensation. This simplicity is advantageous because it allows researchers to dissect and understand the underlying mechanisms of these behaviors with greater precision. In *C. elegans*, specific behavioral functions are often controlled by individual neurons, rather than the more complex neural networks seen in

vertebrates. This direct relationship between neuron function and behavior offers valuable insights into the functionality of neural signal transmission and the overall workings of the nervous system (Corsi et al*.,* 2015).

The neural circuits of *Caenorhabditis elegans* are designed to control various behaviors, including locomotion. Within these circuits, 302 neurons play diverse roles, with 75 motoneurons specifically innervating the body wall muscles that generate the force required for movement (Gjorgjieva et al., 2014). The locomotion of *C. elegans* is characterized by an undulatory fashion, which involves dorsoventral body bends that propel the worm either forward or backward. This undulatory motion is regulated by a combination of neural activity, proprioceptive feedback, and interactions with the environment. The neural circuits generate and propagate these components to ensure coordinated and efficient movement.

GABAergic neurons are crucial elements within these neural circuits, providing inhibitory signals that modulate locomotor patterns. Two main classes of GABAergic motoneurons, the DD and VD neurons, play significant roles in this process. The DD neurons have cell bodies in the ventral nerve cord, with their dendrites positioned ventrally and their neuromuscular junctions dorsally. They inhibit the dorsal muscles, facilitating the alternation between muscle contraction and relaxation necessary for locomotion. Conversely, VD neurons, also located in the ventral nerve cord, have dorsal dendrites and ventral neuromuscular junctions, and they inhibit the ventral muscles. This arrangement ensures that muscle contractions on opposite sides of the body are properly coordinated (Gjorgjieva et al., 2014)

The primary function of GABAergic neurons in locomotion is to provide cross-inhibition between the dorsal and ventral muscle groups. This cross-inhibition is essential for generating the alternating contraction and relaxation patterns that produce the characteristic sinusoidal movement of *C. elegans*. During forward locomotion, cholinergic motoneurons excite muscles on one side of the body while GABAergic motoneurons inhibit muscles on the opposite side, ensuring smooth and coordinated undulations. A similar mechanism occurs during backward locomotion but involves different sets of neurons responsible for excitation and inhibition (Gjorgjieva et al., 2014)

In addition to their roles in muscle inhibition, GABAergic neurons are part of a broader system that integrates sensory feedback to modulate locomotor output. Proprioceptive feedback from stretches receptors and mechanosensory neurons provides critical information about body

posture and environmental interactions. This sensory feedback allows the nervous system to adjust muscle activity in response to external stimuli, ensuring that locomotor patterns are adaptable to varying mechanical loads and environmental conditions (Gjorgjieva et al., 2014). This integration of sensory input with neural circuit activity enables *C. elegans* to navigate through its environment effectively.

When *C. elegans* transitions to a liquid environment, its sensory neurons detect the change in viscosity and texture, prompting a behavioral shift. The worm adopts a C-shaped swimming motion, which is more suited for movement in fluid mediums. This transition is mediated by the neurotransmitter serotonin, which modulates the activity of motor neurons to produce the swimming pattern. Conversely, the crawling movement on solid ground is recognized by sensory neurons and induced via the neurotransmitter dopamine. This intricate regulation ensures that *C. elegans* can effectively navigate and adapt to varying environmental conditions, showcasing the versatility and efficiency of its nervous system (Goodman, 2006; Vidal-Gadea et al., 2011).

The relationship between neural circuits, GABAergic neurons, and locomotion in *C. elegans* is one of complex coordination and modulation. GABAergic neurons deliver essential inhibitory signals that balance the excitatory inputs from cholinergic motoneurons, facilitating smooth and controlled movements. The incorporation of sensory feedback further refines this process, allowing *C. elegans* to adapt its locomotion to different environmental challenges such as pollutants.

1.3 Protein homeostasis and the formation of protein aggregates

The precise regulatory mechanisms of neural circuits and GABAergic neurons that facilitate proper locomotion are paralleled by the critical role of protein homeostasis in maintaining neural function. The maintenance of proteostasis, or protein homeostasis, is crucial for cellular function and is primarily regulated by molecular chaperones and intracellular proteolytic systems, such as autophagy and the ubiquitin-proteasome system (UPS) (Kaushik & Cuervo, 2015). Molecular chaperones play a vital role in assisting newly synthesized proteins to fold correctly, preventing the aggregation of misfolded proteins inside cells. Essentially, chaperones either help cellular unfolded proteins refold into their stable conformations or promote their degradation, depending on the nature of the extracellular stressors present (Finka et al., 2016).

Heat-shock proteins (HSPs) are a well-known class of molecular chaperones that are significant in maintaining proteome balance (Schopf et al., 2017). These proteins facilitate conformational

changes and support the folding of client proteins, often requiring ATP and the assistance of small heat-shock proteins (sHSPs) (Kaushik & Cuervo, 2015). During stressful conditions, such as elevated temperatures, HSPs are upregulated to protect cells from proteotoxic stress by stabilizing unfolded or misfolded proteins and preventing their aggregation. A visual representation of the proteostasis network is shown in Figure 5.

As organisms age, several alterations, such as a decline in mitochondrial function and decreased metabolic efficiency, limit ATP production. Consequently, the ability of chaperones to recognize and refold unfolded proteins diminishes with age (Hartl, 2017; Soares et al., 2019) leading to an accumulation of misfolded proteins within cells. This accumulation can cause cellular dysfunction and contribute to age-related diseases.

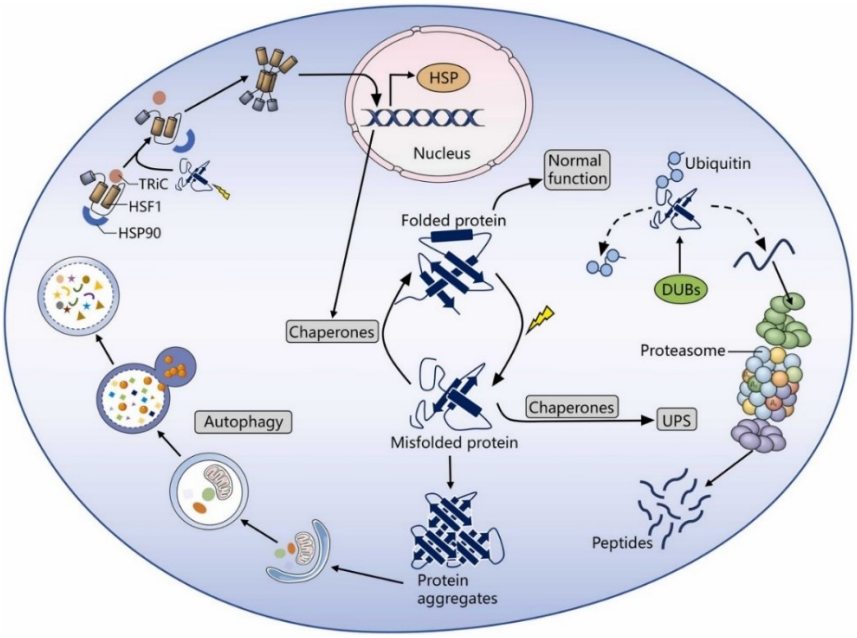

Figure 5. Overview of proteostasis network components and protein quality control implemented by the proteostasis network. (Ma et al., 2023)

Besides molecular chaperones, proteolytic systems are essential for maintaining protein balance within cells. Two main systems, autophagy and proteasome activity, are responsible for clearing damaged and misfolded proteins. Autophagy is a catabolic process that allows the orderly degradation and recycling of dysfunctional proteins and aging organelles. Moderate autophagy

acts as an adaptive response to stress, promoting cellular homeostasis and survival (Carroll et al., 2018).

The ubiquitin-proteasome system (UPS) is a key proteolytic mechanism in mammalian cells. It facilitates protein degradation through a series of steps: attaching ubiquitin molecules to substrate proteins and then breaking them down through proteolytic cleavage by the proteasome. This system plays a crucial role in maintaining protein quality control, responding to cellular stress, and the aging process. As organisms age, proteasome activity decreases, diminishing the UPS's ability to eliminate abnormal, denatured, and damaged proteins (Ma et al., 2023)

Proteins are more prone to transitioning into an insoluble, aggregated state when their cellular abundance surpass normal thresholds or when there are imbalances between the subunits of oligomeric complexes (Vendruscolo et al., 2011; Chiti and Dobson, 2017). This tendency becomes more common with age, as demonstrated in the nematode *C. elegans* (Walther et al., 2015)

Most resulting aggregates are amorphous and lack long-range structural organization, but a subset of smaller proteins often contains unstructured regions (Dunker et al., 2008). These smaller proteins are capable of forming ordered fibrillar aggregates. These aggregates, referred to as amyloid or amyloid-like, are defined by β-strands that align perpendicular to the fibril axis, resulting in a cross-β structure (Chiti & Dobson, 2017). Amyloid aggregates lead to the formation of insoluble deposits, which are characteristic of several age-related proteinopathies, such as Alzheimer’s, Parkinson’s, and Huntington’s diseases (Ross & Poirier, 2004).

The connection between protein homeostasis (proteostasis) and neurodegeneration is a central focus in the study of neurodegenerative diseases using *C. elegans* as a model organism. Proteostasis is crucial for maintaining cellular function and viability, particularly within the nervous system. When proteostasis mechanisms fail, it leads to the accumulation of misfolded and aggregated proteins, which is a hallmark of neurodegenerative diseases such as Alzheimer's disease (AD) and Parkinson's disease (PD) (Klaips et al., 2018; Powers et al., 2009). Many cell types show a decrease in UPS activity and autophagy during aging (Hamer et al, 2010; Cuervo and Wong, 2014). It is assumed that this is the reason for general protein aggregation postmitotic cells, such as muscles and neurons, in *C. elegans* and to one predisposition to neurodegenerative diseases (David et al., 2010; Hamer et al., 2010; Walther et al., 2015)

Environmental pollutants, such as heavy metals and nanoparticles, can disrupt proteostasis and accelerate neurodegeneration. Studies have shown that pollutants like mercury and nano silica collapse proteostasis, promoting the aggregation of proteins and advancing neurodegenerative processes in *C. elegans* models. This disruption is evident across various age groups, with pollutants shifting age-related neurodegeneration from older to younger nematodes. Exposure to nano silica has been demonstrated to promote amyloid protein aggregation, intensifying neurodegenerative effects. Anti-amyloid drugs have been found to mitigate these effects, highlighting the importance of maintaining proteostasis in combating pollutant-induced neurodegeneration (Scharf et al., 2016, Scharf et al., 2022)

Aging naturally impacts proteostasis, leading to the accumulation of damaged and aggregated proteins over time (Hipp et al., 2019). This decline in proteostasis is a significant factor in the increased vulnerability to neurodegenerative diseases observed in older individuals. Intrinsic aging is associated with a collapse in proteostasis, which can be exacerbated by exposure to environmental pollutants. Studies have demonstrated widespread proteome remodeling and aggregation in aging *C. elegans*, a process that is accelerated by neurotoxicants like mercury and nano silica (Walther et al., 2015; Scharf et al., 2016; Scharf et al., 2022)

Maintaining proteostasis is linked to resilience against neurodegenerative diseases. Interventions that enhance proteostasis, such as anti-aging and anti-amyloid drugs, have been shown to reduce neurodegeneration and extend lifespan in *C. elegans* models. An anti-amyloid compound ethosuximide has been found to protect against silica nanoparticle-induced neurotoxicity (Scharf et al., 2016). This suggest that proteostasis mechanisms could be a viable strategy to mitigate the impact of neurotoxic pollutants and delay the onset of neurodegenerative diseases.

Additional evidence involves the polyglutamine (polyQ) repeats, which are associated with Huntington's disease (HD). In *C. elegans*, polyQ proteins with extended repeats form aggregates that impair proteostasis and lead to neurodegeneration. Longer polyQ repeats promote protein aggregation and reduce locomotion, mimicking the neurodegenerative process observed in HD (Morley et al., 2002). This model has been used to track the effects of aging and environmental stressors on proteostasis and neurodegeneration. The aggregation of polyQ proteins in neurons disrupts cellular homeostasis, leading to cell death and behavioral deficits. This illustrates the critical role of proteostasis in managing protein aggregation and maintaining neuronal health (Morley et al., 2002; von Mikecz, 2023).

Disruptions in proteostasis, whether due to intrinsic aging or external pollutants, lead to the accumulation of toxic protein aggregates, driving neurodegenerative processes. Enhancing proteostasis mechanisms offers promising pathways to combat neurodegenerative diseases and improve resilience against environmental neurotoxicants (Scharf et al., 2022). This intricate interplay between proteostasis and neurodegeneration underscores the importance of maintaining cellular protein balance to safeguard neural health.

2. AIM OF THE THESIS

Despite the extensive production and use of silica nanoparticles (NPs) in industrial and consumer products, their long-term neurotoxic effects remain poorly understood. While research has mostly explored the acute impacts of silica NPs, particularly on cellular toxicity, there is limited knowledge about their chronic effects on neural systems. The submitted Ph.D. thesis work aims to address this research gap by investigating the long-term effects of silica NPs on the model organism *Caenorhabditis elegans (C. elegans*). The primary objectives are to investigate how silica NPs affect neurodegeneration and behavioral defects over extended periods, from young adult to middle-age, identify vulnerable age groups, and elucidate the molecular mechanisms underlying the observed neurotoxicity.

To achieve these aims, the study first investigates protein homeostasis, or proteostasis, in *C. elegans*, with a specific focus on polyglutamine (polyQ) repeat tract aggregation in body wall muscle cells. This foundational step is crucial for understanding if disruptions in proteostasis contribute to aging and cellular dysfunction.

The next objective is to determine how silica NPs influence protein aggregation in these neurons and to assess the resultant neurodegeneration and behavioral defects. By employing reporter worms expressing fluorescent proteins under specific neuronal promoters, the study aims to provide a detailed analysis of the neurotoxic effects of silica NPs on neurotransmission and motor control.

Proteomic analysis will be investigated to figure out differentially expressed proteins between silica nanoparticle-treated and mock-treated control groups. This analysis aims to elucidate the molecular mechanisms underlying the observed neurotoxicity and to highlight key proteins and pathways disrupted by silica nanoparticle exposure. The objective is to provide insights into the specific cellular processes and genetic networks implicated in the neurodegenerative effects induced by silica NPs.

The study investigates the development and applications of a single-worm tracking platform to automate the quantification of thrashing behavior and swimming tracks in *C. elegans*. This will facilitate the large-scale studies and advancing our understanding of molecular pathways of nanoparticle-induced neurodegeneration.

3. MATERIAL AND METHODS

Devices

Centrifuge Centrifuge 5417R	Eppendorf AG, Hamburg, Germany
Centrifuge Centrifuge 5430R	Eppendorf AG, Hamburg, Germany
Electrophoresis system	Bio-Rad Laboratories, Inc., Hercules, CA, USA
Electronic analytical balance	Sartorius AG, Göttingen, Germany
Friocell incubator	MMM Medcenter Einrichtungen GmbH, Planegg, Germany
Imager Li-Cor Odyssey Fc 2800	Li-Cor Biosciences GmbH, Bad Homburg, Germany
Innova 4200 Incubator Shaker	New Brunswick Scientific, Co., Inc., Enfield, CT, USA
Multimix roller	Renner GmbH, Darmstadt, Germany
PowerPac Universal	Langenselbold, Germany
Precision scale	Sartorius AG, Göttingen, Germany
Safety cabinet Hera Safe KS-12	Kendro Laboratory Products GmbH, Langenselbold, Germany
Shaker Vortex Genie 2	Bender + Hobein AG, Zurich, Switzerland
Sonifier Branson Sonifier 250-CE	G. Heinemann, Schwäbisch Gmünd, Germany
Stereomicroscope Stemi 2000-C	Carl Zeiss AG, Göttingen, Germany
Stereo microscope SMZ18	Nikon, Tokyo, Japan
Thermoblock Techne Dri-Block DB3	INTEGRA Biosciences GmbH, Biebertal, Germany
Thermomixer Comfort	Eppendorf AG, Hamburg, Germany

Consumables

6-well microtiter plates	Greiner-Bio One GmbH, Frickenhausen, Germany
96-well microtiter plates	Greiner-Bio One GmbH, Frickenhausen, Germany
Centrifuge tubes (15 mL and 50 mL)	Sarstedt AG & Co. KG, Nümbrecht, Germany
Cover glasses (thickness no. 1, 22 x 22 mm)	Menzel glasses, Braunschweig, Germany

Cryo tubes (2 mL filling volume)	Sarstedt AG & Co. KG, Nümbrecht, Germany
Nitrocellulose membrane Amersham Protran	Cytiva, Inc., Marlborough, MA, USA
Pasteur pipettes (3.2 mL filling volume)	Carl Roth GmbH & Co. KG, Karlsruhe, Germany
Petri dishes (92 x 16 mm and 150 x 20 mm)	Peter Oehmen GmbH, Essen, Germany
Reaction vessels (various volumes)	Eppendorf AG, Hamburg, Germany
SuperFrost Plus slides	Menzel glasses, Braunschweig, Germany
Whatman blotting paper 3MM CHR	Cytiva, Inc., Marlborough, MA, USA

Chemicals

2-Mercaptoethanol (C_2H_6OS)	Sigma Aldrich GmbH, Steinheim, Germany
5-Fluoro-2'-deoxyuridine (FUdR)	Sigma Aldrich GmbH, Steinheim, Germany
Acrylamide/bis-acrylamide solution (30%)	Sigma Aldrich GmbH, Steinheim, Germany
Agarose ($C_{12}H_{18}O_9$)	Carl Roth GmbH & Co. KG, Karlsruhe, Germany
Ammonium chloride (NH_4Cl)	Sigma Aldrich GmbH, Steinheim, Germany
Ammonium persulfate ($(NH_4)_2S_2O_8$)	Sigma Aldrich GmbH, Steinheim, Germany
Bacto Agar	BD GmbH, Heidelberg, Germany
Bacto Proteose Peptone No. 3	BD GmbH, Heidelberg, Germany
Bacto Yeast Extract	BD GmbH, Heidelberg, Germany
Brilliant blue R250 ($C_{37}H_{34}N_2Na_2O_9S_3$)	Sigma Aldrich GmbH, Steinheim, Germany
Bromophenol blue ($C_{19}H_{10}Br_4O_5S$)	Sigma Aldrich GmbH, Steinheim, Germany
Calcium chloride ($CaCl_2$)	Sigma Aldrich GmbH, Steinheim, Germany
Calcium chloride hexahydrate ($CaCl_2$ x 6 H_2O)	Carl Roth GmbH & Co. KG, Karlsruhe, Germany
Cholesterol ($C_{27}H_{46}O$)	Sigma Aldrich GmbH, Steinheim, Germany
Citric acid monohydrate ($C_6H_8O_7$ x H_2O)	Carl Roth GmbH & Co. KG, Karlsruhe, Germany
Copper (II) sulfate pentahydrate ($CuSO_4$ x 5 H_2O)	Sigma Aldrich GmbH, Steinheim, Germany

Disodium hydrogen phosphate dihydrate (Na_2HPO_4 x 2 H_2O)	Carl Roth GmbH & Co. KG, Karlsruhe, Germany
Disodium salt EDTA ($C_{10}H_{14}N_2Na_2O_8$)	Carl Roth GmbH & Co. KG, Karlsruhe, Germany
Double distilled water (ddH_2O)	N/A
Dipotassium hydrogen phosphate (K_2HPO_4)	Carl Roth GmbH & Co. KG, Karlsruhe, Germany
Ethanol pure ÿ 99.5% (EtOH)	Sigma Aldrich GmbH, Steinheim, Germany
ECL System Amersham	Cytiva, Inc., Marlborough, MA, USA
Fat-free milk powder	Sigma Aldrich GmbH, Steinheim, Germany
Formaldehyde (CH_2O 37%)	Sigma Aldrich GmbH, Steinheim, Germany
Fungizone (Amphotericin B)	Sigma Aldrich GmbH, Steinheim, Germany
Glycerol ($C_3H_8O_3$)	Carl Roth GmbH & Co. KG, Karlsruhe, Germany
Glycine ($C_2H_5NO_2$)	Carl Roth GmbH & Co. KG, Karlsruhe, Germany
Iron(II) sulfate heptahydrate ($FeSO_4$ x 7 H_2O)	Carl Roth GmbH & Co. KG, Karlsruhe, Germany
LB medium (Luria/Miller)	Carl Roth GmbH & Co. KG, Karlsruhe, Germany
Magnesium sulfate, anhydrous ($MgSO_4$)	Carl Roth GmbH & Co. KG, Karlsruhe, Germany
Magnesium sulfate heptahydrate ($MgSO_4$ x 7 H_2O)	Sigma Aldrich GmbH, Steinheim, Germany
Manganese(II) chloride tetrahydrate ($MnCl_2$ x 4 H_2O)	Carl Roth GmbH & Co. KG, Karlsruhe, Germany
N,N,N',N'-Tetramethylethylenediamine (TEMED) ($C_6H_{16}N_2$)	Sigma Aldrich GmbH, Steinheim, Germany
Polysorbate 20 (Tween 20) ($C_{58}H_{114}O_{26}$)	Sigma Aldrich GmbH, Steinheim, Germany
Ponceau S ($C_{22}H_{12}N_4Na_4O_{13}S_4$)	Sigma Aldrich GmbH, Steinheim, Germany

Potassium chloride (KCl)	Carl Roth GmbH & Co. KG, Karlsruhe, Germany
Potassium dihydrogen phosphate (KH_2PO_4)	Carl Roth GmbH & Co. KG, Karlsruhe, Germany
Protein marker Precision Plus Protein Kaleidoscope Prestained Protein Standards	Bio-Rad Laboratories, Inc., Hercules, CA, USA
Serotonin hydrochloride	Sigma Aldrich GmbH, Steinheim, Germany
Silver nitrate ($AgNO_3$)	Sigma Aldrich GmbH, Steinheim, Germany
Sodium acetate (CH_3COONa)	Sigma Aldrich GmbH, Steinheim, Germany
Sodium azide (NaN_3)	Sigma Aldrich GmbH, Steinheim, Germany
Sodium chloride (NaCl)	Carl Roth GmbH & Co. KG, Karlsruhe, Germany
Sodium carbonate ($CaCO_3$)	Sigma Aldrich GmbH, Steinheim, Germany
Sodium dodecyl sulfate ($C_{12}H_{25}NaO_4S$)	Sigma Aldrich GmbH, Steinheim, Germany
Sodium hydroxide (NaOH)	Carl Roth GmbH & Co. KG, Karlsruhe, Germany
Sodium thiosulfate ($Na_2S_2O_3$.$5H_2O$)	Sigma Aldrich GmbH, Steinheim, Germany
Sodium hypochlorite solution (NaClO in H_2O, 12% Cl)	Carl Roth GmbH & Co. KG, Karlsruhe, Germany
Sodium hydrogen phosphate dihydrate (Na_2HPO_4 x 2 H_2O)	Sigma Aldrich GmbH, Steinheim, Germany
Silicon dioxide AEROSIL 90 (SiO_2) (diameter 20 nm)	Evonik Industries AG, Hanau, Germany
Silicon dioxide AEROSIL 200 (SiO_2) (diameter 12 nm)	Evonik Industries AG, Hanau, Germany
Silicon dioxide BULK (SiO_2) (diameter 500 nm)	Kisker Biotech GmbH & Co. KG, Steinfurt, Germany
Silicon dioxide, monodisperse (SiO_2) (diameter 50 nm)	Kisker Biotech GmbH & Co. KG, Steinfurt, Germany
Thiacloprid (THI)	Sigma Aldrich GmbH, Steinheim, Germany

Thiamethoxam (TMX)	Sigma Aldrich GmbH, Steinheim, Germany
Tris hydrochloride ($NH_2C(CH_2OH)_3$ x HCl)	Sigma Aldrich GmbH, Steinheim, Germany
Tris(hydroxymethyl)aminomethane (Trizma Base) ($C_4H_{11}NO_3$)	Sigma Aldrich GmbH, Steinheim, Germany
Tripotassium citrate monohydrate ($C_6H_5K_3O_7$ x H_2O)	Sigma Aldrich GmbH, Steinheim, Germany
Zinc(II) sulfate heptahydrate ($ZnSO_4$ x 7 H_2O)	Sigma Aldrich GmbH, Steinheim, Germany

Solutions and buffers

Nematode Growth Medium (NGM) for agar plates

Bacto Agar	15 g
NaCl	2.25 g
Bacto Proteose Peptone No. 3	1.9 g
Bacto Yeast Extract	3.75 g

Fill with 750 mL ddH_2O and autoclave the solution. Then heat to below 55°C. Allow them to cool, then add the solutions A, B, C and D.

Solution A

Cholesterol	0.5 g

Dissolve in 100 mL EtOH.

Solution B

$CaCl_2$	11.08 g

Dissolve in 100 mL ddH_2O and autoclave.

Solution C

$MgSO_4$ x 7 H_2O	24.65 g

Dissolve in 100 mL ddH_2O and autoclave.

Solution D

KH_2PO_4	108.3 g

K_2HPO_4	36 g

Dissolve in 1000 mL ddH_2O and autoclave.

M9 buffer

KH_2PO_4	3.0 g
Na_2HPO_4 x 2 H_2O	7.52 g
NaCl	0.5 g
NH_4Cl	1.0 g

Dissolve in 1000 mL ddH_2O and autoclave.

Bleaching solution

ddH_2O	5 mL
NaClO x H_2O	3 mL
4M NaOH	2 mL

Mix in a 15 mL falcon and use immediately or store for a short time in the dark store

LB medium

LB medium (Luria/Miller)	25 g

Dissolve in 1000 mL ddH_2O and autoclave.

S-Medium

S-Basal	0.5 L
1M potassium citrate pH 6.0	5 mL
Trace Metals Solution	5 mL
1M calcium chloride	1.5 mL
1M Magnesium sulfate	1.5 mL
Solution A	0.5 mL
Fungizone (250 µg/ mL stock solution)	205 µL

Basal

NaCl	5.85 g
K_2HPO_4	1.0 g
KH_2PO_4	6.0 g

Dissolve in 1 L ddH_2O and autoclave.

1M potassium citrate pH 6.0

$C_6H_8O_7$ x H_2O	20 g
$C_6H_5K_3O_7$ x H_2O	293.5 g

Dissolve in 1 L ddH_2O and check the pH value, if necessary, adjust to pH 6.0. Then autoclave the solution.

Trace Metals Solution

Disodium salt EDTA	1.86 g
$FeSO_4$ x 7 H_2O	0.69 g
$MnCl_2$ x 4 H_2O	0.2 g
$ZnSO_4$ x 7 H_2O	0.29 g
$CuSO_4$ x 5 H_2O	0.025 g

Dissolve in 1 L ddH_2O and autoclave. Store the solution in a cool, dark place.

1M $CaCl_2$

$CaCl_2$ x 6 H_2O	54 g

Dissolve in 200 mL ddH_2O and autoclave.

1M $MgSO_4$

$MgSO_4$ (anhydrous)	120.4 g

Dissolve in 1 L ddH_2O and autoclave.

Fungicide “Fungizone”

Stock solution	250 µg / mL
Final concentration	0.1 µg / mL
Volume to be pipetted	205 µL

Sodium azide 10%

Agarose	50 mg
100mM NaN3	100 µL
ddH2O	900 µL

Place in 2 mL reaction tubes and heat at 96°C until everything is dissolved. Then cool and store at room temperature.

Silver staining

Solution A:

Ethanol	25 mL
Acetic acid	5 mL

Dissolve in 40 mL ddH2O and fill it up to 50 mL.

Solution B:

Ethanol	15 mL
Sodium acetate	2.05 g
Sodium thiosulfate (5H2O)	0.1 g

Dissolve in 40 mL ddH2O and fill it up to 50 mL.

Solution C:

Silver nitrate	0.05 g

Dissolve in 40 mL ddH2O and fill it up to 50 mL.

Solution D:

Sodium carbonate	1.25 g

Dissolve in 40 mL ddH2O and fill it up to 50 mL.

Solution E:

Sodium carbonate	1.25 g
Formaldehyde (37%)	14.4 µL

Dissolve in 40 mL ddH2O and fill it up to 50 mL.

Solution F:

EDTA

Dissolve in 40 mL ddH2O and fill it up to 50 mL.

SDS-PAGE

10% sodium dodecyl sulfate

SDS	25 g

Dissolve in 150 mL ddH2O and then measure the pH value, if necessary to pH 7.2. Then fill up to 250 mL and store at room temperature.

2 M sodium chloride

NaCl	11.69 g

Dissolve in 100 mL ddH2O and autoclave.

1 M or 0.5 M Tris-HCl

Tris-HCl	15.76 g (1 M) or 7.88 g (0.5 M)

Dissolve in 50 mL ddH2O and then measure the pH value, if necessary, adjust to pH 8.0 (1M) or pH 6.8 (0.5M). Then fill up to 100 mL and autoclave.

10% Bromophenol blue

Bromophenol blue	0.1 g

Dissolve in 1 mL ddH2O and store at -20°C.

Ammonium persulfate

APS	10 g

Dissolve in 100 mL ddH2O and aliquot into 600 µL reaction tubes, then store at -20°C.

SDS lysis buffer

2 M NaCl	3.75 mL
1 M Tris-HCl pH 8.0	0.5 mL
10% SDS pH 7.2	10 mL
ddH2O	35.75 mL

Mix in a 50 mL falcon and use immediately or store for a short time. Store at room temperature.

2x loading buffer

ddH2O	4.2 mL
0.5 M Tris-HCl pH 6.8	1 mL
Glycerin	0.8 mL
10% SDS pH 7.2	1.6 mL

2-Mercaptoethanol	0.4 mL
10% Bromophenol blue	20 µL

Aliquot into 1 mL reaction tubes and store at -20°C in the dark.

Resolving gel buffer

Trizma Base	90.8 g
SDS	2 g

Dissolve in 900 mL ddH2O and then measure the pH value, if necessary to pH 8.8. Then fill up to 1000 mL and store at room temperature.

Stacking gel buffer

Trizma Base	30.3 g
SDS	2 g

Dissolve in 900 mL ddH2O and then measure the pH value, if necessary to pH 6.8. Then fill up to 1000 mL and store at room temperature.

Resolving gel 12%

ddH2O	2 mL
Separating gel buffer	9 mL
Acrylamide/bis-acrylamide 30%	7.5 mL
APS	180 µL
TEMED	36 µL

Mix continuously during preparation and use immediately.

Stacking gel 4%

ddH2O	4 mL
Stacking gel buffer	5 mL
Acrylamide/bis-acrylamide 30%	1.8 mL
APS	100 µL
TEMED	20 µL

Mix continuously during preparation and use immediately.

Running buffer

Trizma Base	3 g
Glycine	14.4 g
10% SDS	10 mL

Dissolve in 1000 mL ddH2O and use immediately.

Coomassie staining solution

Brilliant Blue R250	1.25 g
ddH2O	225 mL
Pure ethanol	225 mL
Acetic acid 100%	50 mL

Mix and store at room temperature.

Destaining solution

Pure ethanol	450 mL
Acetic acid 100%	100 mL
ddH2O	450 mL

Ponceau S staining solution

Ponceau S	5 g
Acetic acid 100%	5 mL

Dissolve in 500 mL ddH2O and store at room temperature.

Preparation of silicon dioxide suspensions

Commercially available stock suspensions of monodisperse silicon dioxide (25 mg/mL) and BULK silicon dioxide (50 mg/mL) are used from Kisker Biotech GmbH & Co. KG. To produce stock suspensions of AEROSIL 90 and AEROSIL 200 (Evonik Industries AG) with a concentration of 25 mg/mL, 125 mg of the respective particles are weighed and 5 mL ddH2O are added. These suspensions are homogenized using the *Branson Sonifier 250-CE* ultrasonic homogenizer for 10

minutes at a duty cycle of 20% and an output control of 1. The mixture is sonicated during the cooled with ice throughout the process. Finally, the suspensions are vortexed before use.

Silicon dioxide, monodisperse 50nm and Silicon dioxide, BULK are synthesized by Stoeber method. AEROSIL 90 (20 nm) and AEROSIL 200 (12 nm) are synthesized by HTFH method (high-temperature flame hydrolysis). Diameters were identified by dynamic light scattering. High-temperature hydrolysis ("", HFTH) (Piechulek et al., 2019 and Limke et al., 2024).

Preparation of Thiacloprid (THI) and Thiamethoxan (TMX) suspensions

THI and TMX were suspended in H_2O and sonicated preceding the experiments with an ultrasonic homogenizer (Branson Sonifier 250-CE, G. Heinemann, Schwabisch Gmünd, Germany). A 50 mM stock solution of inorganic-mercury (I–Hg;i HgCl2; Carl Roth GmbH, Karlsruhe, Germany) was prepared by suspension in H_2O and stored at −20 °C in the dark (Scharpf et al., 2022).

Caenorhabditis elegans Strains

All strains were purchased from Caenorhabditis Genetics Center (University of Minnesota, Minneapolis, MN, USA):

Bristol N2 (wild type);

LX975 vsls97 [tph-1p::DsRed2 + lin-15(+)];

BZ555 egls1 [dat-1p::GFP];

AM140 rmIS132 [unc-54p::Q35::YFP];

EG1285 oxIs12 [unc-47p::GFP + lin-15(+)] and

RW1596 myo-3(st386) V; stEx30 [Pmyo-3::GFP+ rol-6(su1006)].

Particle Exposures in Liquid Media

Nematodes were synchronized by isolating eggs with hypochlorite/NaOH and allowed to hatch on NGM plates at 20 °C. As L4 larvae, animals were transferred to liquid medium (S-medium, pH 5.7 and 0.1 µg/mL fungizone) on 96-well plates with 12mg/mL freshly prepared *E. coli* OP50 [30,40].

For age-resolved experiments, nematodes were supplemented with 5-fluoro-2′-deoxyuridine (FUdR, 1.5 mM final concentration) to maintain synchronization when not stated otherwise. On day 1 of adulthood, worms were mock-treated (H_2O or dispersant) or exposed to nano silica, nano silver or BULK silica at the indicated concentrations. All experiments were performed at 20 °C.

Microscopy and Quantification of Neurodegeneration

Living reporter nematodes were analyzed from young (day 2) to middle age (day 11) on 5% agarose pads with 10 µM NaN3 at room temperature. Neurodegeneration was monitored by epifluorescence microscopy with a 60×/1.4 NA Plan Apo objective (Ix70, Olympus, Tokyo, Japan) in 2- to 11-day-old adult hermaphrodite reporter worms. Discontinuous dotted staining pattern along dendrites, processes and axons in the respective neurons was quantified as beading. Micrographs were taken with a stereo microscope (SMZ18, Nikon Europe B.V., Amsterdam, The Netherlands) with an SHR Plan Apo 2x objective. The reporter DsRed2 was detected with 561 nm excitation/575–615 nm emission. The reporter green fluorescent protein (GFP) was detected with 488 nm excitation/510–550 nm emission. Image processing was performed with the NIS Elements software (NIKON) (https://www.microscope.healthcare.nikon.com/products/software/nis-elements).

Behavior assay

Swimming behavior (%): Methods were as previously described (Piechulek and von Mikecz, 2018). Briefly, the locomotion behavior in liquid S-complete medium was quantified every second day with a stereo microscope in young and old *C. elegans*, e.g. from 2-day-old (young) to 11-day-old (old) worms. 40–65 worms (n) were quantified per condition.

Manual thrashing assay: *C. elegans* were either mock-treated or exposed with silica NPs 200 µg/mL and 625 µg/mL and BULK silica 200 µg/mL in liquid culture. 2-day-old to 11-day-old adult nematodes were transferred from 96-well microplates to 24-well microplates. Swimming behavior in liquid medium was quantified by counting the thrashes of individual worms manually in a time period of 30 seconds (Hering et al., 2022). Swimming was filmed with a NIKON SMZ800 microscope equipped with a DS-Fi2 digital camera. Videos were recorded with NIS Elements Software (NIKON).

Single worm tracking (SWT): Experiment designs and parameters of SWT in this study were developed from the original protocol of Koopman et al., 2020 to fit our current hardware

(microscope NIKON SMZ800) and our experimental settings. In specific, worms were prepared as in 'Particle Exposures in Liquid Media' described above. *C. elegans* were then either mock-treated or exposed with different particles in liquid culture in 96-well-microplates. 2-day-old to 11-day-old adult nematodes were transferred from 96-well-microplates to agar-loaded 6-well-microplates with 2 mL of M9 buffer. Number of thrashes and swimming traces were filmed with 20 fps (frames per second) in 30 seconds with a NIKON SMZ800 microscope equipped with a DS-Fi2 digital camera. Videos were recorded with NIS Elements Software (NIKON) and analyzed by WF-NTP software created by Koopman et al., 2020. Due to our current laboratory settings, parameters of the software such as minimum size, maximum size, px to mm factor, maximum move distance, minimum length, memory, and bend threshold have been adjusted according to the instruction of parameter modifications in the reference paper (Koopman et al., 2020) in order to get the worms in the recorded videos recognized and tracked by the software properly. Various tracking patterns of individual worms and number of thrashes were then generated by the automated system.

Sample Preparation for Proteomic Analysis

GABAergic reporter *C. elegans* (strain EG1285) were transferred as larval stage L4 to 6-well plates containing liquid medium, 20 mg/mL *E. coli* OP50, and FUdR (1.5 mM final concentration) to maintain age- synchronization. On day 1 of adulthood, nematodes were either mock-exposed (H_2O) or exposed to 200 µg/mL silica NPs. Seventy-two hours after exposure, the worms in each group were collected in cryotubes and stored in liquid nitrogen. Six independent experiments were conducted with 8,000–12,000 worms per condition per experiment.

SDS PAGE and mass spectrometry

GABAergic reporter *C. elegans* (strain EG1285) were transferred as larval stage L4 to 6-well plates containing liquid medium, 20 mg/mL *E. coli* OP50, and FUdR (1.5 mM final concentration) to maintain age- synchronization. On day 1 of adulthood, nematodes were either mock-exposed (H_2O) or exposed to 200 µg/mL silica NPs. Seventy-two hours after exposure, the worms were collected and lysed. Total proteins were separated according to molecular weight by SDS-PAGE and visualized using silver staining. A specific band was excised and analyzed by mass spectrometry at the Quantitative Proteomics Lab (Biological-Medical Research Center, BMFZ, Heinrich-Heine-University, Duesseldorf). Protein samples were prepared for mass spectrometric analysis by in-gel digestion, essentially as described by Brenig at al. (2020). Briefly, 5 µg of protein

per sample was loaded into 4–12% Bis(2-hydroxyethyl) amino-tris(hydroxymethyl) methanpolyacrylamide gels (Novex NuPAGE, Thermo Fisher Scientific) and stained with Coomassie Brilliant Blue. Protein-containing bands were further processed for mass spectrometric analysis by reduction with dithiothreitol, alkylation of cysteine residues with iodoacetamide and digestion with trypsin in ammonium bicarbonate solution. Finally, peptides were extracted from the gel pieces and vacuum dried, and 500 ng was prepared in 0.1% (v/v) trifluoroacetic acid in water for mass spectrometric analysis.

Statistical Analyses

Data are presented as mean ± SD from at least three independent biological replicates, unless stated otherwise. Violin plots, bar graphs and line graphs were created in OriginPro 2022 (Origin Lab Corporation). Normality was determined by Shapiro- Wilk test. Depending on the normality distribution of the data, statistical differences were determined using Kruskal–Wallis test with Dunn's post hoc test or one-way ANOVA with Tukey's post hoc test. Statistical analyses were performed in OriginPro (2022) (Origin Lab Corporation). P values of <0.05 were considered statistically significant (*, $p < 0.05$; **, $p < 0.01$; ***, $p < 0.001$, ****, $p < 0.0001$).

4. RESULTS

Proteostasis is a critical cellular process responsible for ensuring the proper synthesis, folding, and degradation of proteins, thereby maintaining cellular function and health. Disruptions in proteostasis can lead to protein aggregation, a hallmark of many age-related diseases and a key indicator of neurodegeneration in *C. elegans*. These protein aggregates are often composed of misfolded proteins that accumulate over time, impairing cellular functions and contributing to the decline in neural integrity. To show that silica NPs induce protein aggregation in *C. elegans*, reporter worms for polyglutamine (polyQ) repeat tracts in body wall muscle cells were used.

Protein aggregation of polyglutamine repeat tracts in body wall muscle cells

To investigate the protein aggregation of polyglutamine (polyQ) in *C. elegans*, reporter worms expressing a homopolymeric glutamine repeat fused to yellow fluorescent protein (Q35::YFP) under the control of the unc-54 promoter in the body wall muscle cells were utilized. In one-day-old worms (Figure 6A), no visible aggregation was detected, as indicated by the smooth, continuous fluorescence along the muscle cells. By day three (Figure 6B), the onset of aggregation became apparent, and particularly concentrated in the head and tail regions, with initial signs of fluorescent foci formation. In four-day-old worms (Figure 6C), aggregation was extensive and widespread throughout the entire length of the muscle cells, with numerous distinct fluorescent aggregates clearly visible. These findings suggest that protein aggregation may serve as an indicator of proteolytic stress intrinsic aging in polyQ reporter worms. Following the identification of these three distinct phenotypes, their quantification was subsequently conducted (Figure 7).

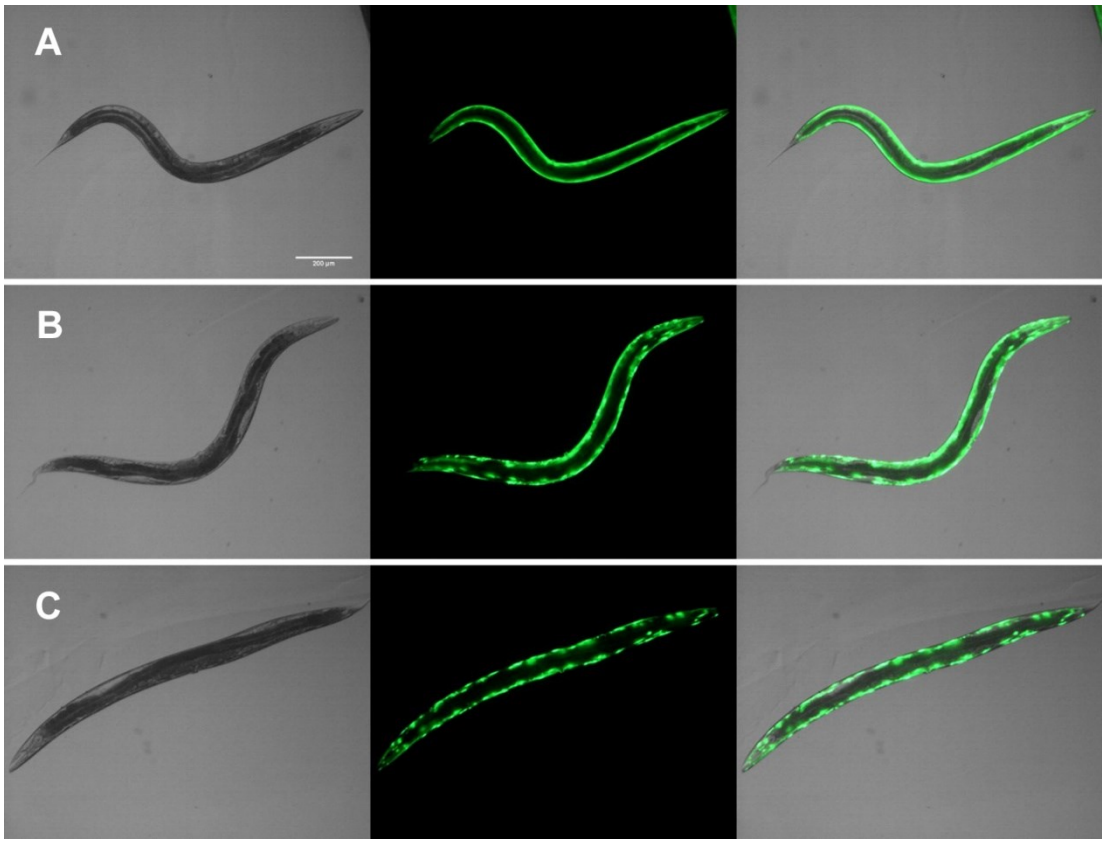

Figure 6. Different phenotypes of protein aggregation in polyQ35 reporter *C. elegans.*

There were three phenotypes of protein aggregation: (A) no aggregation in one-day-old worms, (B) head/tail aggregation in three-day-old worms, and (C) complete aggregation in four-day-old worms. Representative DIC (left), fluorescent (center) and merging DIC-fluorescent (right) micrographs of adult *C. elegans* stably expressing a homopolymeric glutamine repeat fused to yellow fluorescent protein (Q35::YFP) under the control of the *unc-54* promoter in the body wall muscle cells. Bar 200 µm.

The quantification of protein aggregation phenotypes revealed an increasing number of worms exhibiting polyQ aggregation in body wall muscle cells during aging. In fact, the percentage of worms with no aggregation decreases from nearly 100% on day two to approximately 90% on day three, and ultimately reaches 0% in four-day-old *C. elegans* (Figure 7A). No worms exhibited aggregation in the head/tail region on day two (Figure 7B); however, by day three, this number increased to 60% ($p < 0.0001$) before declining to around 10% by day four. The percentage of worms showing complete aggregation increased significantly from 0% on day two to nearly 100% by day four (Figure 7C), indicating that all worms initially showing head/tail aggregation progressed to complete aggregation by day four. The combined graph consolidates these changing trends (Figure 7D), highlighting the sharp decline in worms with no aggregation and the corresponding

rise in complete aggregation. These results underscore the progressive nature of polyQ aggregation in *C. elegans*, correlating with aging and the decline in proteostasis.

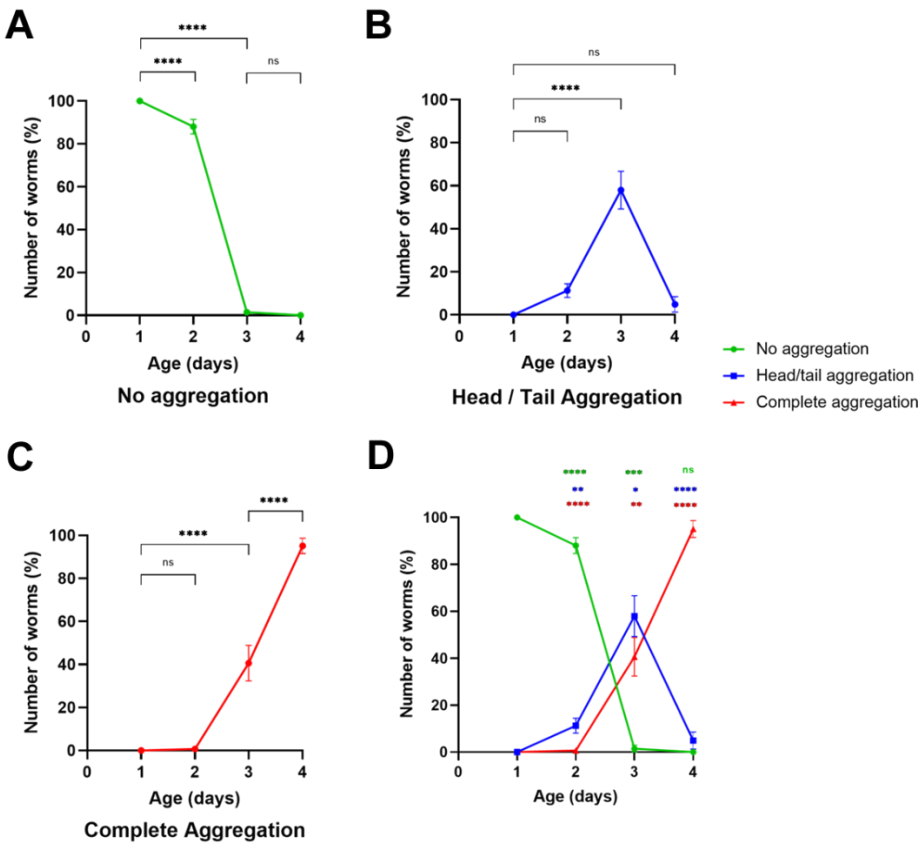

Figure 7. Quantification of protein aggregation phenotypes in 2-day-old to 4-day-old PolyQ35 reporter *C. elegans*.

Worms were fed live *E. coli* OP50 and grown on agar plates at 20°C. Protein aggregation phenotypes of nematodes were classified according to the three categories described in Figure 6. Values represent means ± SD from three independent experiments with n = 65-101 per group per experiment (one way ANOVA with Tukey's post-hoc test $p < 0.05$). *, $p<0.05$; ** $p<0.01$, *** $p<0.001$, **** $p<0.0001$

These observations raised questions regarding the relationship between protein aggregation and neurodegeneration in *C. elegans*. The vulnerability of neuronal cells, to protein aggregation remained an open question that necessitates further investigation. To address this, the subsequent steps involved analyzing the effects of silica NPs on neurons that using common neurotransmitters such as serotonin, dopamine, and GABA in young worms (two-day-old) to middle age worms (11-day-old), and quantification of the related neural behaviors across these age groups.

4.1 Silica NPs accelerated protein aggregation in serotonergic, dopaminergic and GABAergic neurons as well as neuromuscular defects in young and middle-aged worms.

To investigate the effects of silica NPs on serotonergic neurons, reporter worms expressing the reporter protein DsRed2 under the control of the tryptophan hydroxylase (*tph-1*) promoter in serotonergic neurons were either left untreated (H_2O) or exposed to silica NPs 50 nm or BULK silica (500 nm). In control worms, the serotonergic neurons ADF, NSM, and HSN exhibited a healthy morphology, characterized by a continuous and elongated fluorescence pattern. In contrast, worms exposed to silica NPs displayed a fragmented, punctate fluorescence pattern in these neurons, indicative of neurodegeneration (Figure 8A, 8B and 8C).

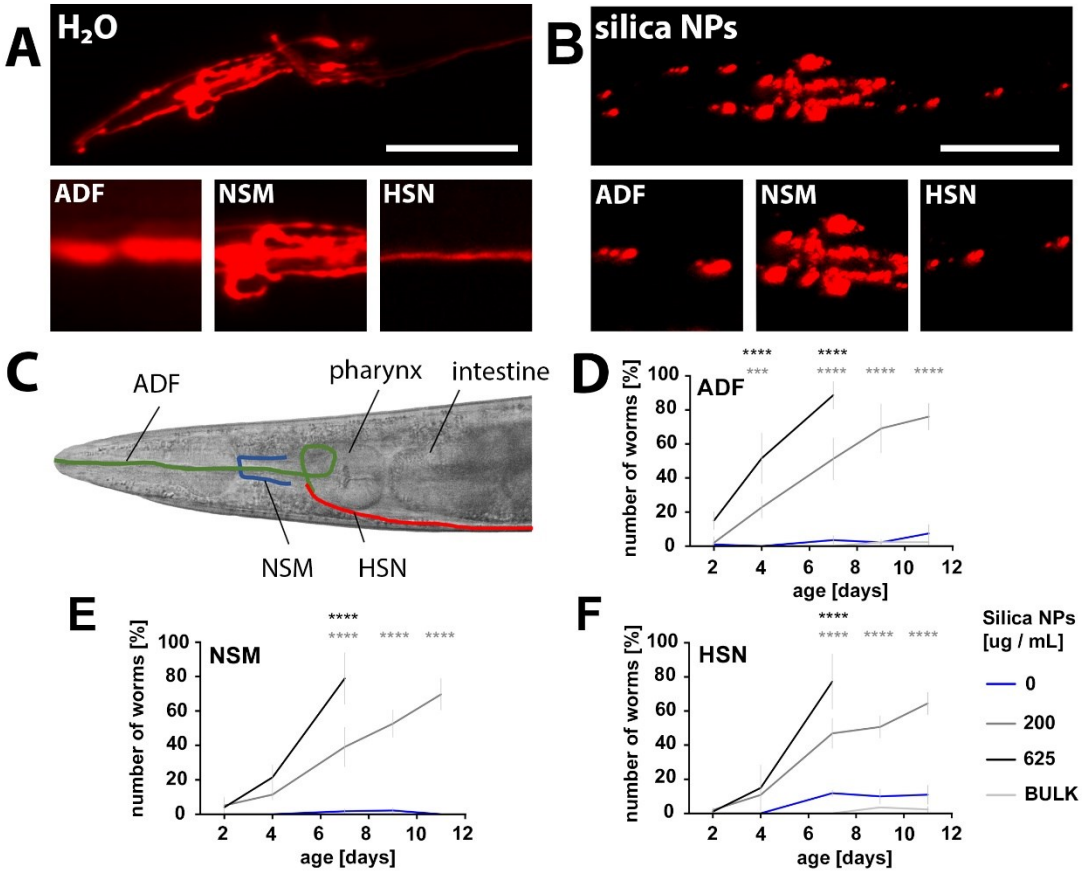

Figure 8. Neurodegeneration in serotonergic neurons of *C. elegans* exposed to silica nanoparticles.
Representative fluorescent micrographs of nine-day-old adult *C. elegans* stably expressing DsRed2 under the control of tryptophan hydroxylase (*tph-1*) in serotonergic neurons. Reporter worms were mock-treated (H_2O) (A) or exposed to 200 µg/mL Silica NPs (B) at 20 °C. The insets show blow-ups of the ADF, NSM and the HSN neurons. A discontinuous punctate fluorescence pattern was categorized as neurodegeneration. (C) Schematic representation of an adult *C.*

elegans illustrating the locations of serotonergic neurons ADF (green), NSM (blue), and HSN (red). (D-F) Quantification of neurodegeneration in two- to eleven-day-old worms that either were mock-exposed or exposed to 200 µg/mL or 650 µg/mL silica NPs, or 200 µg/mL BULK silica. Values represent means ± SD from three independent experiments with n = 27–70 nematodes per condition per experiment (one-way ANOVA with Tukey's post hoc test). Scale bars, 50 µm. *, $p < 0.05$; **, $p < 0.01$; ***, $p < 0.001$; ****, $p < 0.0001$; BULK, Bulk silica (500 nm); SD, standard deviation

However, after 72 hours of exposure, while there was no significant aggregation in NSM and HSN neurons (Figure 8E and Figure 8F) compared to control worms, a significant increase in aggregation ($p<0.001$) was observed in ADF neurons, with approximately 20% of worms treated with 200 µg/mL showing aggregation (Figure 8D). The ADF neurons demonstrated the highest susceptibility to silica NP-induced neurotoxicity. From 7 days old onwards, worms exhibited aggregation in all serotonergic neurons, and by 11 days old, aggregation in ADF neurons reached nearly 80%, while HSN neurons showed about 60% aggregation. At the highest concentration of 625 µg/mL, the worms did not survive beyond day 9. Across all three neuron types, exposure to silica NPs significantly accelerated age-dependent neurodegeneration compared to the control group. Additionally, the study included a dose-response analysis, demonstrating that higher concentrations of silica NPs (625 µg/mL) exacerbated neurodegeneration, thereby strengthening the causal link between silica NP exposure and neuronal damage in *C. elegans*.

Silica NPs - induced neurodegeneration has been observed by protein aggregation in serotonergic reporter worms. However, the connection between neurodegeneration and behavioral defects remained unclear. To investigate the behavioral defects induced by silica NPs, we analyzed the swimming behavior e.g. thrashing rate per 30 seconds.

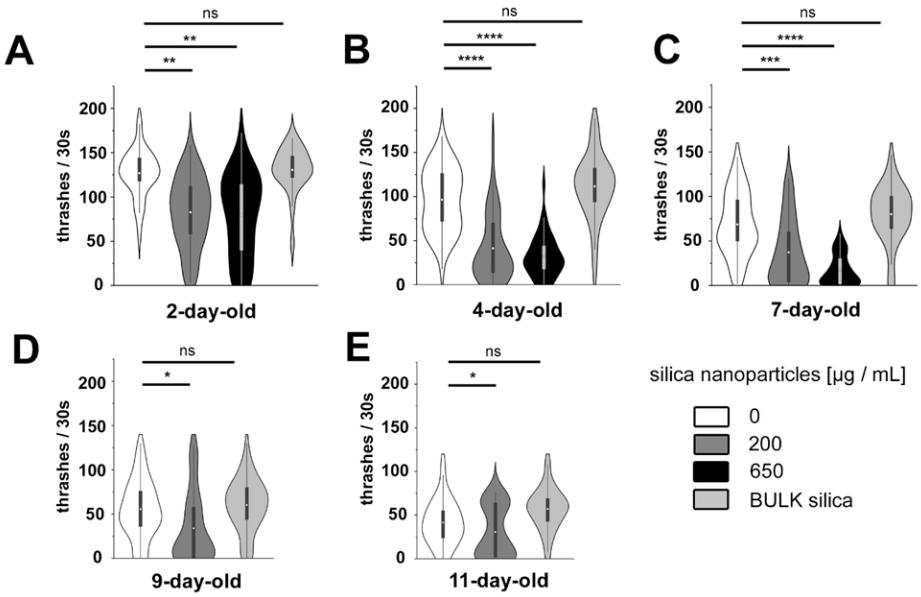

Figure 9. Silica nanoparticles accelerated neuromuscular defects in serotonergic reporter *C. elegans*.
(A–E) Serotonergic reporter worms were cultured at 20 °C and fed with *E. coli* OP50. Locomotion fitness was quantified in 2- to 11-day-old worms that were either mock-treated (distilled water), 200 µg/mL silica NPs, 650 µg/mL or BULK silica. (A–E) Violin plots represent means ± SD from three independent experiments with n = 15 worms per condition per experiment. *, $p < 0.05$; **, $p < 0.01$; ***, $p < 0.001$; °C, degree Celsius; ns, not significant; s, seconds; SD, standard deviation.

The study conducted a detailed analysis of the neuromuscular effects of silica NPs on *C. elegans* across different age-groups and concentrations, revealing significant dose-dependent and age-dependent impacts on locomotion fitness. After the first 24-hour exposure, the untreated control group displayed a mean thrashing rate of approximately 132 thrashes per 30 seconds, indicating robust neuromuscular activity (Figure 9A). Upon exposure to 200 µg/mL silica NPs, there was a significant reduction in thrashing rate to about 106 thrashes ($p < 0.01$). This reduction became more pronounced at 650 µg/mL, with a frequency around 80 thrashes per 30 seconds ($p < 0.01$). In contrast, BULK silica exposure resulted in only a slight, insignificant reduction, highlighting the specific neurotoxic effects of silica NPs.

From the age of 4 days onwards, all groups, including both the mock control and treated groups, exhibited a reduction in thrashing rates, reflecting a natural decline in neuromuscular activity with age (Figure 9B-E). However, exposure to 625 µg/mL silica NPs resulted in the most significant reduction in thrashing rate compared to both the 200 µg/mL silica NP group and the mock control group ($p < 0.001$), with average thrashing rates of 32, 41, and 96 thrashes per 30 seconds, respectively. This indicated that the effects on neuromuscular activity were dose-dependent.

Although the untreated middle-aged (11-day-old) worms exhibited a remarkably low thrashing rate (approximately 41 thrashes per 30 seconds) compared to young 2-day-old worms (131 thrashes), they still maintained a significantly higher thrashing rate compared to the 200 µg/mL silica NP-treated worms at the same age, which had a mean thrashing rate of 31 thrashes per 30 seconds ($p < 0.05$).

Overall, these results demonstrated that silica NPs induce a clear dose-dependent and age-dependent decline in both serotonergic neurons and neuromuscular fitness in *C. elegans*. Young worms exhibited significant reductions in thrashing rates even at lower concentrations of silica NPs (200 µg/mL), whereas this effect was less pronounced in middle-aged worms. The heightened vulnerability of young worms (2-day-old) to silica NP-induced neurotoxicity underscores the substantial impact of nanoparticulate silica on protein aggregation in neurotransmission, and neuromuscular health. Thus, the investigation was expanded to include dopamine, another common neurotransmitter involved in numerous behavioral processes in worms.

Silica NPs accelerated protein aggregation in dopaminergic neurons and induced neuromuscular defects

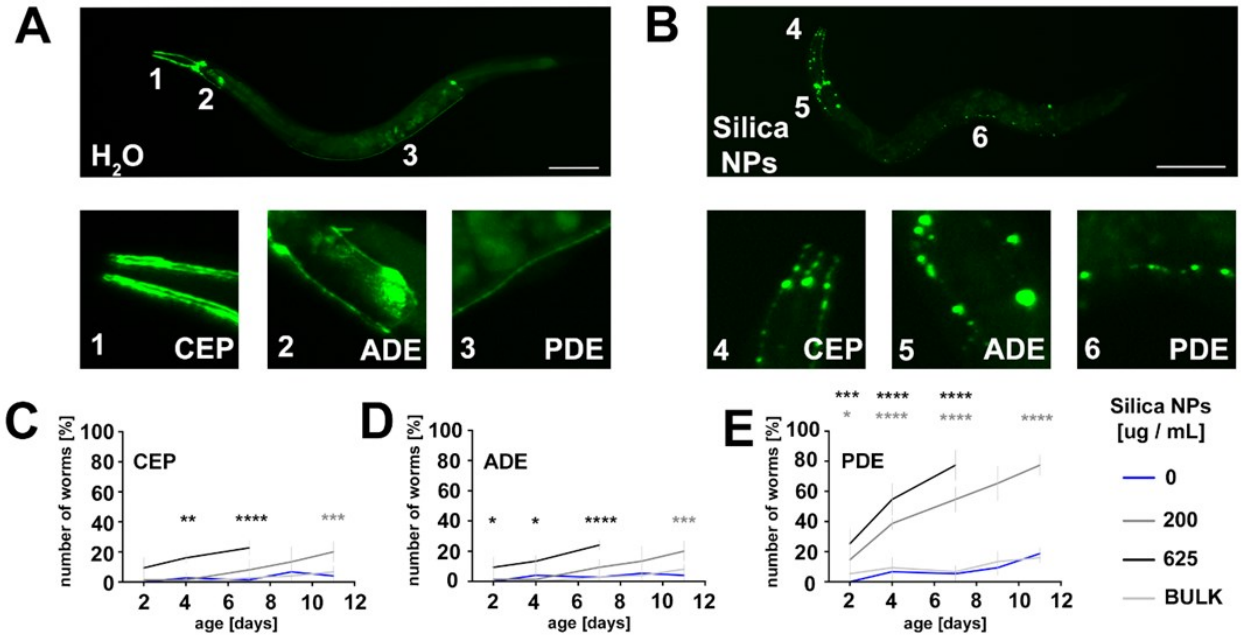

Figure 10. Neurodegeneration in dopaminergic neurons of *C. elegans* exposed to silica nanoparticles. Representative fluorescent micrographs of 9-day-old adult *C. elegans* stably expressing green fluorescent protein (GFP) under the control of the dopamine transporter (*dat-1*) promoter in dopaminergic neurons. Reporter worms were mock-treated (H_2O) (A) or exposed to 200 µg/mL silica NPs (B) at 20 °C. The insets show blow-ups of the CEP, ADE, and

PDE. A discontinuous punctate fluorescence pattern was categorized as neurodegeneration. (C-E) Quantification of neurodegeneration in 2- to 11-day-old worms that were either mock-exposed or exposed to 200 µg/mL 650 µg/mL silica NPs, or 200 µg/mL BULK silica. Values represent means ± SD from three independent experiments with n = 25-30 nematodes per condition per experiment (one-way ANOVA with Tukey's post hoc test). Scale bars, 50 µm. *, $p < 0.05$; **, $p < 0.01$; ***, $p < 0.001$; ****, $p < 0.0001$. SD, standard deviation.

To examine the impact of silica NPs on dopaminergic neurons, reporter worms expressing green fluorescent protein (GFP) under the control of the dopamine transporter (*dat-1*) promoter specifically in their dopaminergic neurons were investigated. These worms were either left untreated (H_2O) or exposed to silica NPs or BULK silica for analysis. In control worms, the neurons CEP, ADE, and PDE exhibited a healthy morphology, characterized by a continuous and elongated fluorescence pattern. In contrast, worms exposed to silica NPs displayed a fragmented, punctate fluorescence pattern in these neurons, indicative of neurodegeneration (Figure 10A and 10B). Specifically, for CEP and ADE neurons (Figure 10C and 10D), neurodegeneration increased gradually with age in both the control group and the BULK silica-treated group, reaching approximately 5% by 11 days. In contrast, exposure to 200 µg/mL silica NPs resulted in a significant increase in neurodegeneration, with about 20% of worms affected by 11 days ($p < 0.001$). Although younger worms in this group displayed a gradual increase in neurodegeneration compared to the control group, the effect was more significantly pronounced in 11-day-old nematodes. At 625 µg/mL, neurodegeneration was also significantly higher, with also nearly 20% of worms exhibiting neurodegenerative patterns by day 7, e.g., four days earlier than the 200 µg/mL treated group ($p < 0.0001$). These findings demonstrated a clear dose-dependent and age-dependent increase in neurodegeneration in CEP neurons, with higher concentrations of silica NPs and older worms causing more severe neurodegenerative effects.

PDE neurons (Figure 10E) exhibited the highest susceptibility to silica NP-induced neurodegeneration. Significant neurodegeneration was observed in PDE neurons as early as day 2 with exposure to 200 µg/mL silica NPs, in contrast to ADE and CEP neurons where significant neurodegeneration was not apparent until day 11. Notably, in middle-aged worms (11-day-old) treated with 200 µg/mL silica NPs, neurodegeneration in PDE neurons reached approximately 80%, whereas neurodegeneration in ADE and CEP neurons at the same age was only around 20%. These findings highlight the heightened vulnerability of PDE neurons to silica NP-induced neurodegeneration, demonstrating the highest levels of neurodegeneration across all concentrations and age groups. Overall, neurodegeneration in the dopaminergic neurons of *C. elegans* was both age-dependent and dose-dependent. CEP and ADE neurons appeared resilient

to silica NPs, as neurodegeneration was not observed until middle age; however, they still exhibited a dose-dependent response with increasing NP concentrations. Notably, PDE neurons were the most vulnerable, showing significant neurodegeneration at the very early stage of 2-day-old. These findings underscored the differential neurotoxic impact of silica NPs on various dopaminergic neurons, highlighting the distinct susceptibilities of each neuron type to nanoparticle-induced neurotoxicity.

Next, we analyzed the thrashing per 30 seconds to investigate behavior defects induced by silica NPs. Neurodegeneration induced by silica NPs has been observed through protein aggregation in dopaminergic reporter worms. However, the relationship between neurodegeneration and behavioral defects remains unclear. The study conducted a detailed analysis of the neuromuscular effects of silica NPs on *C. elegans* across different ages and concentrations, revealing significant dose-dependent and age-dependent impacts on locomotion fitness. After 24 hours of exposure, the control group exhibited a mean thrashing rate of 127 thrashes per 30 seconds, indicating strong neuromuscular activity, but the exposure to 200 µg/mL silica NPs significantly ($p < 0.0001$) reduced this rate to 82 thrashes which further decreased to 79 thrashes at 650 µg/mL (Figure 11A). BULK silica exposure did not impact behavioral defects at any age, as the thrashing rates remained comparable to those of the mock control group. From day 4 onwards (Figure 11B, 11C, 11D and 11E), all groups showed a natural decline in thrashing rates with age. Notably, 625 µg/mL silica NPs caused the most significant reduction in 7-day-old worms, with average thrashing rates of 11 thrashes, compared to 24 thrashes for the 200 µg/mL group, and 84 thrashes for the control group ($p < 0.0001$). Although untreated 11-day-old worms had a lower thrashing rate (61 thrashes) compared to 2-day-old worms (127 thrashes), they still maintained a higher rate than the 200 µg/mL silica NP-treated worms at the same age, which had a mean rate of 17 thrashes per 30 seconds ($p < 0.001$).

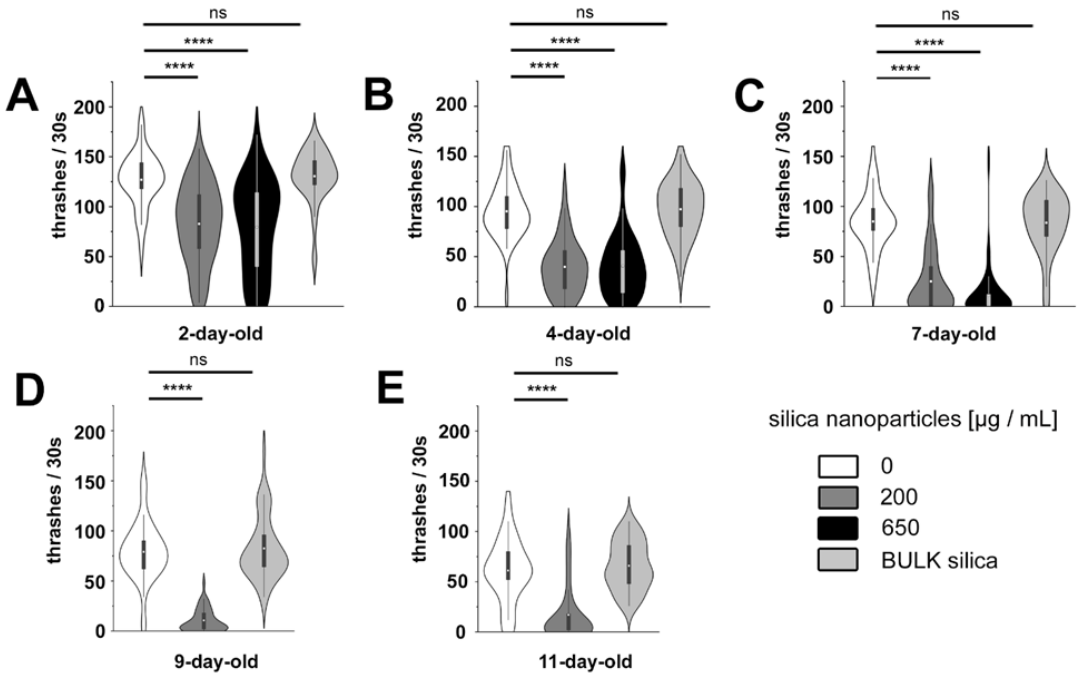

Figure 11. Silica nanoparticles accelerated neuromuscular defects in dopaminergic reporter *C. elegans*.
(A–E) Serotonergic reporter worms were cultured at 20 °C and fed with *E. coli* OP50. Locomotion fitness was quantified in 2- to 11-day-old worms that were either mock-treated (distilled water), 200 µg/mL silica NPs, 650 µg/mL or BULK silica. (A–E) Violin plots represent means ± SD from three independent experiments with n = 15 worms per condition per experiment. *, $p < 0.05$; **, $p < 0.01$; ***, $p < 0.001$; °C, degree Celsius; ns, not significant; s, seconds; SD, standard deviation.

In conclusion, this study demonstrated the significant impact of silica NPs on dopaminergic neurons and neuromuscular function in *C. elegans*. PDE neurons were the most susceptible, showing early and severe neurodegeneration, while CEP and ADE neurons displayed resilience until middle age. Additionally, silica NP exposure caused a dose-dependent reduction in thrashing rates, indicating neuromuscular defects. These findings underscore the differential neurotoxic effects of silica NPs on neuronal integrity and behavior, suggesting their broader implications for aging and proteostasis. Thus, the investigation was expanded to include GABA, another common neurotransmitter involved in numerous behavioral processes in worms.

Silica NPs accelerated protein aggregation in GABAergic neurons and induced neuromuscular defects

To examine the impact of silica NPs on GABAergic neurons, reporter worms expressing green fluorescent protein (GFP) under the control of the *unc-47* promoter specifically in GABAergic neurons were investigated (Figure 12A). The reporter worms were either left untreated (H_2O) or

exposed to silica NPs or BULK silica for analysis. In mock-exposed control worms (H_2O), GABAergic motor neurons were preserved (Figure 12B). In contrast, treatment with silica NPs resulted in a significant loss of GABAergic neurons, particularly in the anterior-most and posterior-most regions (Figure 12B-C, insets).

Quantitative analyses (Figures 12D-12H) reveal a dose-dependent and age-dependent increase in neurodegeneration. In 2-day-old worms (Figure 12D), exposure to 200 µg/mL silica NPs significantly increased neuron loss compared to controls ($p < 0.001$), with an even greater effect at a high concentration of 650 µg/mL. The mean neuron loss increased from 0.5 in controls to approximately 1 in the 200 µg/mL silica NP-treated group, and nearly 2 in the 650 µg/mL group. This trend continued in 4-day-old worms, with neuron loss reaching about 2.5 and 3 in the 200 µg/mL and 650 µg/mL groups, respectively ($p < 0.0001$), peaking in 7-day-old worms. In older worms (9-day-old and 11-day-old), neuronal loss remained around 2.5 in the 200 µg/mL group. However, the 650 µg/mL silica NP concentration proved lethal for most worms by this age. In contrast, BULK silica did not cause significant neurodegeneration, highlighting the nano specific toxicity of silica NPs. Considering the crucial roles of GABA in motor control and neural circuit stability, with fewer GABAergic neurons, the balance of muscle excitation and inhibition could be disrupted. This might manifest as motor control issues, such as impaired locomotion or muscle spasm. The disruption of GABAergic inhibition could result in hyperactivity of neural circuits, impaired motor coordination, and overall neural instability.

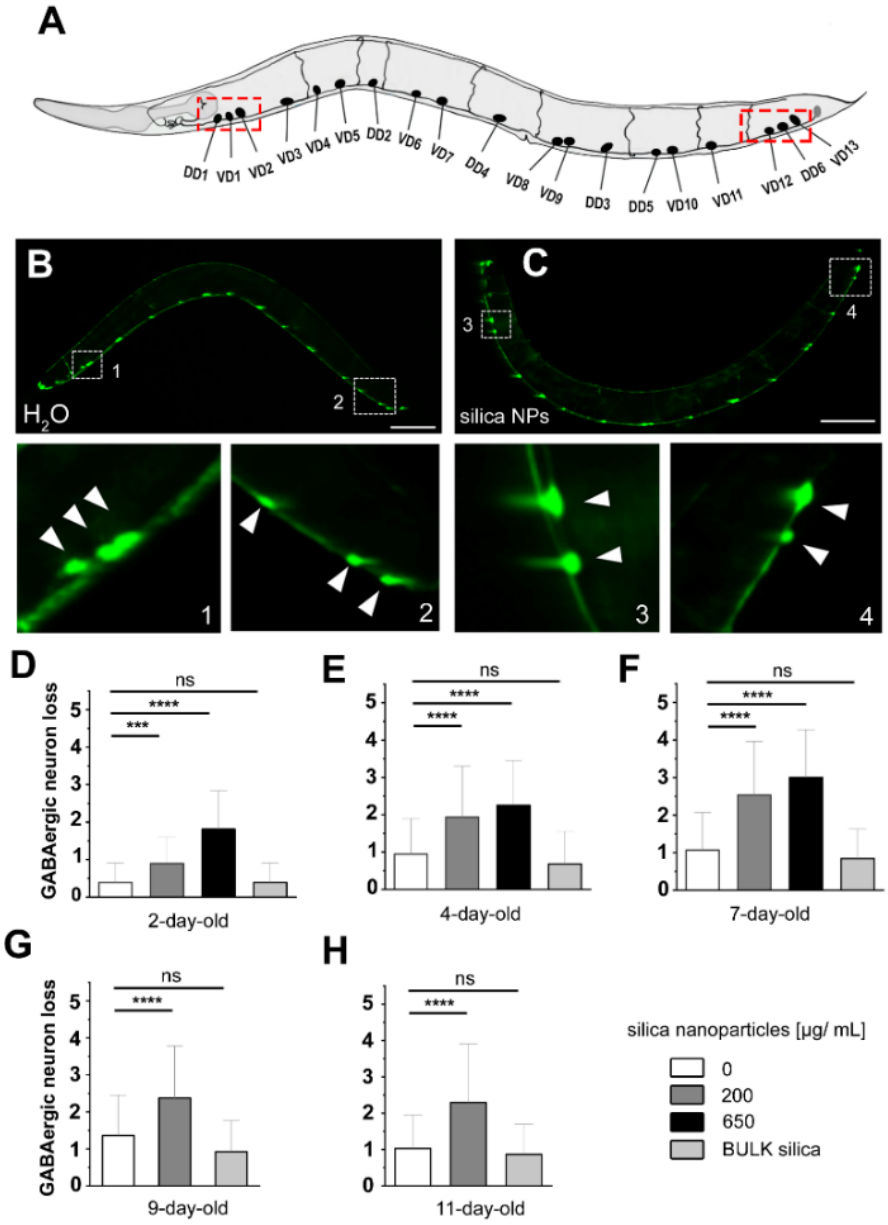

Figure 12. Silica NPs induce GABAergic neuron loss during the adult life of the nematode *C. elegans*.
(A) Scheme of the positions of GABAergic D-type motor neurons in *C. elegans*. Red boxes indicate the anterior-most and posterior-most regions of vulnerable neurons. (B, C) Representative fluorescent micrographs of 4-day-old adult *C. elegans* stably expressing green fluorescent protein (GFP) under the control of promotor *unc-47* in GABAergic neurons. Reporter worms were mock-treated (B) or exposed to 200 µg/mL silica NPs at 20°C (C). The insets show blow-ups of the anterior and posterior regions of D-type motor neurons. Arrows indicate the vulnerable neurons. (D-H) Quantification of GABAergic neuron loss from 2- to 11-day-old worms that were mock-exposed, exposed to 200 µg/mL silica NPs or 650 µg/mL silica NPs or BULK silica. Bar graphs represent means ± SD from three independent experiments with n = 25 per condition per experiment (one-way ANOVA with Tukey's post hoc test). Statistical significance is denoted as

follows: *, p < 0.05; **, p < 0.01; ***, p < 0.001; ****, p < 0.0001. BULK, Bulk silica (500 nm); ns, not significant; s, seconds; SD, standard deviation. Scale bars, 100 μm.

Silica NPs have been shown to induce neurodegeneration, evidenced by the loss of GABAergic D-type motor neurons in reporter worms. Since GABAergic D-type motor neurons are intimately associated with locomotion, this neuronal loss suggests potential behavioral impairments. To elucidate behavioral effects induced by silica NPs, we analyzed the thrashing rate over a 30-second period in young to middle-age reporter *C. elegans*.

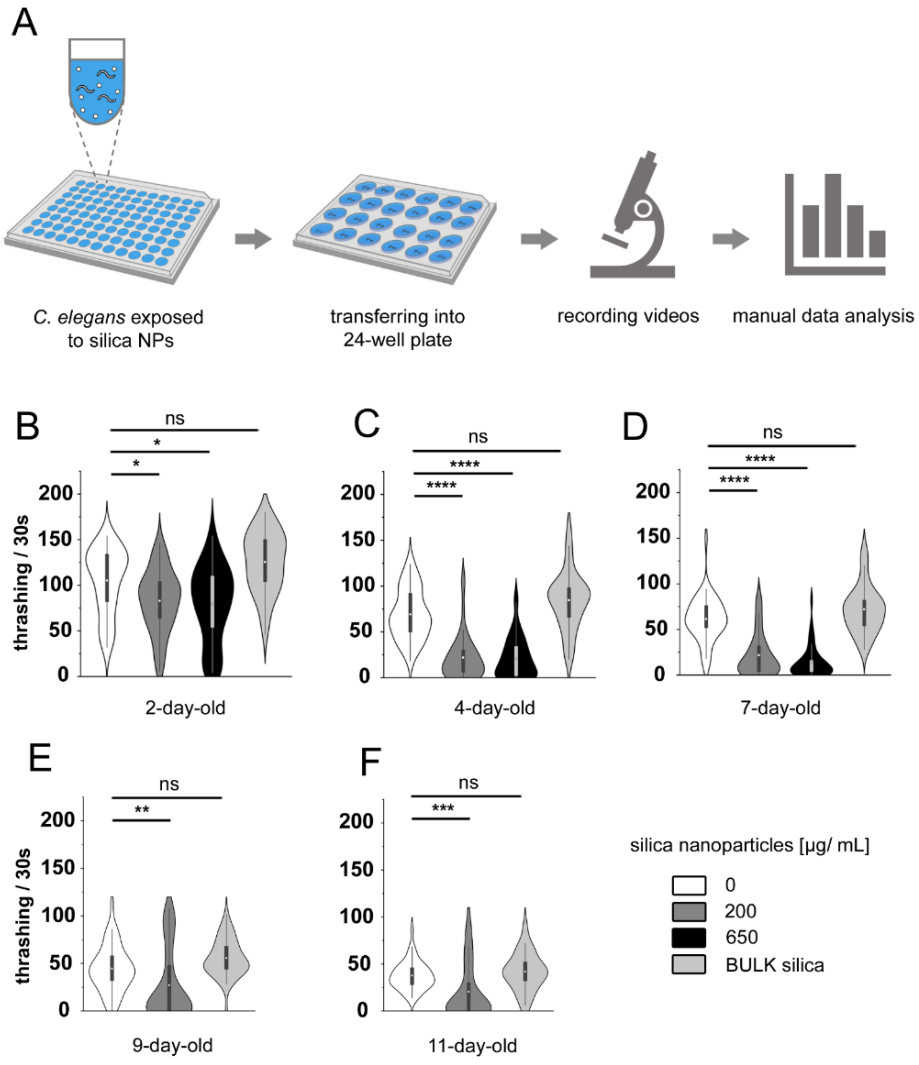

Figure 13. Silica NPs modulate neurobehavior in aging GABAergic reporter worms. (A) Schematic of protocol steps presenting different operational procedures for manual data analysis in *C. elegans*. Adult hermaphrodite *C. elegans* were mock-exposed or exposed to 200 µg/mL silica NPs in 96-well microtiter plates. At a certain age, 1-2 wells were transferred into 24-well plates for recording videos. The videos were then manually analyzed. (B–F) Violin plots represent the locomotion fitness of 2- to 11-day-old worms. Adult hermaphrodite GABAergic reporter worms (strain

EG1285) were cultured at 20 °C and fed with *E. coli* OP50. Locomotion fitness was quantified as the thrashing rate per 30 seconds from 2- to 11-day-old worms. Worms were either mock-treated or exposed to 200 µg/mL silica NPs, 650 µg/mL silica NPs, or 200 µg/mL BULK silica. Violin plots shows means ± SD from three independent experiments, with n = 15 worms per condition per experiment. Statistical significance is denoted as follows: *, $p < 0.05$; **, $p < 0.01$; ***, $p < 0.001$; ****, $p < 0.0001$. BULK, Bulk silica (500nm); ns, not significant; s, seconds; SD, standard deviation.

The results provide an evaluation of the neuromuscular impacts of silica NPs on GABAergic reporter worms (*C. elegans*), focusing on increasing age. Following 24 hours of exposure (Figure 13B), the control group demonstrated a high mean thrashing rate of 105 thrashes per 30 seconds, indicative of robust neuromuscular function. In contrast, exposure to 200 µg/mL silica NPs significantly reduced ($p < 0.05$) this rate to 82 thrashes, with a further decline to 79 thrashes at 650 µg/mL (Figure 13C). Importantly, exposure to BULK silica did not affect the thrashing rates at any age, as these remained comparable to those of the mock control group. Starting from day 4 (Figures 13C-F), all groups exhibited a natural decline in thrashing rates with age. The most pronounced reduction was observed in 7-day-old worms exposed to 650 µg/mL silica NPs, which had an average thrashing rate of 14 thrashes per 30 seconds, compared to 21 thrashes in the 200 µg/mL group and 61 thrashes in the control group ($p < 0.0001$). Although untreated 11-day-old worms had a lower thrashing rate (37 thrashes) compared to 2-day-old worms (105 thrashes), they still maintained a higher rate than the 200 µg/mL silica NP-treated worms at the same age, which exhibited a mean rate of 20 thrashes per 30 seconds ($p < 0.001$). These results underscore significant, dose-dependent, and age-dependent neuromuscular deficits induced by silica NPs, directly correlating with the observed loss of GABAergic neurons in previous figures. The substantial reduction in thrashing rates, particularly at higher NP concentrations and in older worms, aligns with the neurodegeneration of GABAergic neurons. This neuronal loss may critically impair the inhibitory functions of GABA, leading to disrupted neuromuscular activity and diminished motor control. The findings highlight the specific vulnerability of GABAergic neurons to silica NP exposure, emphasizing the need for further research to elucidate the underlying mechanisms of this toxicity.

Preserved entanglement of sarcomere filaments in silica NP-treated and untreated C. elegans

The observed reduction in thrashing rates may be attributed to the effects of silica NPs on the body wall muscle tissues of *C. elegans*, leading to deficits in locomotion control. To investigate this hypothesis, we utilized another strain of reporter worms expressing green fluorescent protein (GFP) under the control of the myosin-3 promoter (*myo-3*) specifically in body wall muscles. This

approach enabled us to assess potential damage to sarcomere filaments caused by silica NPs exposure (Figure 14).

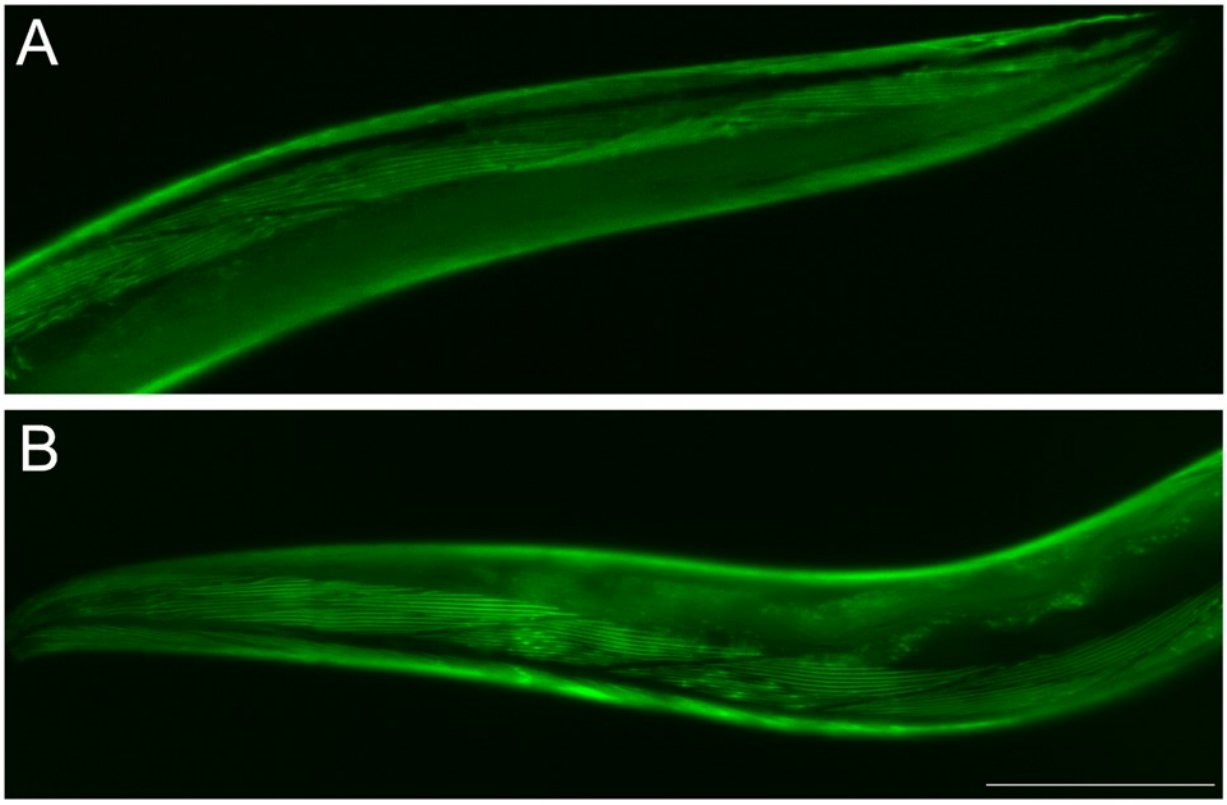

Figure 14. Intact entanglement of sarcomeres filaments in silica NPs treated and mock-treated *C. elegans*. Representative fluorescent micrographs of 4-day-old adult *C. elegans* stably expressing green fluorescent protein (GFP) under the control of myosin-3 promoter (*myo-3*) in body wall muscles. Reporter worms were cultured at 20°C and fed with *E. coli* OP50, then subjected to (A) mock-treatment (H_2O), or (B) 200 µg/mL silica NPs. Scale bars, 100 µm.

The primary observation was the consistent and well-organized pattern of sarcomere filaments in both the control and silica NP-exposed worms. The GFP fluorescence revealed the striated pattern of sarcomeres, indicating intact muscle structure. There was no apparent disruption, disorganization, or fragmentation of the sarcomere filaments in silica NP-exposed worm compared to unexposed controls. This visual comparison suggested that exposure to silica NPs does not induce structural damages to muscle tissues in *C. elegans*.

While this figure focuses specifically on muscle structure, it's important to consider these findings in the context of previous figures demonstrating silica NP-induced neurodegeneration and locomotor deficits. The absence of gross muscle damage suggests that the observed neuromuscular impairments might primarily be resulted from neuronal dysfunction rather than

direct muscle toxicity. However, further investigation, potentially using higher resolution imaging techniques, might be needed to rule out subtle alterations in muscle structure or function that are not detectable at this level of analysis.

4.2 Gene expression profiles of silica-exposed GABAergic reporter worms

Given the significant loss of GABAergic neurons and the associated deficits in thrashing behavior observed following silica nanoparticles exposure, it is crucial to further investigate the underlying molecular mechanisms. A proteomic analysis was performed to compare the gene expression profiles between the silica-exposed *C. elegans* cohort expressing green fluorescent protein (GFP) under the control of promotor *unc-47* in GABAergic neurons, and the respective mock-exposed (H_2O) cohort. Proteomics enable identification and quantification of the differentially expressed proteins, thus providing a profile of specific cellular processes and pathways disrupted by silica NP exposure. This analysis is essential for elucidating the molecular basis of the observed neurotoxicity (Figure 15).

Figure 15A and 15B provides a Volcano plot and Venn diagram summarizing the distribution of identified genes in the proteomic analysis. Out of 3306 total genes analyzed, 817 were downregulated, 621 were upregulated, and 1868 remained unchanged in response to silica NP exposure. This highlights the significant impact of silica NPs on gene expression, with a substantial number of genes showing altered regulation.

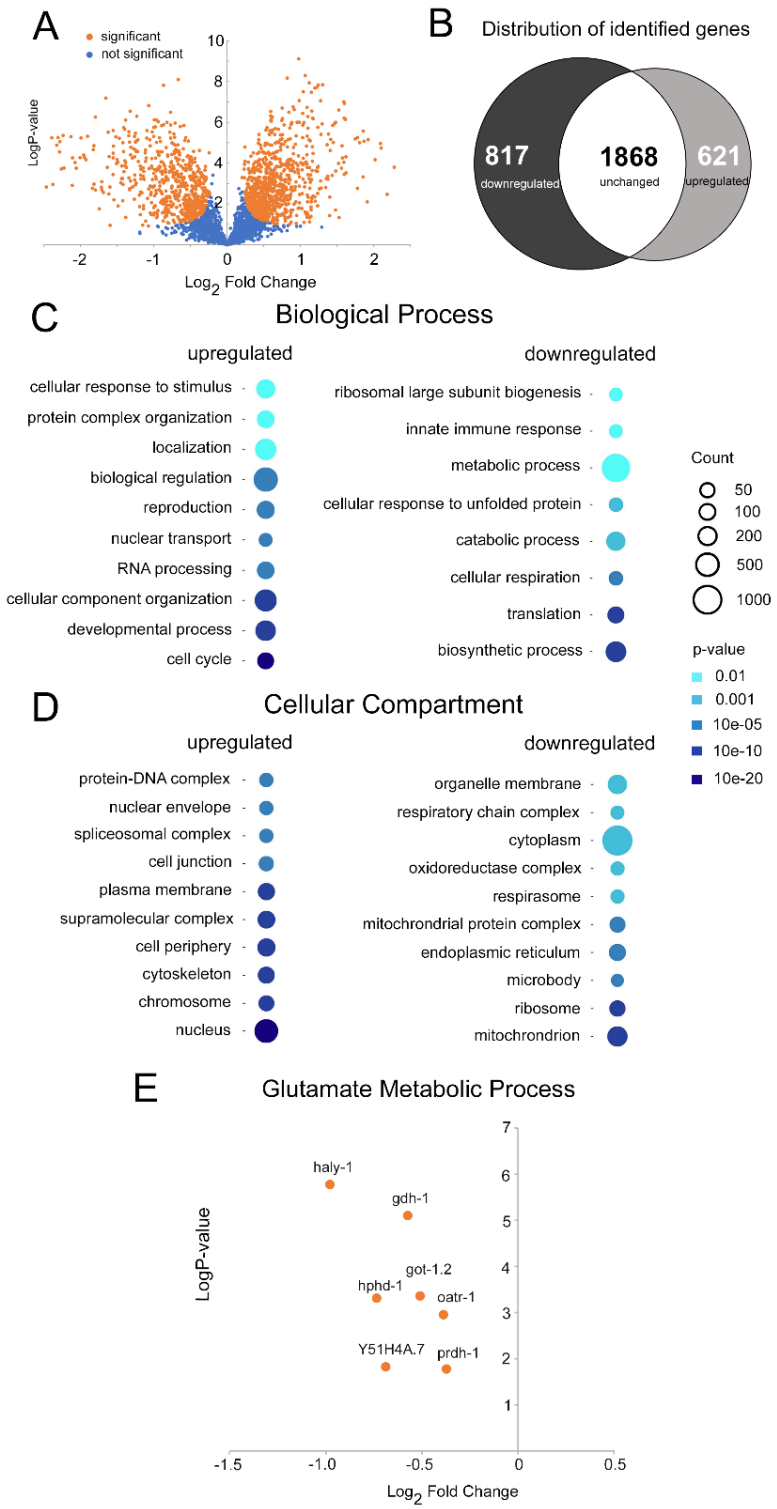

Figure 15. Gene expression of silica NPs - exposed GABAergic reporter worms. (A) Volcano plots representing the differentially expressed genes (DEGs) identified in the proteomic analysis of GABAergic reporter worms exposed to silica NPs compared to mock control. *C. elegans* were mock-exposed (distilled water) or exposed to 200 µg/mL silica NPs for 3 days. Total protein was purified and subjected to mass spectrometry. Reads were mapped according to the *C. elegans* reference genome. Genes and gene ontologies (GOs) were categorized using databases of UniProt, Panther Database and WormBase. Genes with a p-value smaller than 0.05 were considered significantly different (highlighted in orange). (B) The Venn diagram depicts the distribution of genes identified in the proteomic analysis, categorized as upregulated, downregulated, or unchanged. (C) Enriched gene sets corresponding to upregulated and downregulated biological processes, and (D) cellular compartment were identified through GO analysis using the Panther Database. (E) The graph illustrates DEGs identified in the proteomic analysis, specifically focusing on the glutamate metabolic process. Proteomics analysis was conducted across six independent experiments (biological replicates), with n = 8,000–12,000 per condition per experiment. *haly-1*, histidine ammonia-lyase; *gdh-1*, glutamate dehydrogenase-1; *got-1.2*: glutamate oxaloacetate transaminase-1.2; *hphd-1*: Hydroxyacid-oxoacid transhydrogenase; *oatr-1*, ornithine aminotransferase; *prdh-1*, proline dehydrogenase-1.

To gain further insights into the functional implications of these gene expression changes, Gene Ontology (GO) enrichment analysis based on PANTHER classification was performed. The result of GO analysis was presented according to biological process (Figure 15C) and cellular

compartment (Figure 15D). Upregulated genes in biological process are primarily involved in cellular responses to stimuli, protein complex organization, and nuclear transport (Figure 15C), suggesting an activation of stress response pathways and cellular reorganization in response to silica NP exposure. Conversely, downregulated genes are enriched in ribosome biogenesis, metabolic processes, and cellular respiration, indicating a potential suppression of protein synthesis, energy production, and overall metabolic activity.

Upregulated genes are primarily involved in critical biological processes, suggesting a coordinated cellular response to silica NP exposure. A significant category is cellular responses to stimuli, including genes involved in stress responses such as heat shock proteins and inflammatory response elements, indicating attempts to mitigate silica NP-induced cellular damage. Another key category is protein complex organization, involving increased expression of chaperones and co-chaperones, which assist in proper protein folding and prevent aggregation. Proteasome activity-related genes are also upregulated, suggesting enhanced degradation of damaged proteins. Nuclear transport is crucial for the regulation of gene expression. The upregulation of these genes suggests that *C. elegans* cells are actively modulating the transport of transcription factors, regulatory proteins, and other molecules into and out of the nucleus. This process is essential for altering gene expression profiles in response to silica NP-induced stress.

Conversely, downregulated genes are enriched in processes crucial for normal cellular function, indicating suppression of essential activities. Ribosome biogenesis is notably affected, with reduced expression of genes involved in ribosomal subunit synthesis and assembly, suggesting decreased protein synthesis capacity.

Metabolic processes are also significantly impacted, with downregulation of genes in glycolysis, the citric acid cycle, and lipid metabolism, indicating an overall decline in metabolic activity. Additionally, reduced expression of genes in amino acid and nucleotide biosynthesis could impair macromolecule production necessary for growth and repair. Cellular respiration is another majorly affected category, with decreased expression of genes encoding components of the mitochondrial respiratory chain and oxidative phosphorylation, indicative of impaired mitochondrial function and reduced ATP production. Downregulation of genes involved in ROS detoxification could lead to increased oxidative stress and cellular damage.

Figure 15D highlights significant alterations in gene expression within the specific cellular compartments GO of *Caenorhabditis elegans* exposed to silica NPs. The upregulation of genes associated with the protein-DNA complex suggests increased DNA binding and regulatory activity,

likely enhancing transcriptional responses to silica NP-induced stress. Genes linked to the nuclear envelope and nucleus point to heightened nuclear processes, possibly involving DNA repair and gene expression regulation. The spliceosomal complex's upregulation indicates increased RNA splicing activity, essential for mRNA processing. Upregulated genes related to cell junctions and plasma membranes imply enhanced cell-cell communication and membrane integrity, maintaining cellular cohesion and barrier functions under stress. Additionally, increased expression of cytoskeletal genes suggests active reorganization of cellular architecture, crucial for maintaining cell shape, intracellular transport, and mechanical stability under NP exposure.

Upregulated genes in the nucleus, cytoskeleton, and protein-DNA complexes suggests an enhanced stress response and cellular reorganization efforts, indicative of increased transcriptional activity, RNA processing, and maintenance of cellular architecture. Conversely, the downregulation of genes associated with mitochondrial function, protein synthesis, and metabolic processes points to compromised cellular functionality. Specifically, reduced expression in the respiratory chain complex, oxidoreductase complexes, and ribosomes suggests impaired energy production, reduced ATP synthesis, diminished oxidative phosphorylation, and decreased protein synthesis capabilities which corresponded to the reduction of translation found in the biological process GO above.

The downregulation of genes associated with organelle membranes and the respiratory chain complex indicates impaired mitochondrial function and energy production, leading to decreased ATP synthesis and overall cellular energy deficits. Reduced expression of cytoplasmic genes reflects a general decline in metabolic activities. Downregulation of oxidoreductase complexes and the respirasome suggests diminished oxidative phosphorylation and electron transport chain activity, further confirming compromised mitochondrial function. Consistent with these observations, mitochondrial gene downregulation highlights significant mitochondrial dysfunction, contributing to increased oxidative stress and reduced metabolic efficiency. Decreased expression of endoplasmic reticulum and ribosomal genes suggests reduced protein synthesis and folding capacity, which can lead to the accumulation of misfolded proteins and heightened cellular stress. Finally, the downregulation of microbody genes implies potential disruptions in lipid metabolism.

Especially, a specific biological process, glutamate metabolism, which is crucial for neuronal GABAergic synthesis was downregulated (Figure 15E). The graph shows several key genes involved in glutamate metabolism that are significantly downregulated in silica NP-exposed worms: *gdh-1* (Glutamate dehydrogenase) or *got-1.2* (Glutamate oxaloacetate transaminase).

This finding suggests that silica NPs target glutamate signaling pathways, potentially contributing to the observed neurotoxic effects.

Overall, this comprehensive proteomic analysis reveals that silica NP exposure significantly alters gene expression in GABAergic reporter worms, affecting various biological processes and cellular compartments, particularly those related to neuronal functions, stress responses, and energy metabolism. These findings provide valuable insights into the molecular mechanisms underlying silica NP-induced neurotoxicity on GABAergic neurons and confirm the potential risks associated with nanoparticle exposure.

Specific protein resilience in silica-NPs treated C. elegans revealed by silver stained SDS-PAGE gel.

To gain additional insights into the protein-level changes associated with silica NP exposure, we conducted a silver staning analysis. This technique allows us to visualize the overall protein profiles and identify proteins that possibly exhibit resistance to silica NP-induced proteolysis (Figure 16).

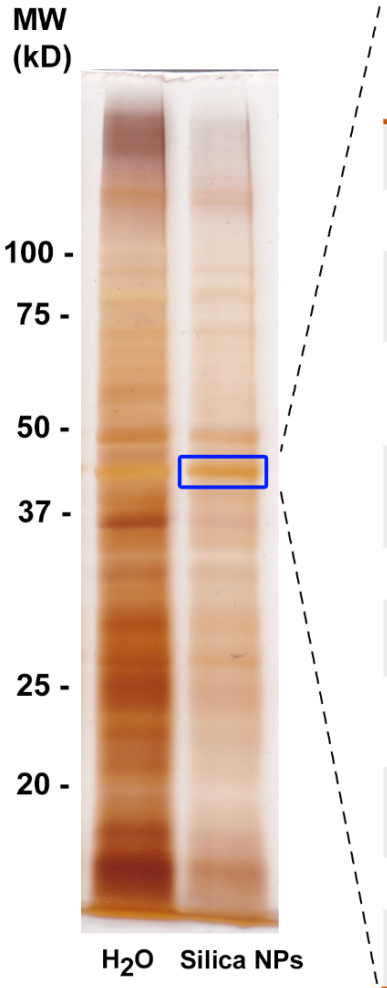

Protein names	Genes	Gene Ontology (biological process)
SHSP domain protein	hsp-43	protein refolding; heat response
elongation factor 1-gamma	eef-1G	translational elongation
26S proteasome regulatory subunit rpn-6.1	rpn-6.1	lifespan, proteasome assembly; ubiquitin-dependent catabolic process
Isocitrate dehydrogenase	idh-1	isocitrate metabolic process; NADP metabolic process
Uncoordinated protein 87	unc-87	actin/myosin assembly; negative regulation of muscle filament
Galectin domain protein	lec-2	carbohydrate binding;galactoside binding
Perilipin-1 homolog	plin-1	embryo development or egg hatching
Pyruvate dehydrogenase E1 alpha	pdha-1	acetyl-CoA biosynthesis
Diphosphomevalonate decarboxylase	CELE_ Y48B6A.13	cholesterol biosynthesis; mevalonate pathway
Actin	act-4	actin cytoskeleton organization
Actin	act-5	microvillus assembly; larval development; eating behavior; tube formation

Figure 16. Reduction of the amount of total protein by silica nanoparticles reveals proteins with specific resilience.

4-day-old adult hermaphrodite *C. elegans* reporters for GABAergic neurons (oxIs12 [unc-47p::GFP + lin-15(+)]) were mock-exposed (H_2O) or exposed to silica nanoparticles (200 µg/mL). (A) The worms (n=8000-10000) were lysed, total protein separated by 1D SDS-PAGE, and visualized by Silver staining (protein lanes, right). Proteins within a resilient band (blue box) were subjected to further analysis by mass spectrometry, and identified. (B) Genes and gene ontologies (GOs) of resilient proteins were categorized using UniProt databases. H_2O, distilled water; kD, kilo Dalton; MW, molecular weight; NPs, nanoparticles; PAGE, polyacrylamid gel electrophoresis; SDS, sodium dodecyl sulfate.

Figure 16 shows representative a silver-stained SDS-PAGE gel comparing the protein profiles of reporter worms mock-exposed (H_2O) and exposed to silica NPs (200 µg/mL). The silver-stained gel reveals a general reduction in the amount of total protein in silica NP-treated worms compared to the control group. However, certain protein bands, highlighted by the blue box, appear with unchanged intensity after silica NP exposure, suggesting that these proteins possess a specific resilience to NP-induced proteolysis.

These resilient protein bands were further analyzed using liquid chromatography to identify the specific proteins involved. The table lists the identified proteins, their corresponding genes, and their associated gene ontology (GO) terms, providing insights into their biological functions. The identified proteins include SHSP domain protein (*hsp-43*), which is involved in protein refolding and heat response and suggests a role in cellular stress response. Elongation factor 1-gamma (*eef-1G*) is essential for translational elongation during protein synthesis, while the 26S proteasome regulatory subunit (*rpn-6.1*) is a key component of the proteasome responsible for protein degradation. Isocitrate dehydrogenase (*idh-1*) functions in isocitrate and NADP metabolic processes, and uncoordinated 87 (*unc-87*) is involved in actin/myosin assembly and muscle filament regulation. Additionally, the identified proteins include galectin domain protein (*lec-2*), which participates in carbohydrate and galactoside binding. Perilipin-1 homolog (*plin-1*) plays a role in embryo development or egg hatching, and pyruvate dehydrogenase E1 alpha (*pdha-1*) is crucial for acetyl-CoA biosynthesis. Diphosphomevalonate decarboxylase (*CELE_Y48B6A.13*) is involved in cholesterol biosynthesis and the mevalonate pathway. Actin proteins (*act-4* and *act-5*) are structural components vital for actin cytoskeleton organization, microvillus assembly, larval development, eating behavior, and tube formation.

The presence of these resilient proteins, particularly those involved in stress response, protein synthesis, and degradation, suggests that *C. elegans* may activate specific cellular mechanisms to mitigate the detrimental effects of silica NP exposure. However, the overall reduction in total protein content indicates that silica NPs still exert a significant impact on protein expression, potentially disrupting various cellular processes. This observed resilience could indicate an adaptive response where certain proteins are upregulated or remain stable to preserve essential cellular functions. Despite the activation of these protective mechanisms, the significant reduction in overall protein levels suggests that the protective responses are not entirely sufficient to counteract the stress induced by silica NPs.

4.3 Development of a single worm tracking (SWT) platform and automatic quantification

To validate the proteomics results indicating disrupted molecular pathways due to silica exposure, behavioral phenotyping was introduced. To this end, a prominent neuromuscular behavior in locomotion, the thrashing rate per 30 seconds, was investigated concerning sensitivity to silica NPs and GABAergic neurons' functionality. Furthermore, the development of an automated thrashing analysis system aims to pave the way for obtaining reliable and generalizable results within a shorter timeframe.

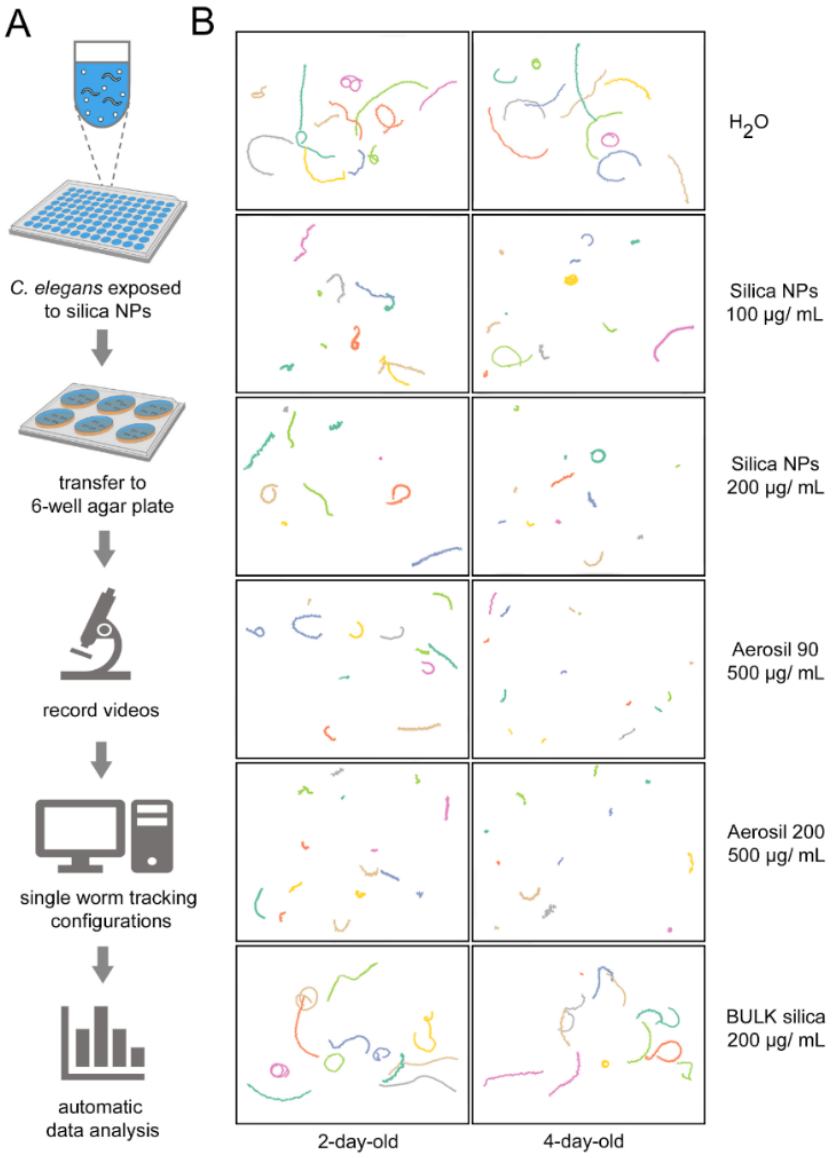

Figure 17. Tracking of individual worms using a single worm tracking (SWT) system across various particle types, concentrations, and worm ages.

(A) Schematic illustrating the protocol steps outlining different operational procedures for automated data analysis in *C. elegans* utilizing the SWT platform. Adult hermaphrodite *C. elegans* were mock-exposed or exposed to 200 µg/mL silica NPs in 96-well plate. At a certain age, 1-2 wells were then transferred in agar-loaded 6-well plate with 2 mL M9 buffer for recording videos. (B) Swimming tracks were recorded for 2-day-old and 4-day-old worms in different conditions. Worms were subjected to either mock treatment (distilled water) or exposure to silica NPs 100 µg/ mL, silica NPs 200 µg/ mL, Aerosil 90 at 500 µg/ mL, Aerosil 200 at 500 µg/ mL, or BULK silica at 200 µg/ mL. Mock treated and BULK silica treated groups had active movement patterns, whereas worms exposed to Aerosil 90, Aerosil 200 and silica NPs showed noticeably reduced tracking movement.

This step investigated the tracking of individual *C. elegans* worms using a single worm tracking (SWT) system, which was reconfigured from SWT software (Koopman et al., 2020) in terms of experiment designs and software parameters to fit into our lab settings (Figure 17A). This system examined various particle types, concentrations, and worm ages (Figure 17B). The control group treated with distilled water and BULK silica exhibits relatively uniform and active movement patterns in both 2-day-old and 4-day-old worms. This activity served as a baseline for comparison with the nanoparticle-treated groups. For the groups exposed to silica NPs at 100 µg/mL and 200 µg/mL, there was a noticeable reduction of movement activity compared to the control, with the effect being more pronounced at higher concentration. This suggested a dose-dependent impact of silica NPs on worm motility. The groups exposed to Aerosil 90 and Aerosil 200 at 500 µg/mL displayed even more significant reductions in movement. The tracking patterns indicated limited and less coordinated movements, particularly in 4-day-old worms. This suggests that aerosol particles may have a more substantial detrimental effect on worm motility compared to standard silica NPs.

The developed SWT system has effectively demonstrated a reduction in the locomotion of the worms by revealing a shorter movement pattern. This system provides valuable qualitative insights into the altered mobility of the worms under various experimental conditions. However, to achieve a comprehensive and quantitative assessment of their locomotion, it is essential to count the actual thrashes of the worms.

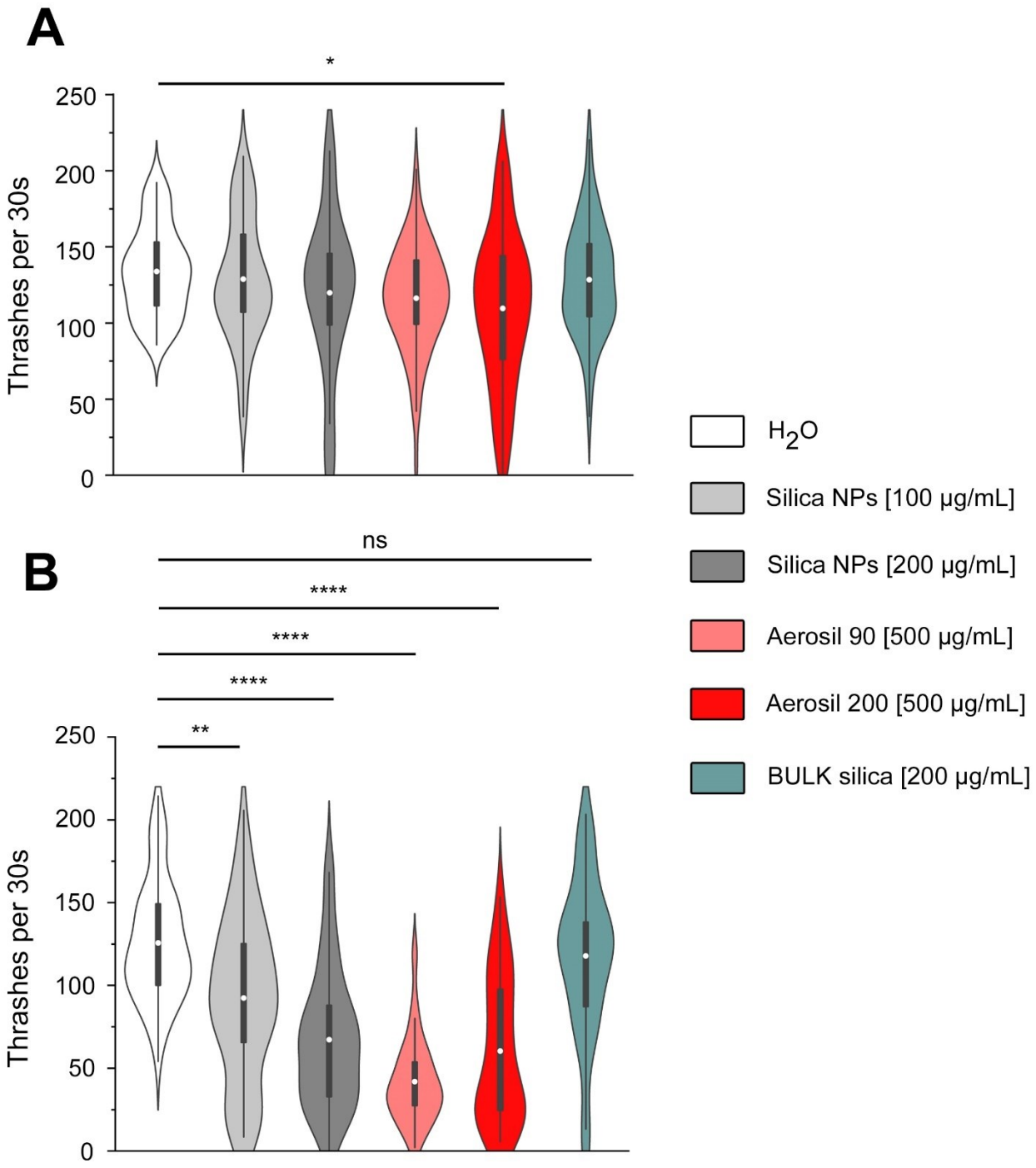

Figure 18. Automatic quantification of locomotion fitness test in individual worms using a single worm tracking (SWT) system across various particle types, concentrations, and worm ages.

Adult hermaphrodite *C. elegans* (N2) were cultured at 20°C and fed with *E. coli* OP50. Worms were subjected to either mock treatment (distilled water) or exposure to silica NPs 100 µg/ mL, silica NPs 200 µg/ mL, Aerosil 90 at 500 µg/ mL, Aerosil 200 at 500 µg/ mL, or BULK silica at 200 µg/ mL. The number of thrashes per 30 seconds were analyzed by the

SWT platform for 2-day-old **(A)** and 4-day-old worms **(B)**. Violin plots represent means ± SD from three independent experiments with n = 15 - 25 worms per condition per experiment. *, p < 0.05; **p < 0.01; ***p < 0.001; °C, degree Celsius; ns, not significant; s, seconds; SD, standard deviation.

The results showed that 2-day-old worms treated with distilled water (control) exhibited a relatively high thrashing frequency, averaging 134 thrashes per 30 seconds (Figure 18A). In contrast, worms exposed to silica nanoparticles at concentrations of 100 µg/mL and 200 µg/mL, as well as those treated with Aerosil 90 at 500 µg/mL, demonstrated a slight reduction in thrashing activity. Notably, worms treated with Aerosil 200 at 500 µg/mL showed a significant decrease in thrashing ($p < 0.05$) averaging 110 thrashes per 30 seconds. The group treated with BULK silica exhibited a thrashing frequency comparable to that of the control group. Figure 18B illustrates the results for 4-day-old worms, revealing more pronounced differences in thrashing behavior. The control group maintained a high average thrashing rate of 125 thrashes per 30 seconds. However, groups treated with silica nanoparticles at concentrations of 100 µg/mL and 200 µg/mL exhibited average thrashing rates of 92 and 67 thrashes, respectively. Worms exposed to Aerosil 90 and Aerosil 200 at 500 µg/mL showed mean thrashing rates of 41 and 60 thrashes, respectively. These reductions in thrashing behavior were statistically significant ($p<0.001$).

The locomotion fitness test reveals that exposure to silica NPs and Aerosil significantly impacts the thrashing behavior of *C. elegans*, with a more pronounced effect observed in older worms. The SWT platform opens up extensive possibilities for research in *C. elegans*. It enables detailed studies of neurotransmission, allowing for the assessment of the effects of agonists and antagonists on *C. elegans* behavior. Additionally, the platform is also useful for investigating aging, genetic mutants, and disease models, providing insights into the decline in motor function and the impact of neurodegenerative diseases. Additionally, SWT facilitates the analysis of exposome factors and their combinations, enabling the understanding of cumulative effects of environmental exposures. It can be applied to study the behavior of wild nematodes, offering ecological insights. Furthermore, SWT is particularly effective for studying neurotoxicant pollutants, assessing their **impact** on neural function and chemotactic behavior in *C. elegans*.

4.4 Neuromuscular defects were induced by other pollutants like thiacloprid or were accelerated by mixtures with silica nanoparticles.

Silica NPs have demonstrated detrimental effects on the nervous systems of *C. elegans*, leading to behavioral defects. To investigate mixed neurotoxicity, we examined whether other well-known

neurotoxicants, such as the pesticides thiacloprid or thiamethoxam, either alone or in combination with silica NPs, could amplify these effects.

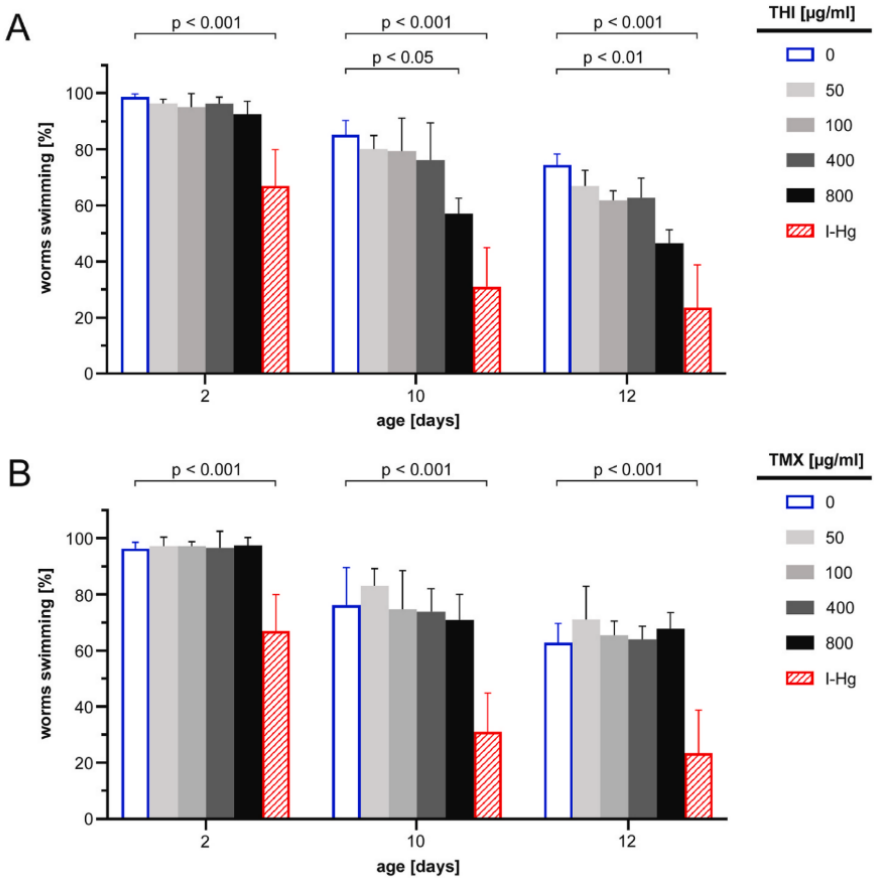

Figure 19. Quantification of locomotion behaviors in thiacloprid- or thiamethoxam-exposed *C. elegans*.
Wild type (N2) *C. elegans* were fed live *E. Coli* OP50 and cultured in 96 well plate liquid S-complete medium at 20 °◦C. The locomotion phenotype swimming was plotted against adult worm age. All graphs showed an age-related decline of swimming from young worms (2-day-old) to middle-aged (10- and 12-day- old) worms. Phenotypes were scored in hermaphrodite worms exposed to H_2O, inorganic mercury (I–Hg), and increasing concentrations of the neonicotinoids thiacloprid (A), or thiametoxam (B). The color code of different neonicotinoid concentrations is given on the right. Values represent means ± SD from three independent experiments with n = 40–65 for each treatment. Significance (p) is compared between treatment groups and respective untreated controls. I–Hg, inorganic mercury; THI, thiacloprid; TMX, thiametoxam.

Locomotion of *C. elegans* is characterized by wave-like bends along the nematode's body. To explore the chronic neurological impact of neonicotinoids on body wall muscle cells, thiacloprid (THI) and thiamethoxam (TMX) were studied using age-resolved swimming tests in adult *C. elegans*, from young to middle-aged, following the approach by Piechulek and von Mikecz (2018). Wild-type adult *C. elegans* were grown in liquid culture assays and either left untreated or

chronically exposed to varying concentrations of THI or TMX (Figure 19A and 19B). The untreated control group showed the typical age-associated decline in swimming performance between 2 and 12 days. Similarly, worms treated with 50 to 400 µg/mL THI exhibited an age-related decline in swimming behavior similar to that of untreated controls (Figure 19A). However, worms exposed to 800 µg/mL THI showed a significant acceleration in the decline of swimming ability, particularly in 10- and 12-day-old worms (Figure 19A). This accelerated decline was also seen in middle-aged worms treated with 800 µg/mL THI or the neurotoxicant I-Hg (Figure 19A, red color). Notably, I-Hg accelerated the decline in swimming across all age groups, including both young and middle-aged worms, whereas THI specifically affected the middle-aged worms.

To investigate another neonicotinoid, age-resolved swimming tests were also conducted with TMX. However, TMX concentrations ranging from 50 to 800 µg/mL did not significantly accelerate the age-related decline in swimming compared to untreated worms (Figure 19B). In contrast, I-Hg, used as a positive control, significantly expedited this aging phenotype in 2-, 10-, and 12-day-old worms.

We subsequently explored conditions that accelerate the THI-induced reduction in swimming fitness. Neonicotinoid THI is typically applied with amorphous silicon dioxide, such as silica nanoparticles, under realistic conditions to enhance its bioavailability (Goswami et al., 2022; Zhu et al., 2022).To replicate this in our experiments, we added silica nanoparticles (100 µg/mL) to a non-significant concentration of THI (400 µg/mL) that alone did not markedly reduce thrashing (Figure 20).

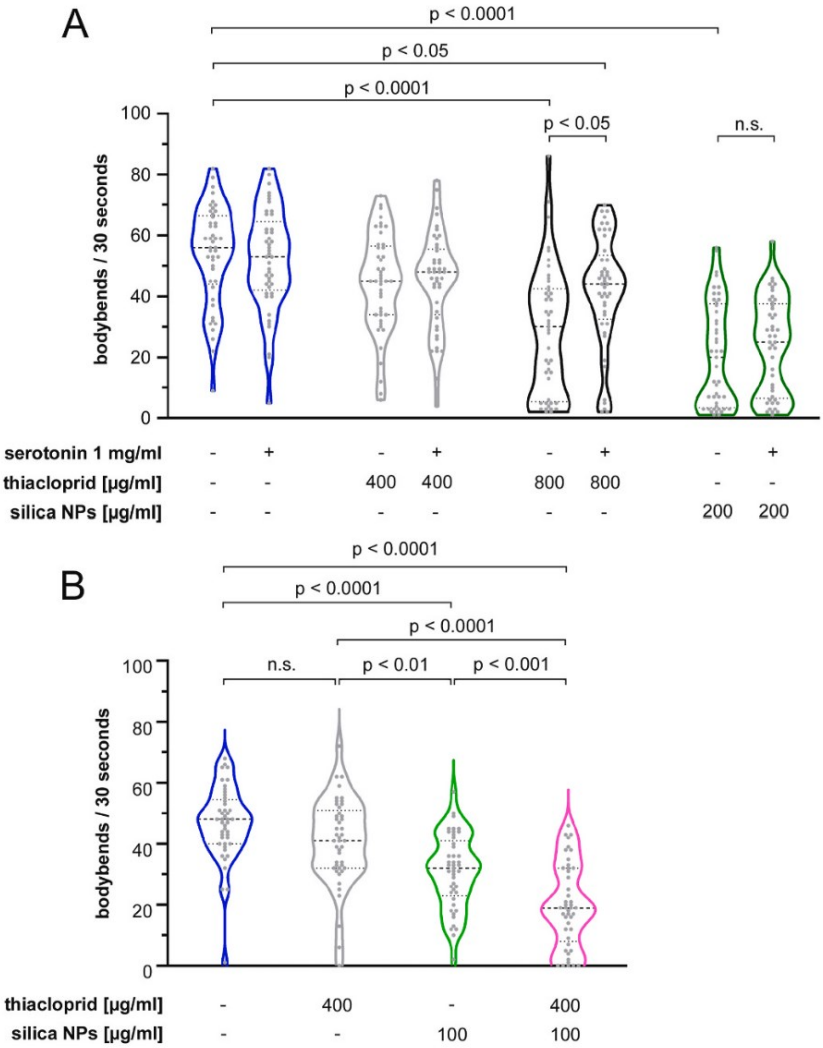

Figure 20. Thiacloprid-induced reduction of thrashing is rescued by exogenous serotonin, but accelerated by co-exposure with silica nanoparticles. (A, B) Wild type (N2) *C. elegans* were fed live *E. coli* OP50 and cultured in 96 well plate liquid S-complete medium at 20 °C. Young adult *C. elegans* were mock-treated (H_2O) or treated with the neonicotinoid thiacloprid, serotonin or silica NPs as indicated. Locomotion fitness was quantified in two-day-old worms by scoring the number of body bends per 30 seconds. Values represent means ± SD from three independent experiments with n = 15 per condition per experiment. Significance (p) is compared between the mock-treated and treated groups as indicated. NPs, nanoparticles; n.s., not significant.

The experiment was conducted to assess the impact of various interventions on neuromuscular fitness in 1-day-old adult *C. elegans* hermaphrodites. Worms were treated with increasing doses of THI (400 and 800 µg/mL) and their swimming fitness was evaluated by measuring thrashing rates (Figure 20A). Without serotonin pretreatment, mock-treated control worms had a median

thrashing rate of 56 per minute, while worms treated with 400 µg/mL and 800 µg/mL THI had mean rates of 45 and 30 thrashes per minute, respectively. Worms exposed to neurotoxic nano silica showed a median of 20 thrashes per minute. With exogenous serotonin pretreatment, the thrashing rates of control and 400 µg/mL THI-treated worms remained similar, but the rate for 800 µg/mL THI-treated worms increased significantly to 44 thrashes per minute, indicating serotonin mitigated the THI-induced reduction in locomotion. However, serotonin did not significantly improve thrashing rates in nano silica-treated worms. This suggests that serotonergic neurotransmission is a target of THI neurotoxicity.

Next conditions were analyzed that might exacerbate the THI-induced decline in swimming fitness. To replicate this scenario, silica nanoparticles (100 µg/mL) were added to a THI concentration (400 µg/mL) that did not significantly reduce thrashing on its own (Figure 20B). Remarkably, the co-incubation of THI and nano silica led to a significant reduction in thrashing in 2-day-old *C. elegans* compared to worms treated with only one of the chemicals (THI 400 µg/mL versus the THI-silica NP mixture, $p < 0.0001$; silica NPs 100 µg/mL versus the THI-silica NP mixture, $p < 0.001$). This suggests that combinations of neonicotinoids with other substances might have additive effects, which need further validation in future experiments using LOEL concentrations of THI and silica NPs.

5. DISCUSSION

The rising application of nanoparticles (NPs) in both industry and consumer products has caused their concentration to build up in environmental repositories such as soil and sediments. Although much of nanotoxicology research has concentrated on immediate effects, the chronic impacts, particularly those that manifest over time, are not well understood This doctoral thesis explores the prolonged impacts of silica nanoparticles on *Caenorhabditis elegans*, with a focus on neurodegeneration, behavioral impairments, and underlying mechanisms. The show that silica NPs lead to significant neuronal loss in GABAergic D-type motor neurons, and decreased locomotion. Additionally, silica NPs accelerate protein aggregation in serotonergic and dopaminergic neurons, which correlates with increased behavioral defects.

Proteomic analysis revealed that exposure to silica NPs significantly downregulates key genes involved in the glutamate metabolic process, essential for GABA synthesis. The notable reduction in *gdh-1* (Glutamate dehydrogenase) and *got-1.2* (Glutamate oxaloacetate transaminase) confirm the observed loss of GABAergic neurons. Although it remains to be determined if lack of GABA causes nano silica-induced degradation of anterior- and posterior-most D-type motor neurons. Furthermore, the development of a single-worm tracking (SWT) platform now enables the automated and scalable quantification of thrashing rates and locomotion patterns. This platform proved effective across various experimental conditions, overcoming the limitations of manual methods and opening up possibilities for high-throughput screening of xenobiotics, drugs, and mutant strains of *C. elegans* under different environmental conditions and concentrations.

5.1 Loss of GABAergic D-type motor neurons constitutes a novel crucial characteristic of neurodegeneration in *Caenorhabditis elegans*.

Previous studies showed that silica NPs penetrated the pharyngeal tissue and vulval cells of *Caenorhabditis elegans* hermaphrodites. This translocation of silica NPs was associated with a premature decline in pump frequency and an early onset of the internal hatch phenotype (Pluskota et al., 2009; Scharf et al., 2013). Additionally, silica NPs have been shown to induce amyloid structures in the nucleus or nucleolus of individual intestinal cells (Scharf et al., 2013). Moreover, silica NPs promoted protein aggregation in single serotonergic and dopaminergic neurons (Limke et al., 2024; Piechulek & von Mikecz, 2018; Scharf et al., 2016) . In this thesis, these findings are corroborated, confirming the effects of silica NPs in *C. elegans* on protein aggregation, neurodegeneration and neurotransmission. However, this study extends the understanding of

silica NP-induced neurodegeneration by highlighting significant loss of specific GABAergic neurons. Complete anterior- and posterior-most GABAergic D-type motor neurons of the ventral axis are lost after exposure to nano silica. This novel finding indicates that the neurotoxic effects of silica NPs are more extensive than previously recognized, affecting a broader range of neuronal types and leading to additional neurodegenerative outcomes, namely neuronal loss.

When GABAergic reporter worms were treated with silica NPs, we observed significant loss of GABAergic neurons, particularly in the anterior regions (DD1, VD1, VD3) and posterior regions (DD6, VD12, VD13). Previous studies have demonstrated that the GABAergic nervous system is vulnerable to damage from various metal nanoparticles and heavy metals. Particularly, neurodegeneration and structural abnormalities in GABAergic neurons have been reported following exposure to Pb, Hg, and Cu (Du & Wang, 2009). The neurotoxicity of CdTe QDs (Cadmium Telluride Quantum Dots) has been observed at concentrations of 0.1–1 µg/L, affecting both the development and function of RME motor neurons in nematodes (Zhao et al., 2015). Additionally, *C. elegans* fed with *E. coli* pre-treated with ZnO-NPs exhibited impaired locomotive behaviors, due to damage to D-type GABAergic motor neurons (How & Huang, 2023). Our study specifically highlights the impact of silica NPs on D-type motor neurons (VDs and DDs), rather than RME, DVB, or AVL neurons within the GABAergic nervous system. The silica NPs used in our experiments were sized approximately 50 nm in diameter, significantly larger than the CdTe QDs (3.6 nm) used in study of Zhao et al., 2015. This size difference may explain the lack of observed effects on RME neurons in our experiments. The size of nanoparticles plays a crucial role in their biological effects. In fact, our findings, in conjunction with other research (Limke et al., 2024; Piechulek & von Mikecz, 2018; Scharf et al., 2016), indicate that BULK silica with a diameter of 500 nm does not exhibit significant effects on *C. elegans* which corroborates the nano-specificity of the neurotoxic silica effects.

The findings from this thesis, which demonstrate significant GABAergic neuronal loss in *C. elegans* treated with silica nanoparticles, may provide valuable insights into the potential mechanisms underlying epilepsy in humans. GABAergic neurons are essential for maintaining inhibitory neurotransmission, and their dysfunction or loss is a hallmark of certain types of epilepsy, such as temporal lobe epilepsy (Sarlo & Holton, 2021). The observed GABAergic neuronal loss in *C. elegans* mirrors the neuronal losses seen in human epilepsy, suggesting that similar pathological processes may occur. This connection is particularly relevant as it underscores the critical role of GABAergic neurons in preventing the hyperexcitability of neural circuits, which can lead to seizures. By demonstrating how environmental factors like silica

nanoparticles can induce GABAergic neuronal loss, our research highlights a possible environmental risk factor for epilepsy, thereby expanding our understanding of the disease's etiology.

Furthermore, our study's findings may have direct implications for understanding epilepsy in humans. In *C. elegans*, the loss of GABAergic neurons leads to altered motor behaviors, indicative of an imbalance between excitatory and inhibitory signals. This excitatory - inhibitory imbalance is a fundamental mechanism in the development of epileptic seizures in humans (Bonansco & Fuenzalida, 2016). The hyperexcitability of neural circuits resulting from GABAergic dysfunction can trigger seizure activity, highlighting the importance of maintaining a balanced neurotransmitter system for normal brain function. These parallels between *C. elegans* and human epilepsy not only validate the use of this model organism in studying neurodegenerative diseases but also point to the broader implications of environmental neurotoxins in contributing to neurological disorders. Ethosuximide, known for its efficacy in epilepsy therapy (Buschhoff et al., 2022; Fedotova et al., 2019), has also been shown to reduce serotonergic neurodegeneration induced by nano silica (Scharf et al., 2016). Our next step is to test ethosuximide and GABAergic agonists such as muscimol and gaboxadol on reporter worms for GABAergic neurons using the SWT platform to determine if this drug can rescue the reduced thrashing behavior caused by nano silica exposure.

Thiacloprid has been found to induce paralysis in *C. elegans*, while inorganic mercury does not elicit the same effect (Scharpf et al., 2021). This observation suggests that the neurotoxic mechanisms of these two substances differ significantly. Thiacloprid's ability to induce paralysis could be hypothesized to result from its impairment of neuronal transmission, specifically targeting GABAergic neurons. GABAergic neurons are crucial for inhibitory signaling in the nervous system, and their dysfunction can lead to an imbalance between excitation and inhibition, resulting in motor control issues such as paralysis. In contrast, inorganic mercury may affect other cellular processes or neuron types that do not directly result in paralysis. Thus, the specific impact of thiacloprid on GABAergic neurons highlights its potential to disrupt inhibitory neurotransmission, further emphasizing the need to explore the neural signaling pathways involved in its neurotoxicity with the SWT platform.

5.2 Altered gene expression of GABAergic reporter worms induced by silica nanoparticles.

To analyze the proteomics results, we used the PANTHER classification system (http://www.pantherdb.org, Mi et al., 2019) for large-scale genome and gene function analysis of

4-day-old worms treated with silica nanoparticles compared to mock controls. PANTHER offers significant advantages over individual gene analysis by providing comprehensive functional annotation and statistical tests, categorizing genes into GO terms and protein classes. This approach enables the understanding of broader biological roles and interactions that might be missed with isolated gene analysis. In our study, PANTHER revealed that nano silica-treated worms exhibited significant downregulation in biological processes related to ribosome biogenesis, metabolic processes, and cellular respiration, indicating potential suppression of protein synthesis, energy production, and overall metabolic activity. Notably, glutamate metabolism, crucial for neuronal GABAergic synthesis, was also downregulated.

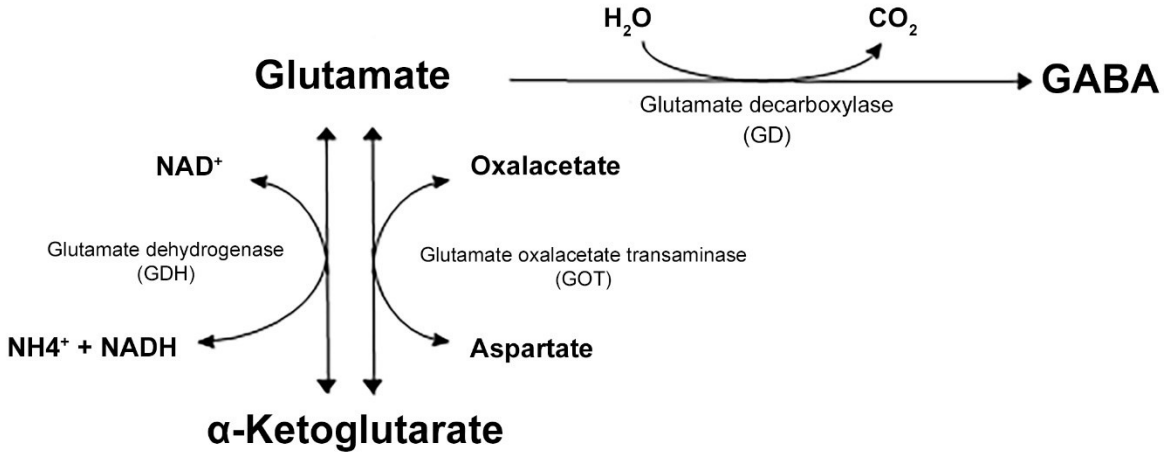

Figure 21. Metabolism of glutamate. Adapted from J. Centelles, 2016

From proteomics results, we found that GO group of glutamate metabolic process has been downregulated. Especially, Glutamate dehydrogenase *gdh-1* and *got-1.2* (Glutamate oxaloacetate transaminase). The downregulation of *gdh-1* (Glutamate dehydrogenase) and *got-1.2* (Glutamate oxaloacetate transaminase) is particularly significant in understanding the loss of GABAergic neurons following silica nanoparticle exposure. *gdh-1* plays a crucial role in the conversion of glutamate to α-ketoglutarate, a key metabolic process that also links to the synthesis of GABA, the primary inhibitory neurotransmitter in the nervous system (Figure 21). The downregulation of *gdh-1* suggests a bottleneck in this conversion process, potentially leading to decreased availability of GABA. This reduction can impair inhibitory signaling, leading to neuronal hyperactivity and subsequent neurodegeneration. In mice, GDH deficiency in the central nervous system disrupts glutamate homeostasis and excitatory/inhibitory balance in hippocampal subregions, leading to impaired hippocampal-prefrontal cortex connectivity and associated

behavioral deficits (Lander et al., 2020). Protein expression levels of the GABA synthesis enzyme glutamate decarboxylase (GAD) GAD67 were decreased in the ventral hippocampus as well

Similarly, *got-1.2* is essential for the transamination reaction that also involves glutamate, converting it to α-ketoglutarate and aspartate (Figure 21). This enzyme is important in amino acid metabolism and neurotransmitter cycling. Downregulation of *got-1.2* disrupts this balance, further impairing glutamate processing and GABA synthesis. The dual impact of reduced *gdh-1* and *got-1.2* expression exacerbates the shortage of GABA, compromising the inhibitory control exerted by GABAergic neurons. Insufficient GABA levels can lead to an imbalance between excitatory and inhibitory neurotransmission, increasing neuronal stress and vulnerability to damage. This metabolic disruption aligns with the observed loss of GABAergic neurons, as they are particularly sensitive to changes in neurotransmitter supply and metabolic stress. Thus, the downregulation of *gdh-1* and *got-1.2* directly correlates with the impaired synthesis of GABA, contributing significantly to the degeneration of GABAergic neurons in *C. elegans* exposed to silica nanoparticles.

5.3 Resilience of specific proteins to silica nanoparticles-induced changes

The concept of resilience in biological systems often pertains to the ability of certain components to maintain their function and integrity despite exposure to stressors. In the context of this thesis, resilience refers to specific proteins that remain unaffected or minimally affected by silica nanoparticle exposure. Among 11 genes found, *rpn-6.1, unc-87, and plin-1* show insignificant differential expression in the proteomic analysis following silica nanoparticles exposure in *C. elegans*. This observation suggests that these genes maintain stable expression levels despite the environmental stress posed by silica NPs, which can provide insights into cellular resilience and potential therapeutic targets.

RPN-6.1 is a regulatory subunit of the proteasome, crucial for protein degradation and maintaining protein quality control. Its stable expression implies that a part of proteasome system continues to function effectively, preventing the accumulation of damaged or misfolded proteins. In the thesis context, this resilience is essential for cellular health, particularly under stress conditions that can increase the load of damaged proteins. The implication is that enhancing proteasome activity could be a protective strategy against environmental and pathological stressors that disrupt protein homeostasis. A study of Vilchez et al. has shown that ectopic expression of *rpn-6* to provides resistance to proteotoxic stress and prolong lifespan, indicating that *rpn-6* may be a promising candidate for mitigating deficiencies associated with age-related protein homeostasis disorders

(Vilchez et al., 2012). This finding leads to a future investigation using the single-worm tracking (SWT) platform to analyze the locomotion of mutants in the *rpn-6* family, assessing their sensitivity to nano silica treatment.

UNC-87 plays a vital role in the assembly and regulation of muscle filaments (Ono et al., 2015), contributing to the structural integrity and function of neuromuscular junctions. Its stable expression under silica NP exposure indicates that the neuromuscular system maintains its functionality, ensuring coordinated movement and response to stimuli. This resilience highlights the importance of structural proteins in maintaining cellular and organismal health under stress. Enhancing the function of structural proteins like *unc-87* could be beneficial in developing treatments for neuromuscular disorders and mitigating the impact of environmental toxins on muscle and nerve function.

PLIN-1 (perilipin-1 homolog) is involved in the regulation of lipid storage and mobilization, essential for maintaining energy balance (Chughtai et al., 2015). The stable expression of *plin-1* under silica NP exposure suggests that lipid metabolism processes are preserved, allowing cells to access energy reserves as needed. This finding underscores the robustness of lipid regulatory mechanisms, which is crucial for cellular survival during metabolic stress.

The resilience of these specific proteins to silica NP-induced changes underscores the robustness of certain cellular pathways and mechanisms in maintaining homeostasis under stress conditions. These resilient proteins enable cells to continue critical functions such as protein synthesis, degradation, metabolism, structural integrity, and communication despite the presence of potentially disruptive nanoparticles. Understanding the mechanisms underlying this resilience can inform the development of strategies to enhance cellular defenses, mitigate the adverse effects of nanoparticle exposure, and improve overall cellular health and function.

5.4 Utility and Advancements of the single worm tracking platform

The development and implementation of the single worm tracking (SWT) platform represent a significant advancement in the study of nanoparticle-induced effects on *C. elegans*. This innovative platform provides several key benefits over traditional methods, enabling more precise, efficient, and high-throughput analysis of worm behavior and locomotion.

Neurotransmission, agonists, antagonists and neurotoxicants

The SWT platform is highly applicable for studying neurotransmission and the effects of agonists and antagonists on *C. elegans*, allowing for detailed analysis of movement phenotypes such as thrashing and crawling. By tracking the locomotion of worms exposed to these compounds, it enables the assessment of impact on neural circuits and synaptic transmission. For example, the effect of the acetylcholine esterase inhibitor aldicarb on cholinergic synaptic transmission can be evaluated efficiently. Aldicarb prevents the breakdown of acetylcholine, leading to an accumulation that causes muscle contraction and subsequent paralysis. By analyzing crawling movies at specified intervals, aldicarb-induced paralysis was analyzed to assess cholinergic synaptic efficiency (Oh & Kim, 2017). The SWT can analyze multiple conditions simultaneously using multi-well plates, making it ideal for screening various agonists and antagonists. This application is important for understanding the role of neurotransmitters and for identifying potential compounds that modulate pollutant-induced defects of neurotransmission.

Aging, Mutants, Disease Models of C. elegans

The SWT platform is a powerful tool for studying aging, mutants, and disease models in *C. elegans*. The external exposome refers to the totality of environmental exposures, including chemicals, and non-chemical factors such as temperature, that an individual encounters throughout the lifetime and how these exposures affect its health. It can track large populations of worms simultaneously, making it ideal for high-throughput screening of genetic mutants and transgenic lines that model human diseases. Movement decline associated with aging can be analyzed when comparing the locomotion of young and old worms (Koopman et al., 2020). The platform can also be used to study neurodegenerative disease models. Worms expressing human disease genes such as amyloid-beta (Aβ) or alpha-synuclein in their muscles show reduced thrashing compared to controls, which aligns with findings in human neurodegenerative diseases (Koopman et al., 2020). The ability to analyze multiple behavioral parameters simultaneously, such as speed, paralysis, and bending frequency, provides comprehensive insights into the phenotypic effects of aging and genetic mutations.

Exposome Factors and Their Combination

The SWT can be utilized to study the effects of various exposome factors and their combinations on *C. elegans*. The external exposome refers to the totality of environmental exposures, including chemicals, and non-chemical factors such as temperature, that an individual encounters throughout the lifetime and how these exposures affect its health. SWT can be used to analyze

thrashes of exposed worms to different environmental stressors, such as temperature changes, toxins, or pollutants, and monitor their behavior to assess the impact on locomotion and overall fitness. Temperature has been proven to have serious impact on the locomotion of an Alzheimer's disease *C. elegans* model (Scharpf et al., 2022). By tracking the movement of worms exposed to single or combined factors (temperature and xenobiotics), the SWT can provide valuable data on the cumulative effects of multiple environmental exposures on health span in *C. elegans* amyloid aggregation disease models.

Wild Nematodes

The SWT can be applied to study the behavior and physiology of wild nematodes in addition to laboratory strains. The platform's ability to analyze large populations collected from nature simultaneously is particularly beneficial for ecological studies, where understanding the diversity and adaptability of nematodes in different habitats is essential. The SWT can help identify behavioral adaptations that wild nematodes have developed in response to their environments, providing a deeper understanding of ecological dynamics and evolutionary processes.

LOELs Concentration of Pollutants

The SWT platform is suitable for determining the Lowest Effect Levels (LOELs) of pollutants by exposing *C. elegans* to varying concentrations of pollutants and analyzing their movement behaviors. This platform can accelerate the manual thrashing analysis in behavior changes, such as reduced thrashing rate or decreased percentage of swimming worms, induced by silica nanoparticles, nano silver, or thiacloprids, indicating the onset of toxic effects at low pollutant concentrations (Piechulek & von Mikecz, 2018; Scharpf et al., 2022). This information is critical for environmental monitoring and risk assessment, as it helps establish safe exposure limits for various pollutants. The ability to handle high-throughput analysis ensures that large datasets can be generated efficiently, providing robust data for regulatory purposes.

6. CONCLUSIONS

This doctoral thesis investigates the long-term effects of silica nanoparticles on *Caenorhabditis elegans*, focusing on neurodegeneration, behavioral impairments and underlined molecular mechanisms. The study showed that exposure to silica NPs leads to significant neuronal loss in GABAergic D-type motor neurons, resulting in reduced locomotion. Additionally, silica NPs accelerate protein aggregation in serotonergic and dopaminergic neurons, correlating with increased behavioral defects.

Proteomic analysis revealed that silica NP exposure significantly downregulates key genes involved in the glutamate metabolic process, crucial for GABA synthesis. The notable reduction in *gdh-1* (Glutamate dehydrogenase) and *got-1.2* (Glutamate oxaloacetate transaminase) may play a role in the loss of GABAergic neurons.

The development of a single-worm tracking (SWT) platform allowed for automated, scalable quantification of thrashing behavior and locomotion patterns. This platform proved robust across various experimental conditions, addressing the limitations of manual methods and facilitating high-throughput screening of pollutants, drugs, aging processes, and various mutants and disease models in *C. elegans*.

Future research should explore the molecular pathways underlying the resilience of certain proteins to silica NP exposure and investigate the synergistic effects of silica NPs with other environmental pollutants or exposome factors. This approach aims to enhance our understanding of how xenobiotics interact with neuronal signaling pathways in organisms within a complex environmental context.

BILIOGRAPHY

Altun, Z. F., & Hall, D. H. (2009). Introduction. *In WormAtlas*. https://doi.org/doi:10.3908/wormatlas.1.1

Apfeld, J., & Kenyon, C. (1999). Regulation of lifespan by sensory perception in Caenorhabditis elegans. *Nature*, *402*(6763), 804–809. https://doi.org/10.1038/45544

Bamber, B. A., Beg, A. A., Twyman, R. E., & Jorgensen, E. M. (1999). The Caenorhabditis elegans unc-49 locus encodes multiple subunits of a heteromultimeric GABA receptor. *The Journal of Neuroscience : The Official Journal of the Society for Neuroscience*, *19*(13), 5348–5359. https://doi.org/10.1523/JNEUROSCI.19-13-05348.1999

Bargmann, C. I. (1998). Neurobiology of the Caenorhabditis elegans genome. *Science (New York, N.Y.)*, *282*(5396), 2028–2033. https://doi.org/10.1126/SCIENCE.282.5396.2028

Bayda, S., Adeel, M., Tuccinardi, T., Cordani, M., & Rizzolio, F. (2019). The History of Nanoscience and Nanotechnology: From Chemical-Physical Applications to Nanomedicine. *Molecules (Basel, Switzerland)*, *25*(1). https://doi.org/10.3390/MOLECULES25010112

Beg, A. A., & Jorgensen, E. M. (2003). EXP-1 is an excitatory GABA-gated cation channel. *Nature Neuroscience 2003 6:11*, *6*(11), 1145–1152. https://doi.org/10.1038/nn1136

Bessa, M. J., Brandão, F., Viana, M., Gomes, J. F., Monfort, E., Cassee, F. R., Fraga, S., & Teixeira, J. P. (2020). Nanoparticle exposure and hazard in the ceramic industry: an overview of potential sources, toxicity and health effects. *Environmental Research*, *184*, 109297. https://doi.org/10.1016/J.ENVRES.2020.109297

Bonansco, C., & Fuenzalida, M. (2016). Plasticity of Hippocampal Excitatory-Inhibitory Balance: Missing the Synaptic Control in the Epileptic Brain. *Neural Plasticity*, *2016*. https://doi.org/10.1155/2016/8607038

Brenner, S. (1974). The genetics of Caenorhabditis elegans. *Genetics*, *77*(1), 71–94. https://doi.org/10.1093/GENETICS/77.1.71

Buschhoff, A. S., Scherließ, R., de Mooij-van Malsen, J. G., Schiffelholz, T., Stephani, U., & Wulff, P. (2022). Intrathecal application of ethosuximide is highly efficient in suppressing seizures in a genetic model of absence epilepsy. *Epilepsy Research*, *184*. https://doi.org/10.1016/J.EPLEPSYRES.2022.106967

Carroll, B., Otten, E. G., Manni, Di., Stefanatos, R., Menzies, F. M., Smith, G. R., Jurk, Di., Kenneth, N., Wilkinson, S., Passos, J. F., Attems, J., Veal, E. A., Teyssou, E., Seilhean, D., Millecamps, S., Eskelinen, E. L., Bronowska, A. K., Rubinsztein, D. C., Sanz, A., & Korolchuk, V. I. (2018). Oxidation of SQSTM1/p62 mediates the link between redox state and protein homeostasis. *Nature Communications 2018 9:1*, *9*(1), 1–11. https://doi.org/10.1038/s41467-017-02746-z

Chen, M., & Von Mikecz, A. (2005). Formation of nucleoplasmic protein aggregates impairs nuclear function in response to SiO2 nanoparticles. *Experimental Cell Research*, *305*(1), 51–62. https://doi.org/10.1016/J.YEXCR.2004.12.021

Chiti, F., & Dobson, C. M. (2017). Protein misfolding, amyloid formation, and human disease: A summary of progress over the last decade. *Annual Review of Biochemistry*, *86*(Volume 86, 2017), 27–68. https://doi.org/10.1146/ANNUREV-BIOCHEM-061516-045115/1

Chughtai, A. A., Kaššak, F., Kostrouchová, M., Novotný, J. P., Krause, M. W., Saudek, V., Kostrouch, Z., & Kostrouchová, M. (2015). Perilipin-related protein regulates lipid metabolism in C. elegans. *PeerJ*, *3*(9). https://doi.org/10.7717/PEERJ.1213

Corsi, A. K., Wightman, B., & Chalfie, M. (2015). A Transparent Window into Biology: A Primer on Caenorhabditis elegans. *Genetics*, *200*(2), 387–407. https://doi.org/10.1534/GENETICS.115.176099

Cuervo, A. M., & Wong, E. (2014). Chaperone-mediated autophagy: roles in disease and aging. *Cell Research*, *24*(1), 92–104. https://doi.org/10.1038/CR.2013.153

David, D. C., Ollikainen, N., Trinidad, J. C., Cary, M. P., Burlingame, A. L., & Kenyon, C. (2010). Widespread Protein Aggregation as an Inherent Part of Aging in C. elegans. *PLOS Biology*, *8*(8), e1000450. https://doi.org/10.1371/JOURNAL.PBIO.1000450

Du, M., & Wang, D. (2009). The neurotoxic effects of heavy metal exposure on GABAergic nervous system in nematode Caenorhabditis elegans. *Environmental Toxicology and Pharmacology*, *27*(3), 314–320. https://doi.org/10.1016/j.etap.2008.11.011

Dunker, A. K., Silman, I., Uversky, V. N., & Sussman, J. L. (2008). Function and structure of inherently disordered proteins. *Current Opinion in Structural Biology*, *18*(6), 756–764. https://doi.org/10.1016/J.SBI.2008.10.002

Fedotova, I. B., Perepelkina, O. V., Nikolaev, G. M., Surina, N. M., & Poletaeva, I. I. (2019). Effect of Ethosuximide on Audiogenic Epilepsy in Krushinsky-Molodkina Rats. *Bulletin of Experimental Biology and Medicine*, *167*(4), 464–466. https://doi.org/10.1007/S10517-019-04550-9

Finka, A., Mattoo, R. U. H., & Goloubinoff, P. (2016). Experimental Milestones in the Discovery of Molecular Chaperones as Polypeptide Unfolding Enzymes. *Annual Review of Biochemistry*, *85*(Volume 85, 2016), 715–742. https://doi.org/10.1146/ANNUREV-BIOCHEM-060815-014124/CITE/REFWORKS

Genome sequence of the nematode C. elegans: A platform for investigating biology. (1998). *Science*, *282*(5396), 2012–2018. https://doi.org/10.1126/SCIENCE.282.5396.2012

Gjorgjieva, J., Biron, D., & Haspel, G. (2014). Neurobiology of caenorhabditis elegans locomotion: Where do we stand? *BioScience*, *64*(6), 476–486. https://doi.org/10.1093/biosci/biu058

Goodman, M. B. (2006). Mechanosensation. *WormBook : The Online Review of C. Elegans Biology*, 1–14. https://doi.org/10.1895/WORMBOOK.1.62.1

Goswami, P., Mathur, J., & Srivastava, N. (2022). Silica nanoparticles as novel sustainable approach for plant growth and crop protection. *Heliyon*, *8*(7). https://doi.org/10.1016/J.HELIYON.2022.E09908

Hamer, G., Matilainen, O., & Holmberg, C. I. (2010). A photoconvertible reporter of the ubiquitin-proteasome system in vivo. *Nature Methods*, *7*(6), 473–478. https://doi.org/10.1038/NMETH.1460

Hartl, F. U. (2017). Protein misfolding diseases. *Annual Review of Biochemistry*, *86*(Volume 86, 2017), 21–26. https://doi.org/10.1146/ANNUREV-BIOCHEM-061516-044518/CITE/REFWORKS

Hemmerich, P. H., & von Mikecz, A. H. (2013). Defining the Subcellular Interface of Nanoparticles by Live-Cell Imaging. *PLOS ONE*, *8*(4), e62018. https://doi.org/10.1371/JOURNAL.PONE.0062018

Hipp, M. S., Kasturi, P., & Hartl, F. U. (2019). The proteostasis network and its decline in ageing. *Nature Reviews. Molecular Cell Biology*, *20*(7), 421–435. https://doi.org/10.1038/S41580-019-0101-Y

How, C. M., & Huang, C. W. (2023). Dietary Transfer of Zinc Oxide Nanoparticles Induces Locomotive Defects Associated with GABAergic Motor Neuron Damage in Caenorhabditis elegans. *Nanomaterials (Basel, Switzerland)*, *13*(2). https://doi.org/10.3390/NANO13020289

J. Centelles, J. (2016). Glutamate transporters: the regulatory proteins for excitatory/excitotoxic glutamate in brain. *Journal of Translational Science*, *2*(1). https://doi.org/10.15761/JTS.1000123

White, J. G., Southgate, E., Thomson, J. N., & Brenner, S. (1986). The structure of the nervous system of the nematode Caenorhabditis elegans. *Philosophical Transactions of the Royal Society of London. B, Biological Sciences*, *314*(1165), 1–340. https://doi.org/10.1098/rstb.1986.0056

Jin, Y., Hoskins, R., & Horvitz, H. R. (1994). Control of type-D GABAergic neuron differentiation by C. elegans UNC-30 homeodomain protein. *Nature 1994 372:6508*, *372*(6508), 780–783. https://doi.org/10.1038/372780a0

Jin, Y., Jorgensen, E., Hartwieg, E., & Horvitz, H. R. (1999). The Caenorhabditis elegans gene unc-25 encodes glutamic acid decarboxylase and is required for synaptic transmission but not synaptic development. *The Journal of Neuroscience : The Official Journal of the Society for Neuroscience*, *19*(2), 539–548. https://doi.org/10.1523/JNEUROSCI.19-02-00539.1999

Johari, S. A. (2014). Toxicity Effect of Colloidal Silver Nanoparticles on Fertilization Capacity and Reproduction Success of Rainbow Trout (Oncorhynchus mykiss). *Journal of Nanomedicine Research*, *Volume 1*(Issue 1). https://doi.org/10.15406/JNMR.2014.01.00001

Jorgensen, E. M. (2005). Gaba. In *WormBook : the online review of C. elegans biology* (Vol. 1). https://doi.org/10.1895/wormbook.1.14.1

Kaupmann, K., Huggel, K., Heid, J., Flor, P. J., Bischoff, S., Mickel, S. J., McMaster, G., Angst, C., Bittiger, H., Froestl, W., & Bettler, B. (1997). Expression cloning of GABAB receptors uncovers similarity to metabotropic glutamate receptors. *Nature 1997 386:6622*, *386*(6622), 239–246. https://doi.org/10.1038/386239a0

Kaushik, S., & Cuervo, A. M. (2015). Proteostasis and aging. *Nature Medicine 2015 21:12*, *21*(12), 1406–1415. https://doi.org/10.1038/nm.4001

Khanna, P., Ong, C., Bay, B. H., & Baeg, G. H. (2015). Nanotoxicity: An Interplay of Oxidative Stress, Inflammation and Cell Death. *Nanomaterials 2015, Vol. 5, Pages 1163-1180*, *5*(3), 1163–1180. https://doi.org/10.3390/NANO5031163

Khataee, A., Movafeghi, A., Nazari, F., Vafaei, F., Dadpour, M. R., Hanifehpour, Y., & Joo, S. W. (2014). The toxic effects of l-Cysteine-capped cadmium sulfide nanoparticles on the aquatic plant Spirodela polyrrhiza. *Journal of Nanoparticle Research*, *16*(12). https://doi.org/10.1007/S11051-014-2774-7

Klaips, C. L., Jayaraj, G. G., & Hartl, F. U. (2018). Pathways of cellular proteostasis in aging and disease. *Journal of Cell Biology*, *217*(1), 51–63. https://doi.org/10.1083/jcb.201709072

Koopman, M., Peter, Q., Seinstra, R. I., Perni, M., Vendruscolo, M., Dobson, C. M., Knowles, T. P. J., & Nollen, E. A. A. (2020). Assessing motor-related phenotypes of Caenorhabditis elegans with the wide field-of-view nematode tracking platform. In *Nature Protocols* (Vol. 15, Issue 6). Springer US. https://doi.org/10.1038/s41596-020-0321-9

Lander, S. S., Chornyy, S., Safory, H., Gross, A., Wolosker, H., & Gaisler-Salomon, I. (2020). Glutamate dehydrogenase deficiency disrupts glutamate homeostasis in hippocampus and prefrontal cortex and impairs recognition memory. *Genes, Brain, and Behavior*, *19*(6). https://doi.org/10.1111/GBB.12636

Limke, A., Poschmann, G., Stühler, K., Petzsch, P., Wachtmeister, T., & Mikecz, A. Von. (2024). *Silica Nanoparticles Disclose a Detailed Neurodegeneration Profile throughout the Life Span of a Model Organism*. 135–153.

Ma, C., Yu, R., Li, J., Chao, J., & Liu, P. (2023). Targeting proteostasis network in osteoporosis: Pathological mechanisms and therapeutic implications. *Ageing Research Reviews*, *90*(March), 102024. https://doi.org/10.1016/j.arr.2023.102024

McIntire, S. L., Reimer, R. J., Schuske, K., Edwards, R. H., & Jorgensen, E. M. (1997). Identification and characterization of the vesicular GABA transporter. *Nature 1997 389:6653*, *389*(6653), 870–876. https://doi.org/10.1038/39908

McIntire, S. L., Jorgensen, E., Kaplan, J., & Horvitz, H. R. (1993). The GABAergic nervous system of Caenorhabditis elegans. *Nature 1993 364:6435*, *364*(6435), 337–341. https://doi.org/10.1038/364337a0

Mebert, A. M., Baglole, C. J., Desimone, M. F., & Maysinger, D. (2017). Nanoengineered silica: Properties, applications and toxicity. *Food and Chemical Toxicology : An International Journal Published for the British Industrial Biological Research Association*, *109*(Pt 1), 753–770. https://doi.org/10.1016/J.FCT.2017.05.054

Melo, J. A., & Ruvkun, G. (2012). Inactivation of conserved C. elegans genes engages pathogen- and xenobiotic-associated defenses. *Cell*, *149*(2), 452–466. https://doi.org/10.1016/J.CELL.2012.02.050

Mi, H., Muruganujan, A., Huang, X., Ebert, D., Mills, C., Guo, X., & Thomas, P. D. (2019). Protocol Update for large-scale genome and gene function analysis with the PANTHER classification system (v.14.0). *Nature Protocols*, *14*(3), 703–721. https://doi.org/10.1038/s41596-019-0128-8

Michaelson, L. (2000). C. elegans: A Practical Approach. *Heredity 2000 85:1*, *85*(1), 99–99. https://doi.org/10.1046/j.1365-2540.2000.0745d.x

Mikecz, A. Von. (2023). Elegant Nematodes Improve Our Understanding of Human Neuronal Diseases , the Role of Pollutants and Strategies of Resilience. *Environmental Science & Technology*. https://doi.org/10.1021/acs.est.3c04580

Moon, C., Park, H. J., Choi, Y. H., Park, E. M., Castranova, V., & Kang, J. L. (2010). Pulmonary Inflammation After Intraperitoneal Administration of Ultrafine Titanium Dioxide (TiO2) At Rest or in Lungs Primed with Lipopolysaccharide. *Journal of Toxicology and Environmental Health, Part A*, *73*(5–6), 396–409. https://doi.org/10.1080/15287390903486543

Morley, J. F., Brignull, H. R., Weyers, J. J., & Morimoto, R. I. (2002). The threshold for polyglutamine-expansion protein aggregation and cellular toxicity is dynamic and influenced by aging in Caenorhabditis elegans. *Proceedings of the National Academy of Sciences of the United States of America*, *99*(16), 10417–10422. https://doi.org/10.1073/PNAS.152161099

Napierska, D., Thomassen, L. C. J., Lison, D., Martens, J. A., & Hoet, P. H. (2010). The nanosilica hazard: another variable entity. *Particle and Fibre Toxicology 2010 7:1*, *7*(1), 1–32. https://doi.org/10.1186/1743-8977-7-39

Neher, D. A. (2001). Role of Nematodes in Soil Health and Their Use as Indicators. *Journal of Nematology*, *33*(4), 161. /pmc/articles/PMC2620512/?report=abstract

Nemmar, A., Albarwani, S., Beegam, S., Yuvaraju, P., Yasin, J., Attoub, S., & Ali, B. H. (2014). Amorphous silica nanoparticles impair vascular homeostasis and induce systemic inflammation. *International Journal of Nanomedicine*, *9*(1), 2279–2789. https://doi.org/10.2147/IJN.S52818

Nemmar, A., Yuvaraju, P., Beegam, S., Yasin, J., Kazzam, E. E., & Ali, B. H. (2016). Oxidative stress, inflammation, and DNA damage in multiple organs of mice acutely exposed to amorphous silica nanoparticles. *International Journal of Nanomedicine*, *11*, 919–928. https://doi.org/10.2147/IJN.S92278

Oh, K. H., & Kim, H. (2017). Aldicarb-induced Paralysis Assay to Determine Defects in Synaptic Transmission in Caenorhabditis elegans. *Bio-Protocol*, *7*(14). https://doi.org/10.21769/BIOPROTOC.2400

Oikonomou, G., & Shaham, S. (2011). The glia of Caenorhabditis elegans. *Glia*, *59*(9), 1253. https://doi.org/10.1002/GLIA.21084

Ono, K., Obinata, T., Yamashiro, S., Liu, Z., & Ono, S. (2015). UNC-87 isoforms, Caenorhabditis elegans calponin-related proteins, interact with both actin and myosin and regulate actomyosin contractility. *Molecular Biology of the Cell*, *26*(9), 1687–1698. https://doi.org/10.1091/MBC.E14-10-1483

Piechulek, A., & von Mikecz, A. (2018). Life span-resolved nanotoxicology enables identification of age-associated neuromuscular vulnerabilities in the nematode Caenorhabditis elegans. *Environmental Pollution*, *233*, 1095–1103. https://doi.org/10.1016/j.envpol.2017.10.012

Pluskota, A., Horzowski, E., Bossinger, O., & Von Mikecz, A. (2009). In Caenorhabditis elegans nanoparticle-bio-interactions become transparent: Silica-nanoparticles induce reproductive senescence. *PLoS ONE*, *4*(8). https://doi.org/10.1371/journal.pone.0006622

Powers, E. T., Morimoto, R. I., Dillin, A., Kelly, J. W., & Balch, W. E. (2009). Biological and chemical approaches to diseases of proteostasis deficiency. *Annual Review of Biochemistry*, *78*, 959–991. https://doi.org/10.1146/ANNUREV.BIOCHEM.052308.114844

Ross, C. A., & Poirier, M. A. (2004). Protein aggregation and neurodegenerative disease. *Nature Medicine 2004 10:7*, *10*(7), S10–S17. https://doi.org/10.1038/nm1066

Sarlo, G. L., & Holton, K. F. (2021). Brain concentrations of glutamate and GABA in human epilepsy: A review. *Seizure - European Journal of Epilepsy*, *91*, 213–227. https://doi.org/10.1016/J.SEIZURE.2021.06.028

Scharf, A., Gührs, K. H., & Von Mikecz, A. (2016). Anti-amyloid compounds protect from silica nanoparticle-induced neurotoxicity in the nematode C. elegans. *Nanotoxicology*, *10*(4), 426–435. https://doi.org/10.3109/17435390.2015.1073399

Scharf, A., Limke, A., Guehrs, K.-H., & von Mikecz, A. (2022). Pollutants corrupt resilience pathways of aging in the nematode C. elegans. *IScience*, *25*, 105027. https://doi.org/10.1016/j.isci.2022.105027

Scharf, A., Piechulek, A., & Von Mikecz, A. (2013). Effect of nanoparticles on the biochemical and behavioral aging phenotype of the nematode caenorhabditis elegans. *ACS Nano*, *7*(12), 10695–10703. https://doi.org/10.1021/nn403443r

Scharpf, I., Cichocka, S., Le, D. T., & von Mikecz, A. (2022). Peripheral neuropathy, protein aggregation and serotonergic neurotransmission: Distinctive bio-interactions of thiacloprid and thiamethoxam in the nematode Caenorhabditis elegans. *Environmental Pollution*, *314*(June), 120253. https://doi.org/10.1016/j.envpol.2022.120253

Schofield, P. R., Darlison, M. G., Fujita, N., Burt, D. R., Stephenson, F. A., Rodriguez, H., Rhee, L. M., Ramachandran, J., Reale, V., Glencorse, T. A., Seeburg, P. H., & Barnard, E. A. (1987). Sequence and functional expression of the GABAA receptor shows a ligand-gated receptor super-family. *Nature 1987 328:6127*, *328*(6127), 221–227. https://doi.org/10.1038/328221a0

Schopf, F. H., Biebl, M. M., & Buchner, J. (2017). The HSP90 chaperone machinery. *Nature Reviews Molecular Cell Biology 2017 18:6*, *18*(6), 345–360. https://doi.org/10.1038/nrm.2017.20

Schulenburg, H., & Félix, M. A. (2017). The Natural Biotic Environment of Caenorhabditis elegans. *Genetics*, *206*(1), 55–86. https://doi.org/10.1534/GENETICS.116.195511

Schuske, K., Beg, A. A., & Jorgensen, E. M. (2004). The GABA nervous system in C. elegans. *Trends in Neurosciences*, *27*(7), 407–414. https://doi.org/10.1016/j.tins.2004.05.005

Silva, B. F., Andreani, T., Gavina, A., Vieira, M. N., Pereira, C. M., Rocha-Santos, T., & Pereira, R. (2016). Toxicological impact of cadmium-based quantum dots towards aquatic biota: Effect of natural sunlight exposure. *Aquatic Toxicology*, *176*, 197–207. https://doi.org/10.1016/J.AQUATOX.2016.05.001

Soares, T. R., Reis, S. D., Pinho, B. R., Duchen, M. R., & Oliveira, J. M. A. (2019). Targeting the proteostasis network in Huntington's disease. *Ageing Research Reviews*, *49*, 92–103. https://doi.org/10.1016/J.ARR.2018.11.006

Teodoro, J. S., Silva, R., Varela, A. T., Duarte, F. V., Rolo, A. P., Hussain, S., & Palmeira, C. M. (2016). Low-dose, subchronic exposure to silver nanoparticles causes mitochondrial alterations in Sprague-Dawley rats. *Nanomedicine (London, England)*, *11*(11), 1359–1375. https://doi.org/10.2217/NNM-2016-0049

Varshney, L. R., Chen, B. L., Paniagua, E., Hall, D. H., & Chklovskii, D. B. (2011). Structural properties of the Caenorhabditis elegans neuronal network. *PLoS Computational Biology*, *7*(2). https://doi.org/10.1371/JOURNAL.PCBI.1001066

Vendruscolo, M., Knowles, T. P. J., & Dobson, C. M. (2011). Protein Solubility and Protein Homeostasis: A Generic View of Protein Misfolding Disorders. *Cold Spring Harbor Perspectives in Biology*, *3*(12), a010454. https://doi.org/10.1101/CSHPERSPECT.A010454

Vidal-Gade, A., Topper, S., Young, L., Crisp, A., Kressin, L., Elbel, E., Maples, T., Brauner, M., Erbguth, K., Axelrod, A., Gottschalk, A., Siegel, D., & Pierce-Shimomura, J. T. (2011). Caenorhabditis elegans selects distinct crawling and swimming gaits via dopamine and serotonin. *Proceedings of the National Academy of Sciences of the United States of America*, *108*(42), 17504–17509. https://doi.org/10.1073/PNAS.1108673108/SUPPL_FILE/SM08.MOV

Vilchez, D., Morantte, I., Liu, Z., Douglas, P. M., Merkwirth, C., Rodrigues, A. P. C., Manning, G., & Dillin, A. (2012). RPN-6 determines C. elegans longevity under proteotoxic stress conditions. *Nature*, *489*(7415), 263–268. https://doi.org/10.1038/NATURE11315

Walther, D. M., Kasturi, P., Zheng, M., Pinkert, S., Vecchi, G., Ciryam, P., Morimoto, R. I., Dobson, C. M., Vendruscolo, M., Mann, M., & Hartl, F. U. (2015). Widespread Proteome Remodeling and Aggregation in Aging C. elegans. *Cell*, *161*(4), 919–932. https://doi.org/10.1016/J.CELL.2015.03.032

Wang, J., Chen, C., Liu, Y., Jiao, F., Li, W., Lao, F., Li, Y., Li, B., Ge, C., Zhou, G., Gao, Y., Zhao, Y., & Chai, Z. (2008). Potential neurological lesion after nasal instillation of TiO2 nanoparticles in the anatase and rutile crystal phases. *Toxicology Letters*, *183*(1–3), 72–80. https://doi.org/10.1016/J.TOXLET.2008.10.001

Wang, Y., Kalinina, A., Sun, T., & Nowack, B. (2016). Probabilistic modeling of the flows and environmental risks of nano-silica. *Science of the Total Environment*, *545–546*, 67–76. https://doi.org/10.1016/j.scitotenv.2015.12.100

Xu, Y., Wang, N., Yu, Y., Li, Y., Li, Y. B., Yu, Y. B., Zhou, X. Q., & Sun, Z. W. (2014). Exposure to Silica Nanoparticles Causes Reversible Damage of the Spermatogenic Process in Mice. *PLOS ONE*, *9*(7), e101572. https://doi.org/10.1371/JOURNAL.PONE.0101572

Yu, Y., Duan, J., Yu, Y., Li, Y., Liu, X., Zhou, X., Ho, K. fai, Tian, L., & Sun, Z. (2014). Silica nanoparticles induce autophagy and autophagic cell death in HepG2 cells triggered by reactive oxygen species. *Journal of Hazardous Materials*, *270*, 176–186. https://doi.org/10.1016/J.JHAZMAT.2014.01.028

Ze, Y., Zheng, L., Zhao, X., Gui, S., Sang, X., Su, J., Guan, N., Zhu, L., Sheng, L., Hu, R., Cheng, J., Cheng, Z., Sun, Q., Wang, L., & Hong, F. (2013). Molecular mechanism of titanium dioxide nanoparticles-induced oxidative injury in the brain of mice. *Chemosphere*, *92*(9), 1183–1189. https://doi.org/10.1016/J.CHEMOSPHERE.2013.01.094

Zhang, Y., Lu, H., & Bargmann, C. I. (2005). Pathogenic bacteria induce aversive olfactory learning in Caenorhabditis elegans. *Nature 2006 438:7065*, *438*(7065), 179–184. https://doi.org/10.1038/nature04216

Zhao, Y., Wang, X., Wu, Q., Li, Y., & Wang, D. (2015). Translocation and neurotoxicity of CdTe quantum dots in RMEs motor neurons in nematode Caenorhabditis elegans. *Journal of Hazardous Materials*, *283*, 480–489. https://doi.org/10.1016/J.JHAZMAT.2014.09.063

Zhu, M., Tang, J., Shi, T., Ma, X., Wang, Y., Wu, X., Li, H., & Hua, R. (2022). Uptake, translocation and metabolism of imidacloprid loaded within fluorescent mesoporous silica nanoparticles in tomato (Solanum lycopersicum). *Ecotoxicology and Environmental Safety*, *232*, 113243. https://doi.org/10.1016/J.ECOENV.2022.113243

LIST OF ABBREVIATION

°C ..... Degrees Celsius

µ ..... Micro

µg ..... Microgram

µm ..... Micrometers

ANOVA ..... Analysis of Variance

ACh ..... Acetylcholine

C. elegans ..... *Caenorhabditis elegans*

dat-1 ..... Dopamine Transporter

DIC ..... Differential Interference Contrast

eef-1G ..... Elongation Factor 1-Gamma

GFP ..... : Green Fluorescent Protein

GO ..... Gene Ontology

H_2O ..... Water

haly-1 ..... Histidine ammonia-lyase

hphd-1 ..... Hydroxyacid-oxoacid transhydrogenase

idh-1 ..... Isocitrate Dehydrogenase

I-Hg ..... Inorganic Mercury

kg ..... Kilogram

kD ..... Kilo Dalton

L ..... Liter

lec-2 ..... Galectin Domain Protein

LOEL ..... Lowest-Observed-Effect Level

mg ..... Milligrams

mm ..... Millimeters

mL ..... Milliliters

MW ..... Molecular Weight

myo-3 ..... Myosin-3 (a gene in *C. elegans*)

NPs ..... Nanoparticles

oatr-1 ..... ornithine aminotransferase

PANTHER ..... Protein ANalysis THrough Evolutionary Relationships (a database)

pdha-1 ..... Pyruvate Dehydrogenase E1 Alpha

plin-1 ..... Perilipin-1 Homolog

polyQ ..... Polyglutamine

prdh-1 ..... proline dehydrogenase-1

rpn-6.1 ..... 26S Proteasome Regulatory Subunit

SD ..... Standard Deviation

SDS-PAGE ..... Sodium Dodecyl Sulfate Polyacrylamide Gel Electrophoresis

SHSP ..... Small Heat Shock Protein

SWT ..... Single worm tracking

THI ..... Thiacloprid

TMX ..... Thiamethoxam

tph-1 ..... Tryptophan Hydroxylase

unc-47 ..... Uncoordinated-47

unc-87 ..... Uncoordinated-87

WF-NTP ..... Wide Field Nematode Tracking Platform

LIST OF FIGURES

ACKNOWLEDGEMENTS

I would like to extend my heartfelt gratitude to everyone who supported me throughout my PhD journey at the IUF – Leibniz Research Institute for Environmental Medicine and Heinrich Heine University in Germany!

My deepest thanks go to Prof. Dr. rer. nat. Anna von Mikecz. I am grateful for the opportunity to work on such an interesting topic and for your intensive and dedicated supervision and support throughout my doctoral thesis.

I am also deeply thankful to Prof. Dr. rer. nat. Dieter Willbold for his willingness to serve as my mentor of my thesis.

I'm also grateful to Dr. Gereon Poschmann, Prof. Dr. Kai Stuehler, Stella Pauls and Dr. Anja Stefanski for their work on the proteomics study, which produced fascinating results.

I would like to express my appreciation to all current and former members of Prof. von Mikecz's research group: Aneta, Inge, Sylwia, Indra and Alex. Your contributions to a cozy working atmosphere, your kindness, and your numerous suggestions and engaging discussions during the research were invaluable. It has been a great pleasure working with you!

A special and warm thank you goes to my family in Vietnam, my girlfriend - Minh Trang Nguyen, my friends and my supportive neighbors who always believed in me and provided me with immense patience and support me during my time in Germany.

Thank you all very much!

DECLARATION

I certify that a part of this thesis has been published in:

1. Indra Hering, Dang Tri Le and Anna von Mikecz (2021) 'How To Keep Up With the Analysis of Classic and Emerging Neurotoxins: Age-Resolved Fitness Tests in the Animal Model *Caenorhabditis elegans* – a Step-By-Step Protocol', EXCLI Journal, 21, pp. 344–353. https://doi.org/10.17179/excli2021-4626.

2. Inge Scharpf, Sylwia Cichocka, Dang Tri Le, Anna von Mikecz (2022) 'Peripheral neuropathy, protein aggregation and serotonergic neurotransmission: Distinctive bio-interactions of thiacloprid and thiamethoxam in the nematode *Caenorhabditis elegans'*, *Environmental Pollution*, 314(June), p. 120253. https://doi.org/10.1016/j.envpol.2022.120253.

I certify that I performed the analysis of proteomics results, which were generated by Prof. Dr. Kai Stuehler's lab unit (Molecular Proteomics Laboratory, BMFZ, Heinrich Heine University Düsseldorf, 40225 Düsseldorf, Germany).

I certify that I wrote the dissertation independently, without unauthorized external assistance and in compliance with the "Principles for Ensuring Good scientific practice at the Heinrich Heine University Düsseldorf".

Duesseldorf, .../...../2024